"SYNTHESIS AND CHARACTERIZATION OF HYDROGELS FOR NOVEL APPLICATIONS"

A THESIS SUBMITTED TO

SAVITRIBAI PHULE PUNE UNIVERSITY

FOR AWARD OF DEGREE OF

DOCTOR OF PHILOSOPHY (Ph.D.)

IN

CHEMISTRY

SUBMITTED BY

MANJUSHA V. PATWADKAR

UNDER THE GUIDANCE OF

Dr. MANOHAR V. BADIGER

POLYMER SCIENCE & ENGINEERING DIVISION

CSIR – NATIONAL CHEMICAL LABORATORY

PUNE – 411008, INDIA

SEPTEMBER 2016

CERTIFICATE

CERTIFIED that the work incorporated in the thesis entitled "**Synthesis and Characterization of Hydrogels for Novel Applications**" Submitted by **Manjusha V. Patwadkar** was carried out by the candidate under my supervision/guidance. Such material has been obtained from other sources has been duly acknowledged in the thesis.

Date :

Place : Pune

Dr. Manohar V. Badiger
(Research Guide)
CSIR-NCL, Pune

DECLARATION

I declare that the thesis entitled "**Synthesis and Characterization of Hydrogels for Novel Applications"** submitted by me for the degree of Doctor of Philosophy is the record of work carried out by me during the period from **18-04-2011** to **20-09-2016** under the guidance of **Dr. Manohar V. Badiger** and has not formed the basis for the award of any degree, diploma, associateship, fellowship, titles in this or any other University or other institution of Higher learning.

I further declare that the material obtained from other sources has been duly acknowledged in the thesis.

Date :

Place : Pune

Manjusha V. Patwadkar

(Research Student)

CSIR-NCL, Pune

Acknowledgements

Completing my PhD degree is probably the most challenging activity of my life. The best and unpleasant moments of my doctoral journey have been shared with many people. It has been a great privilege to spend a few years in the Polymer Science and Engineering Division of the CSIR-National Chemical Laboratory and its members will always remain dear to me.

My first debt of gratitude must go to my research advisor, ***Dr. Manohar V. Badiger.*** *He patiently provided the vision, encouragement and advice necessary for me to proceed through the doctoral program and complete my dissertation. His mentorship was paramount in providing a well-rounded experience consistent with my long-term career goals. He has been a wonderful guide, a marvellous person and an overwhelming influence. He has given me full freedom in my research and one could not imagine have a better mentor than him. His friendly and helping nature binds the group members strongly. I feel privileged to have had an opportunity to be his student and shall forever be indebted to him for his contribution to my growth.*

I wish to thank the ***Director****, CSIR-NCL for providing me all the required facilities to work in NCL.*

I would like to thank my Ph.D. committee ***Dr. Prakash P. Wadgaonkar, Dr. Vaishali S. Shinde, Dr. C. V. Rode, Dr. M. Jayakanan*** *for their support, guidance and helpful suggestions.*

I also owe my gratitude to ***Dr. Sreekumar*** *who has inspired me in my research with stimulating discussions and conversations and for carrying out few experimental studies relating to my thesis work in their labs. I would like to thank* ***Rajith, Vidyanand*** *with whom I carried out experiments related to my thesis work.*

A special word of thanks goes to ***Dr. Mohan G. Kulkarni*** *who taught me start firmly during initial stint at NCL and the field of science during my work as a project assistant. I will be always obliged to him for teaching, guiding me the finest skill and giving excellent training required for the research as well as for his constant efforts to encourage us with several essential habits, like group meeting, seminar, monthly report and daily planning of work. My sincere regards and respect are for him forever.*

Additionally, I am very grateful for the friendship of the entire members of his research group, ***Dr. Mahesh, Dr. Rupali, Dr. Anupa, Dr. Sunita, Dr. Santosh, Dr. Prerna, Dr. Ramesh, Dr. Gahinath Bharate Dr. Ujjwal, Dr. Hemant, Dr. Jiten, Dr. Sachin, Dr. Satish, Dr. Sameera, Dr. Harshal, Dr. Swapnil, Dr. Tushar, Dr. Muntazim, Rupali, Yogini, Vishal, Neelam, Arpita, Vrushali, Pavan, Piyush, Rajesh, Sanjay, Mayur, Niranjan*** *with whom I worked closely and puzzled over many of the same problems.*

In addition, I would like to thank my colleagues ***Dr. Shubhangi, Dr. Aarti, Dr. Vivek, Dr. Vijay, Dr. Nivika, Suresha, Arun, Anumon, Rajeshwari, Ashwini, Neha, Yogesh, Sanoop, Pallavi, Naresh, Bhagyashree, Nidhi, Amarnath, Pratiksh, Lokanadhan*** *for timely help, co-operation and making my stay at NCL pleasant.*

A Special thanks to ***Mr. M. J. Thakkar, Dr. GVN Rathna, Dr. Neelima, Dr. Suresh Bhatt.***

I also wish to thank the Student Academic Office staff, ***Mrs. Puranik, Mrs. Kolhe, Mr. Pavithran, and Mr. Iyer*** *for their extended help.*

I would like to thank administrative and technical staff members ***Mr. U.V. Dhavale****,* ***Mr. Mahajan****,* ***Mr. Bharati, Mr. Kokane*** *who have been kind enough to advise and help in their respective roles.*

I acknowledge the ***CSIR-SRF, RGSTC-Mumbai*** *for providing fellowships to pursue doctoral studies.*

*And last, but definitely not the least, **my family**. As you know, work is not my (entire) life. I really like working, but you are far more important to me.*

*There are no words to acknowledge my parents, **Pappa and Aai** for their blessings, love, care, and continuous support from the initial to the final stages of this journey. Their patience and sacrifice are always a main source of my inspiration and will remain throughout my life. As being a teacher, my father's constant emphasis on the importance of education, ambition and motivation to pursue still higher goal has always been a guiding light for me. It was under their watchful eye that I gained so much drive and an ability to tackle challenges head on.*

*I would like to thank **Sonali, Dipali and Mahesh** (My sisters and brother) who kept supporting and caring about me during my PhD experience.*

*I thank to my **Parents-in-law** for supporting me to pursue my doctoral studies. Without their support this journey could have not been possible. I would like to thank **Nagesh, Yogesh, Bhushan** (my brothers-in-law), **Suchitra, Megha (**my sisters-in-law**)** and entire family just for being there for me, no matter what. I hope that this work makes you proud.....*

*Last but not the least my deepest heartfelt gratitude to my lovely husband **Mangesh** for his faith in me and always being there for me. Thank you for constant and endless love, support, understanding, patience and encouragement throughout my doctoral journey. I would like to give special thanks to my beloved daughter **Swara** for being such a wonderful girl, supported me throughout this journey and always cheering me up. Without their continuous support and tireless efforts this journey would never have been so successful.*

Manjusha

TABLE OF CONTENTS

Abstract

Synthesis and Characterization of Hydrogels for Novel Applications

The aim of this thesis was to design and synthesize hydrogels for novel applications in catalysis, proton conducting membranes for energy storage and sensors. Hydrogels are becoming increasingly important materials in these areas because of their properties such as soft, flexible, hydrophilic, 3D network structure and ease of preparation in different shapes and sizes. Hydrogels are basically 3D network of hydrophilic polymers which are capable of absorbing copious amount of water without loosing their structural integrity. Particularly, for catalytic applications hydrogels have been used as template for preparation and protection of metal nanoparticles and act as nanoreactor for various chemical reactions.

In the area of energy storage applications, hydrogel membranes are beginning to show great potential as proton exchange membranes in fuel cells. Recently, nanofibers embedded with nanoparticles are attracting lot of interest in the area of sensors for toxic metals. Hydrogels have wide range of applications such as, scaffolds/implants in tissue engineering, vehicles for drug delivery, sensors, actuators, enzyme immobilization, stimuli-responsive materials etc. Although, there are a few reports on the hydrogels used/or proposed in catalytic, conducting and sensing applications, there is a great scope for designing hydrogel system with improved properties coupled with antibacterial properties.

In this context, the work was undertaken to design and synthesize Ag-NPs embedded Semi-IPN hydrogels based on Poly(acrylamide) [PAm] and Poly(aspartic acid) [PAS] by free radical polymerization. The formation of Ag-NPs was confirmed by using variety of analytic methods, such as UV-Vis spectroscopy, TEM, EDAX, XRD, and XPS. We demonstrated the use of these Ag-NPs embedded hydrogel in catalytic application for reduction of 4-nitrophenol (4-NP) to 4-aminophenol (4-AP). The swelling property which is the most important parameter for catalytic application for easy diffusion of reactant to approach Ag-NPs to convert into product could be controlled by amount of Poly(aspartic acid) which shows influence on catalytic property of hydrogels. More importantly, the Ag-NPs embedded hydrogel could be

easily separated and used for subsequent repeated cycles without losing the catalytic activity which is the most desired aspects. These hydrogels showed good antibacterial properties which can have bio-medical applications.

We also report on the environmentally friendly route for the synthesis of Ag-NPs incorporated them into Sodium alginate (SA) and Hydrophobically modified ethyl hydroxy ethyl cellulose (EHM-200) hydrogel beads and used them for the catalytic reduction reaction of 4-NP to 4-AP. Sodium alginate could also act as both reducing agent and capping agent for Ag-NPs. EHM-200 helps in enhancing the swelling of the hydrogel as a result, there can be better diffusion of reactants through the hydrogel. The obtained Ag-NPs in the hydrogel beads were characterized by TEM, UV-Vis spectroscopy. In the absence of Ag-NPs and with only $NaBH_4$, the reduction reaction of 4-NP to 4-AP was very slow and the conversion was very low. However, in the presence of Ag-NPs as a catalyst, the reaction rate was faster with high conversion upto $\approx$ 90 %. The isolation of catalyst after the reaction was quite easy and the catalyst could be reused for 2-3 cycles.

We demonstrated incorporation Ag-NPs into Poly(vinyl alcohol)/Poly(aspartic acid) [PVA/PAS] nanofibers and studied their applications in detecting toxic metal, mercury (Hg).

The research work was also focused on development of new hydrogel membranes for proton exchange membrane fuel cells (PEMFC) based on Poly(2-acrylamido-2-methyl-1-propanesulfonic acid) (PAMPS) and sultone modified PVA polymers. Sultone modified PVA content in the hydrogel membrane was varied from 0-15%. The swelling and mechanical strength of the hydrogel membranes were studied. The proton conductivity and ion exchange capacity (IEC) of the hydrogel membranes were studied and the influence of humidity and temperature on the proton conductivity was investigated. The proton conductivities were obtained in the range of (0.6 - 4.30) x 10^{-2} Scm^{-1}. Activation energy (E_a) for proton conductivity was determined and compared with the E_a of commercial membrane, nafion 117. The activation energy decreased with increase in $-SO_3H$ content in the membranes and exhibited higher proton conductivity. The mechanism of proton transfer was explained using both “hop” along via Grotthuss method as well as Vehicle transport of hydrated ions. The tensile strength of the hydrogel membranes varied from 5-30

MPa depending on the humidity content in the hydrogel membrane and the % elongation was in the range of 200-400%. These hydrogel membranes show promise in fuel cell applications.

LIST OF SCHEMES

LIST OF TABLES

LIST OF FIGURES

ABBREVATIONS AND SYMBOLS

Ag	Silver
Au	Gold
Pt	Platinum
Ni	Nickel
PAA	Poly(acrylic acid)
PAMPS	Poly(2-acrylamido-2-methyl-1-propanesulfonic acid)
PHEMA	Poly(2-hydroxy ethyl methacrylate)
PAm	Poly(acrylamide)
PAS	Poly(aspartic acid)
PNIPAM	Poly(N-isopropyl acrylamide)
PEG	Poly(ethylene glycol)
PGMA	Poly(ethylene glycol) methacrylate
EGDMA	Ethylene glycol dimethacrylate
TEGDMA	Tetraethylene glycol dimethacrylate
PVA	Poly(vinyl alcohol)
PVP	Poly(N-vinylpyrrolidone)
PFSA	Perflurosulfonic acid
CS	Chitosan
PSSA	Poly(styrene sulfonic acid)
PEMFC	Proton exchange membrane fuel cell
EHM-200	Hydrophobically modified ethyl hydroxy ethyl cellulose
PEM	Polyelectrolyte membrane
4-NP	4-nitrophenol
4-AP	4-aminophenol
t-BuOK	Potassium tertiarybutoxide
APS	Ammonium Persulfate
KPS	Potassium Persulfate
NMP	N-methylpyrilidone
DMSO-d_6	Deuterated Dimethyl sulfoxide

TEMED	Tetramethylethylenediamine
$AgNO_3$	Silver nitrate
$NaBH_4$	Sodium borohydride
M_W	Weight average molecular weight
nm	Nanometer
MPa	MegaPascal
NPs	Nanoparticles
ppm	Parts per million
MBA	N,N´-Methylenebisacrylamide
FT-IR	Fourier Transform Infrared Spectroscopy
SEM	Scanning Electron Microscopy
NMR	Nuclear Resonance Spectroscopy
TEM	Transmission Electron Microscopy
XRD	X-ray Diffraction
XPS	X-ray Photoelectron Spectroscopy
EDAX	Energy Dispersive X-ray Spectroscopy
SAED	Selected area energy diffraction
UV	Ultra Violet
SPR	Surface Plasmon Resonance
wt%	Weight percent
IEC	Ion Exchange Capacity
RH	Relative humidity
min	Minutes
E_a	Activation energy
Hg	Mercury

Introduction

Chapter – I

In the first chapter, a detailed literature survey was done on hydrogels in terms of their classification, properties and their applications for catalysis, conducting membranes for fuel cell and sensors. Further scope for developing hydrogels for the above applications was highlighted. Characterization techniques such as XPS, XRD, TEM, Electrospinning, etc., used for studying the atomic composition, surface morphology, and making nanofibers were briefly explained.

1.1. Introduction

Hydrogels are three dimensional (3D) polymeric networks, which have the capacity to absorb and hold substantial amount of water in their hydrophilic network. The physical properties of hydrogels resemble living tissues because of their relatively high water content, soft and rubbery nature. Dissolution of hydrogels in water is prevented by crosslinking of polymer chains, which can be provided by covalent bonding, Van der Waals interaction or physical entanglements[1] or crystallites bringing together two or more macromolecular chains.[2] Water can penetrate in between the polymer chains of the polymer network, subsequently causing swelling and formation of a hydrogel.[3] The ability of hydrogels to absorb water arises from the hydrophilic functional groups such as -OH, -CONH, -COOH, -SO_3H, and -NH_2 present in the polymeric structure.

The most interesting property of a polymeric hydrogel is the discontinuous, reversible volume transition between the swollen and collapsed state induced by using the trigger of an external stimuli such as temperature, pH, light, ionic strength, electric and magnetic field etc. The exciting aspects of these hydrogels is that their stimuli responses are smartly and intelligently manifested in changes in volume, shape, phase, optics, mechanics, surface energies, permeation rates etc. Further, gels are soft in nature and mimic the extracellular matrix (ECM) of the body. Therefore, they show promising applications in controlled drug delivery, tissue engineering, actuators, sensors, robotics, optical shutters, molecular separation systems etc.

Besides, these applications hydrogels are now attracting attention in the area of catalysis, conducting materials for fuel cell and sensors for toxic metals. There is a great scope in exploring hydrogels for these novel applications.

1.1.1. Types of hydrogels

Hydrogels can be classified into mainly two types (i) Physical hydrogels (ii) Chemical hydrogels. Physical hydrogels are connected through noncovalent bonds, such as Van der Waals forces, metal-ligand coordination, hydrogen bonding, ionic interactions, hydrophobic interactions, or micro- and nanocrystallite formation.

These physical hydrogels are again classified into polymer and molecular (supramolecular) hydrogels. Polymer physical gels are formed by physical interaction of polymer chains whereas, molecular gels are formed from low-molecular weight organic compounds (molecular weight less than 1000 g mol^{-1}) interacting by noncovalent bonds. The recent development of both polymer and molecular hydrogels has opened up new opportunities in the field of soft materials. **Figure 1.1** shows methods to make physical hydrogels.

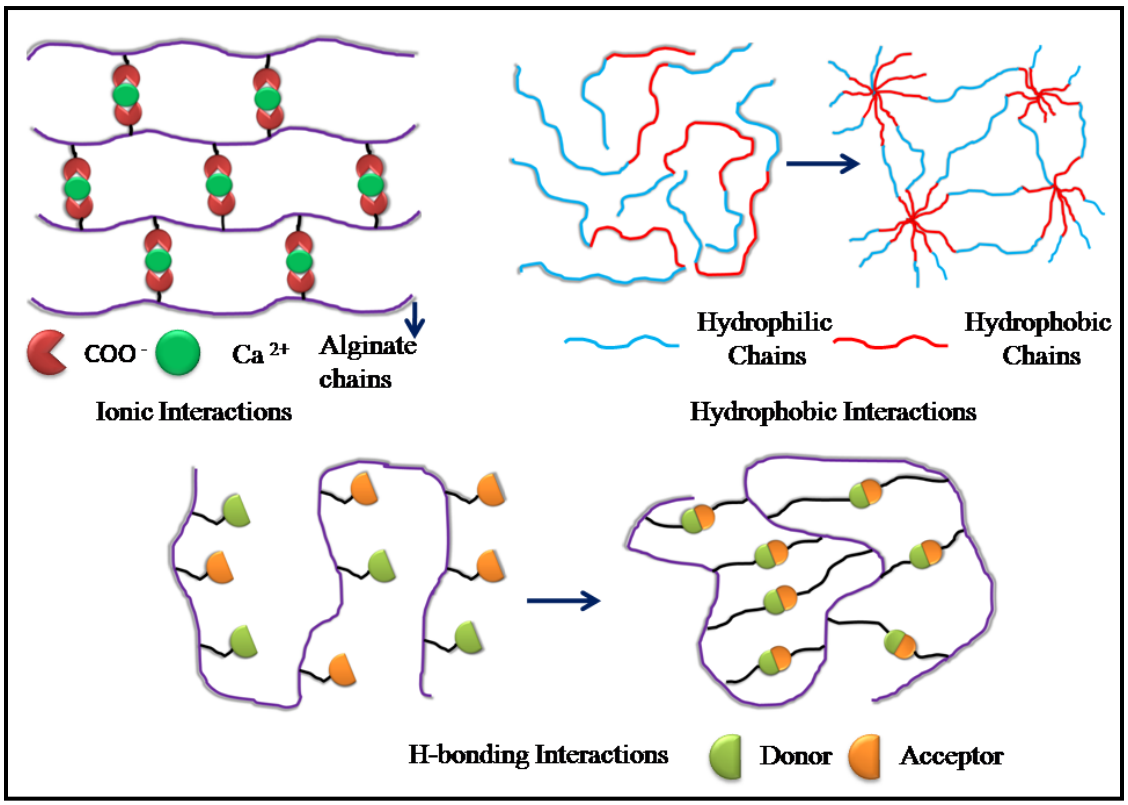

Figure 1.1: *Methods to make physical hydrogels*

However in chemical hydrogels, polymer chains are connected by covalent bonds which are irreversible. Chemical hydrogels are prepared by in-situ crosslinking of monomers using di, tri, tetra/multi functional crosslinking agents during the polymerization reaction.[4] Alternatively, post crosslinking of water-soluble polymers with functional groups can be achieved to make chemically crosslinked hydrogels. **Figure 1.2** shows different methods to make chemical hydrogels.

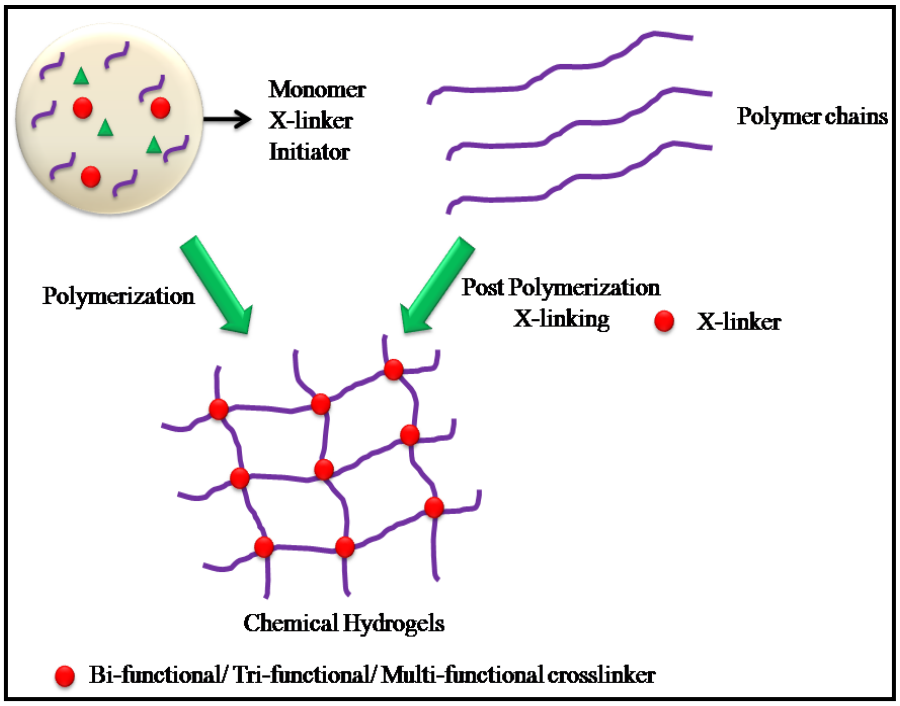

Figure 1.2: *Methods to make Chemical hydrogels*

Based on the chemical structure, the hydrogels can be classified into Homopolymer, Copolymer, Interpenetrating, Semi-interpenetrating hydrogels.

Homopolymeric hydrogels consists of only one type of monomeric unit crosslinked by small amount of crosslinking agents (normally ≈ 5-10 mole %). The common examples of homopolymeric gels include PHEMA, PAA, PAMPS, PAm etc.

Copolymeric hydrogels contain two or more types of monomers crosslinked by different crosslinking agents. The copolymeric hydrogels offer the advantage of the combination of properties of different monomers for the end product. The common examples of copolymeric hydrogels include P(Am-co-AA), P(HEMA-co-IA), P(AA-co-AMPS), P(AMPS-co-HEMA), P(HEMA-co-PGMA) using MBA, EGDMA, TEGDMA as crosslinking agents.

Interpenetrating network (IPN) hydrogels consist of two or more network in which one network is crosslinked in the presence of the other.[5] Generally, IPNs are formed for the purpose of combining individual properties of two or more polymers. The development of IPNs are attractive because they provide free volume space for the easy

encapsulation of drugs in the 3D network structure which are obtained by crosslinking of two or more polymer network.[6] Various properties of IPNs such as porosity, elasticity, swelling and stimuli-responsive behavior can be controlled by the appropriate choice of the network- forming polymers and suitable crosslinking agent and its proportion.[7]

IPNs can be prepared by using various matrices such as polyurethane, polybutadiene, methacrylic acid, L-lysine, glutamic acid, poly vinyl alcohol, poly acrylic acid, gelatin, poly vinyl pyrrolidone, alginate, dextran, guar gum, chitosan, polyethylene glycol etc. for various applications.

In the Semi-inter penetrating network (Semi-IPN) one polymer is linear and penetrates into another crosslinked network without any other chemical bonds.[8] Semi-IPNs can give more effectively rapid response rates to pH or temperature due to the absence of restricting interpenetrating elastic network. For example, Semi-IPN prepared by the incorporation of linear cationic polyallylammonium chloride in acrylamide/acrylic acid copolymer hydrogel, has both higher mechanical strength and fully reversible pH switching for the theophylline release.[9] **Figure 1.3** shows typical representation of the types of hydrogels described above.

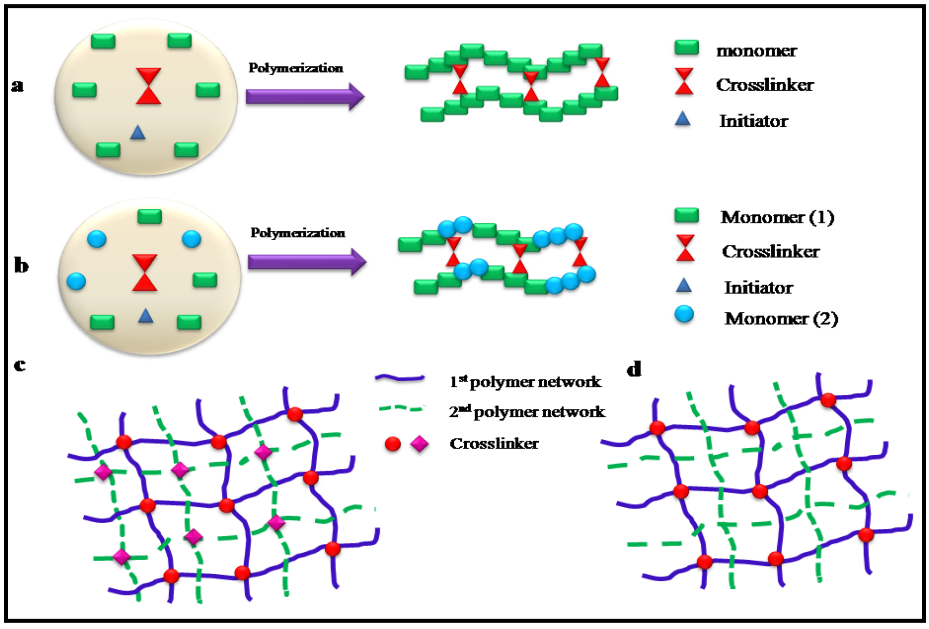

Figure 1.3: *Types of hydrogels a) Homopolymeric hydrogels, b) Copolymeric hydrogels, c) IPNs, d) Semi-IPNs*

1.1.2. Hydrogels in Catalytic Applications

Metal nanoparticles are found to be very efficient catalyst systems because of their large surface area to volume ratio for variety of chemical reactions. For example, use of platinum (Pt) nanoparticles in homogeneous catalytic reactions,[10] use of palladium (Pd) nanoparticles in hydrosilylation reactions[11] and silver (Ag) nanoparticles in olefinic hydrogenation have been reported in the literature.[12-13] An excellent review on the preparation of nanoparticles and their catalytic applications is reported in the literature.[14] However, metallic nanoparticles have a tendency to aggregate and loose their catalytic property. Therefore, in order to overcome the aggregation problem, many protective systems such as polymeric latex particles,[15] dendrimers,[16] hydrogels,[17-18] have been used to stabilize nanoparticles. Amongst these, hydrogels have become very important in the recent past. Hydrogels act as both template and a nano reactor for the chemical reaction to take place. Liu etal.[19] have reported on the nickel nanoparticles in a thermosensitive hydrogel for reduction reaction. Butun and Sahiner[20] have used hydrogel template for metal nanoparticles preparation for catalytic applications. Lu etal.[17] have used a composite hydrogel as a robust carrier for catalytic nanoparticles.

Another advantage with the hydrogel is that toxic metal catalyst can be encapsulated within the hydrogels which can resolve the environmental concern.

Most studied reactions of nanoparticles incorporated hydrogels are catalytic reduction of 4-nitrophenol to 4-aminophenol. Nitrophenols, one of the derivatives of phenols, are present in high levels in the effluents from numerous industries including chemical, petrochemical, pharmaceutical, refineries, oil field activities, coal processing, olive oil production, etc.[21-22] Phenol is toxic to humans and causes headaches, fainting, vertigo and mental disturbance. Additionally, it can cause several severe ecological and environmental problems. Therefore, continuous efforts are being made to reduce nitroaromatic compounds to their corresponding useful amines. [23-25]

Although there are a few reports on the metal nanoparticles incorporated hydrogels for catalytic applications, the influence of hydrogel properties such as degree of swelling, porosity, crosslink density, on the catalytic activity of the metal nanoparticles

is yet to be fully understood. Therefore, there is still a great scope in studying these aspects.

1.1.3. Hydrogels as Proton Exchange Membranes (PEM) in Fuel Cell Applications

Recently, fuel cells have become environmental friendly devices for energy conversion, power generation, and one of the most promising candidates as Zero-emission power sources. They are electrochemical devices which convert the chemical energy obtained from a redox reaction directly into electrical energy. Fuel cell consists of an electrolyte material that is packed between two thin electrodes (Anode and Cathode). The input fuel (mostly hydrogen) passes over the anode and split (using Pt catalyst) into electron and hydrogen ions. The polymer electrolyte membrane (PEM) allows only the H^+ ions to pass through it to the cathode. The negatively, charged electrons travel along an external circuit to the cathode, creating an electric current. When the electrons reach the oxygen side, they combine with H^+ ion and oxygen to form water. The electrons going through the external circuit create a direct conversion of chemical reaction into electrical energy.[26-27] The general schematic of the fuel cell is shown in **Figure 1.4.**

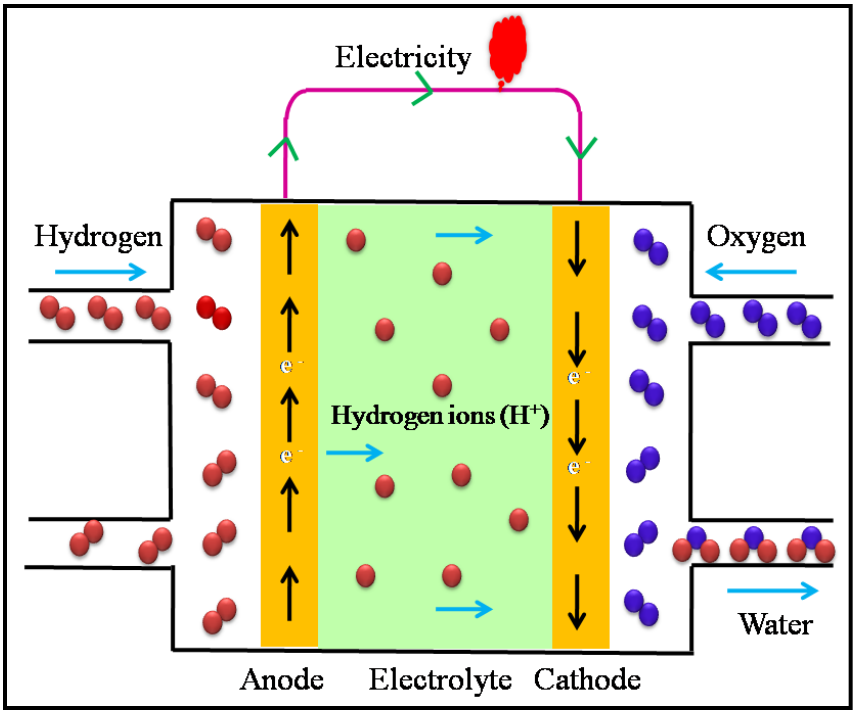

Figure 1.4: *Schematic representation of a fuel cell*

The first working fuel cell was invented by Sir William Grove in 1843 by reacting oxygen and hydrogen on separate platinum electrodes that were immersed in dilute sulphuric acid inside five cells of a gas voltaic battery and using the current produced to electrolyze water in another similar cell.[28-29] However, fuel cells found their first major application when NASA utilized hydrogen-powered fuel cells to produce electricity and water for the Gemini space missions. The high cost and short lifetimes of fuel cells limits their applications to real world.

There are six main types of fuel cell which are categorized depending upon the electrolyte present in them and having commercial importance are (i) alkaline fuel cell (AFC), (ii) phosphoric acid fuel cell (PAFC), (iii) molten carbonate fuel cell (MCFC), (iv) solid oxide fuel cell (SOFC), (v) proton exchange membrane fuel cell (PEMFC) and (vi) direct methanol fuel cell (DMFC)[30-31]

Amongst all, proton exchange membrane fuel cells (PEMFCs) are considered as one of the most promising energy conversion systems. However, their main components (proton exchange membrane, gas diffusion electrodes, bipolar plates, etc.) are still the object of intense fundamental and technological research, especially for durability and cost issues. One of the most interesting challenges to be addressed concerns the proton exchange membrane, which is the heart of the fuel cell.

The most commonly used proton exchange membranes in fuel cells are Perflurosulfonic acid (PFSA) membranes. These membranes are composed of a Polytetrafluoroethylene backbone and perfluorinated pendant side chains terminated by sulfonic acid ($-RSO_3^-$) functional groups responsible for its good proton conductivity and water sorption properties when exposed to water or to a humid environment. The absorbed water serves as a transport medium for protons and gives the membrane good conductivity properties during the operation of the PEMFC. Among the PFSA membranes, the most studied and commercially successful is Nafion® membrane, an ionomer developed and manufactured by DuPont. However, its high cost, high methanol permeability, difficulty in synthesis and processing limits its application in fuel cell.[32-37] To overcome these drawbacks, extensive efforts have been made to develop alternative low-cost membranes as potential PEMs.

Most of the strategies have been developed to modified PFSA polymers, acid functionalized aromatic hydrocarbon-based polymers or a number of sulfonated aromatic polymers such as poly (arylene ethers) (PAE),[38-39] poly (acrylene ether sulfone) (PAES),[40-42] poly (ether ether ketone) (PEEK)[43-44] and polyimide (PI)[45-46] as potential PEMs. Sulfonated or phosphonated polybenzimidazoles (PBI),[47-49] polybenzoxazoles (PBO)[50-51] and polybenzothiazoles (PBT)[52-53] have also been investigated for possible use as PEMs. However, there are still unresolved application issues with these membranes due to low proton conductivity under low humidity conditions, and poor stability during long-term operation.

Acid base blends are another approach for designing fuel cell membrane in which polymers like poly (ethylene oxide) (PEO),[54-55] poly (vinyl alcohol) (PVA), poly (acrylamide) (PAm) and poly (vinylpyrrolidone) (PNVP) are complexed with strong acids, such as sulfuric acid or phosphoric acid. However, these blends show lower proton conductivity (10^{-3} Scm^{-1}) in hydrated and dehydrated state. Another concern with these blend membranes is poor mechanical stability due to high acid content. Therefore, different strategies to improve mechanical strength without sacrificing proton conductivity are copolymerization, grafting, polymer blending and crosslinking.

Recently, water soluble polymers (WSP) are becoming important in designing PEM where they confer additional water retention ability. Several WSPs, such as chitosan (CS),[56-58] poly (ethylene glycol) (PEG), poly(vinyl alcohol) (PVA), poly(vinylpyrrolidone) (PNVP), poly(2-acrylamido-2-methyl-1-propanesulfonic acid) (PAMPS) and Poly(styrene sulfonic acid) (PSSA) are being used for fuel cell PEM, with different architectures resulting from polymer blending, simple crosslinking, Semi-interpenetrating networks (Semi-IPN) and interpenetrating networks (IPN). For example, CS was usually either ionically crosslinked with sulfuric acid[59-60] or incorporated into inorganic particles[61-64] to solve low conductivity and high swelling problems. PVA[65-70] and PEG[71-72]are mostly used as crosslinking partners into Semi-IPN membranes to improve the membrane's toughness and strength. P(NVP) is generally blended with PVA for improving water and methanol sorption selectivity in DMFCs.[73] PSSA and PAMPS were used as a polyelectrolyte in Semi-IPN architectures.[65, 74] PSSA/PAMPS

homopolymer, or as copolymers, were often combined with a PVA network to form Semi-IPN architecture.

In our study, we have made an attempt to modify nonionic PVA by adding partial charges on to the polymer, so as to impart proton conductivity by forming Semi-IPNs with PAMPS.

1.1.4. Hydrogels as Nanofibers for Sensing Applications

Nanofibers, according to National Science Foundation (NSF) have a measured diameter of less than a micrometer with a large surface area to volume ratio, which makes them a great candidate for many applications such as in drug delivery,[75] tissue engineering as nanofiber scaffolds, chemical, biological and optical nanosensor.[76] In addition, nanofibers with nanoparticles are considered for many other applications such as water treatment and wound dressing etc.[77]

Polymeric fibers have been fabricated by several techniques such as: drawing,[78-80] template synthesis,[81-82] phase separation,[83]and Electrospinning.[84-87] Drawing is a process similar to dry spinning which can make one-by-one very long single nanofibers. However, only a viscoelastic material can be made into nanofibers through drawing. The template synthesis uses a nanoporous membrane as a template to make nanofibers of solid or hollow shape. Using this technique nanofibers of various raw materials such as electronically conducting polymers, metals, semiconductors, and carbons can be fabricated. However, the method cannot make one-by-one continuous nanofibers. The phase separation consists of dissolution, gelation, extraction using a different solvent, freezing, and drying resulting in nanoscale porous foam. The process takes relatively long time to transfer the solid polymer into the nano-porous foam. The self-assembly is another process in which individual, pre-existing components organize themselves into desired patterns and functions. However, this technique is time-consuming in processing continuous polymer nanofibers.

Now, electrospinning is gaining popularity due to ease of making nanofibers continuously and the availability of commercial electrospinning equipments with various design parameters.

Recently, Silver nanoparticles (Ag-NPs) have been used as selective chemosensors for heavy metal ions which are generally toxic. Amongst them, mercury (Hg) is considered as one of the most toxic metal for environment.[88-89] Ag-NPs have been used for colorimetric sensors for Hg where in silver forms amalgam with Hg and influence the surface plasmon resonance (SPR) extinction of Ag-NPs.[90] However, the interference due to the analyte medium can make the sensor inefficient. Further, packing of these sensors in general is cumbersome. Therefore, incorporation of Ag-NPs into electrospun fibers is gaining interest where the nanoparticles can be distributed uniformly in the nanofiber structure with high porosity and large surface area. For example, Formo etal.[91] reported on the synthesis of Pt-NPs on the surface of TiO_2 electrospun fibers for catalytic applications. Jin etal.[92] and Wang etal.[93] made Ag-NPs doped PVP nanofibers for antimicrobial application.

1.1.5. Characterization techniques used in this work

1.1.5.1. Electrospinning

Although the term "Electrospinning" was used recently but its fundamental idea dates back more than 60 years earlier. From 1934 to 1944, Formalas published a series of patent including an experimental setup for the production of polymer filaments using electrostatic force.[94]

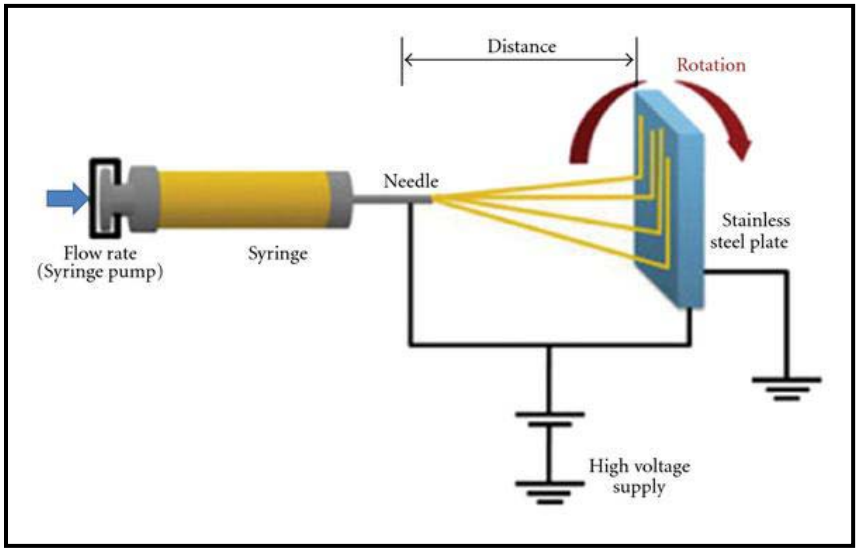

Figure 1.5: *Schematic of nanofibers formation by Electrospinning*

A polymer solution was introduced into the electric field. The polymer fibers were formed, from the solution, between two oppositely charged electrodes. One of the electrodes was placed into the solution and the other onto a collector. When a high voltage is applied, polymer solution becomes charged and electrostatic repulsion overcomes the surface tension and the droplet is stretched which results into fibers which were collected on the collector. Fibers morphology and formation depends on the various factor such as polymer molecular weight, solution properties, applied voltage, distance between the needle and collector. Schematic of Electrospinning setup is shown in **Figure 1.5.**

1.1.5.2. X-ray Photoelectron Spectroscopy (XPS)

XPS is a surface sensitive technique which analyses the electronic structure, atomic composition in the top (~50Å) surface of the material. Each atom in the surface has core electrons with the distinct binding energy, which helps in identification of all elements by XPS. Binding energy (BE) is a direct measure of energy required to remove the electrons concerned from its initial state to vacuum level. Alternatively, it may be called ionization energy also, which is nothing but the minimum energy required to remove an electron from a given orbital. Since the BE is a characteristic property of atoms and ions, XPS provides a direct information of chemical analysis such as oxidation states and surface concentrations and hence is also known as electron spectroscopy for chemical analysis (ESCA).

The principle of this technique is based on the photoelectric effect. Each atom has core electron with the characteristics binding energy. When the X- ray beam bombards on the sample surface, the energy of photon is absorbed by core electron of an atom in a molecule. If the photon energy is large enough, then core electron will escape from the atom and emit out of the surface. The emitted electron with kinetic energy of E_k is referred to as a photoelectron. The binding energy of electron is given by an Einstein relationship:

$$E_b = h\nu - E_k - \Phi \qquad (1)$$

Where, E_k is the kinetic energy, hν is the X-ray photon energy of a photoelectron, E_b is the binding energy of photoelectron, and Φ is the work function as shown in **Figure 1.6.**

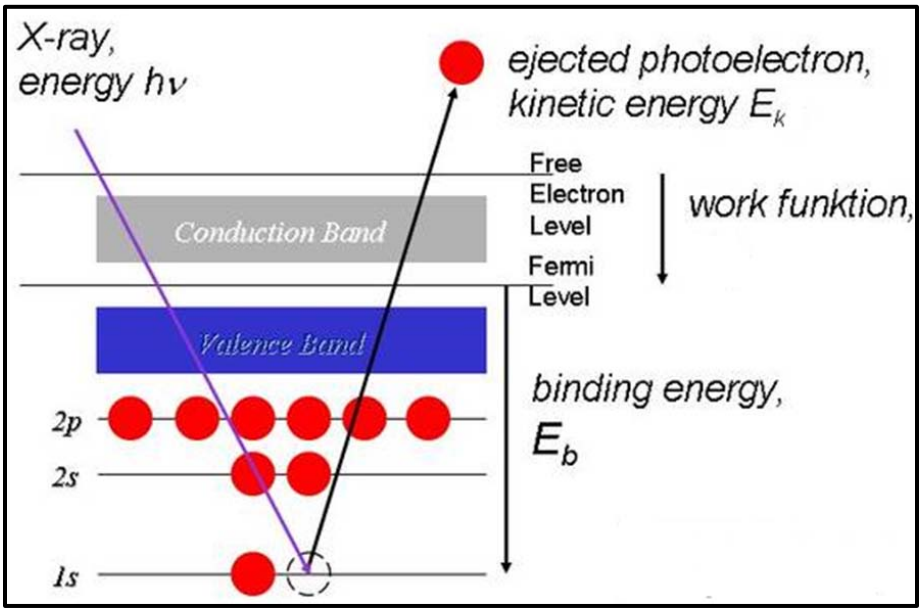

Figure 1.6: *Principle of X-ray Photoelectron Spectroscopy*

The XPS consists of a X-ray source, an energy analyzer for emitted photoelectrons and a detector in an ultra-high vacuum chamber. Al Ka (1486.6 eV /1 eV width) or Mg Ka (1253.6 eV energy /0.7 eV width) are generally used as X-ray sources. High vacuum is normally attained with a combination of several vacuum pumps. Generally, concentric hemispherical analyzer has been explored. Finally the image detector detects the spectra due to photoelectrons.

An electron energy analyzer produces an energy spectrum of intensity (number of photo-ejected electrons versus time) versus binding energy. Each prominent energy peak on the spectrum corresponds to a specific element. For example, B.E of 284.6 eV, corresponds to carbon (C), and 532.5 eV which corresponds to oxygen (O).

XPS can be used to determine the chemical environment of element. Change in binding energy is normally attributed to change in oxidation, effective charge as well as bonding characteristics between atoms. Same element with different environment gives rise to different measurable binding energy.

1.1.5.3. Transmission Electron Spectroscopy (TEM)

The transmission electron microscope is a very powerful tool for material science. It was developed to obtain magnification and hence details of specimen, to a much better level than the conventional optical microscope. In TEM, a beam of electrons is passed through an ultra-thin specimen which interacts with the specimen as it passes through. When the electrons are accelerated to high energy levels (≈ few hundred keV) and focused on a material, they can scatter or back scatter elastically or inelastically, and give many interactions. An image is formed from these interactions and the image is magnified, focused onto an imaging device, such as a fluorescent screen, on a layer of photographic film, or detected by a sensor such as a CCD camera. The electron emission source is either a tungsten or lanthanum hexaboride. Electromagnets are used to accelerate and focus the electrons into a very thin beam by varying the magnetic field of the electromagnetic lenses. The microscope is interiorly evacuated to a low pressure of 10^{-4} Pa. This minimizes scattering of the electrons and increases the mean free path.

TEM is always the first method used to determine the size and size distribution of nanoparticle samples.

1.1.5.4. X-ray Diffraction (XRD)

X-Ray diffraction (XRD) is one of the most important characterization tools used in solid state chemistry and materials science. It represents a non-destructive analytical technique for identification and quantitative determination of crystalline compounds. The diffraction depends on the crystal structure and on the wavelength. Because the wavelength of X-rays is comparable to the size of atoms, they are ideally suited for probing the structural arrangement of atoms and molecules in a wide range of materials. In our study XRD technique was used to characterize the crystalline nature of Ag-NPs.

X-rays are electromagnetic radiation with typical photon energy. The energy of X-ray photon and its wavelength is related by the equation,

$$E = \frac{hc}{\lambda} \qquad (2)$$

Where h is Planck's constant [6.62 x 10^{-34} Js] and c is speed of light. X-ray used in diffraction has wavelengths lying approximately in the range 0.5-2.5 Å. X-rays are produced by collision of high speed electrons with a metal target. All X-ray tubes contain two electrodes, an anode (the metal target) and a cathode. The common X-ray tubes contain copper (Cu) and molybdenum (Mo) which emit 8 and 14 KeV with corresponding wavelength of 1.54 Å and 0.8 Å respectively. Copper makes a good target since it is an excellent heat conductor with a high melting point. X-rays primarily interact with electrons in atoms. If the atoms are arranged in a periodic fashion, as in crystals, the diffracted waves will consist of sharp interference maxima (peaks) with the same symmetry as in the distribution of atoms and hence this diffraction pattern allows to deduce the distribution of atoms in a material. X-ray diffractogram is usually obtained by measuring the diffracted intensity as a function of diffracted angles 2θ (angle between incident and diffracted beams) and orientation of specimen. The peaks in X-ray diffraction pattern are directly related to the atomic distance by Bragg's law.

$$n\lambda = 2d\ sin\theta \qquad (3)$$

Where, 'λ' is wavelength of X-rays and 'd' is d-spacing between atomic planes (interplaner distance) in the crystal, 'θ' is the scattering angle and 'n' is an integral representing the order of diffraction peaks. Bragg's equation can be utilized for the surface analysis by using X-rays of known wavelength and measuring theta, one can determine the d-spacing of various planes in a crystal.

1.2. Summary

This introductory Chapter-I gives a comprehensive review of the literature on hydrogels, types of hydrogels based on crosslinking and chemical structure. The emphasis is given on the applications of hydrogels in the area of catalysis, conducting materials for fuel cell and sensors for toxic metals. Background of hydrogels utilized for these applications and further scope for developing hydrogels for new applications is highlighted. The characterization techniques such as XPS, TEM, XRD and Electrospinning used in this work have been briefly described. Relevant references are given at the end of each chapter.

1.3. References

1. Peppas, N.; Korsmeyer, R., Dynamically swelling hydrogels in controlled release applications. *Hydrogels in medicine and pharmacy* **1987,** 3, 109-136.
2. Hickey, A. S.; Peppas, N. A., Mesh size and diffusive characteristics of semicrystalline poly (vinyl alcohol) membranes prepared by freezing/thawing techniques. *Journal of membrane science* **1995,** 107, (3), 229-237.
3. Langer, R.; Peppas, N. A., Advances in biomaterials, drug delivery, and bionanotechnology. *AIChE Journal* **2003,** 49, (12), 2990-3006.
4. Hennink, W.; Van Nostrum, C. F., Novel crosslinking methods to design hydrogels. *Advanced Drug Delivery Reviews* **2012,** 64, 223-236.
5. Lipatov, Y. S., Polymer blends and interpenetrating polymer networks at the interface with solids. *Progress in Polymer Science* **2002,** 27, (9), 1721-1801.
6. Kulkarni, A. R.; Soppimath, K. S.; Aminabhavi, T. M.; Rudzinski, W. E., In-vitro release kinetics of cefadroxil-loaded sodium alginate interpenetrating network beads. *European Journal of Pharmaceutics and Biopharmaceutics* **2001,** 51, (2), 127-133.
7. Ekici, S.; Saraydin, D., Interpenetrating polymeric network hydrogels for potential gastrointestinal drug release. *Polymer International* **2007,** 56, (11), 1371-1377.
8. Zhang, J.-T.; Bhat, R.; Jandt, K. D., Temperature-sensitive PVA/PNIPAAm semi-IPN hydrogels with enhanced responsive properties. *Acta biomaterialia* **2009,** 5, (1), 488-497.
9. Zhang, Y.; Wu, F.; Li, M.; Wang, E., pH switching on-off semi-IPN hydrogel based on cross-linked poly (acrylamide-co-acrylic acid) and linear polyallyamine. *Polymer* **2005,** 46, (18), 7695-7700.
10. Witham, C. A.; Huang, W.; Tsung, C.-K.; Kuhn, J. N.; Somorjai, G. A.; Toste, F. D., Converting homogeneous to heterogeneous in electrophilic catalysis using monodisperse metal nanoparticles. *Nature Chemistry* **2010,** 2, (1), 36-41.
11. Lewis, L. N.; Lewis, N., Platinum-catalyzed hydrosilylation-colloid formation as the essential step. *Journal of the American Chemical Society* **1986,** 108, (23), 7228-7231.

12. Hutchings, G. J., Heterogeneous catalysts—discovery and design. *Journal of Materials Chemistry* **2009,** 19, (9), 1222-1235.
13. Haruta, M., When gold is not noble: catalysis by nanoparticles. *The Chemical Record* **2003,** 3, (2), 75-87.
14. Roucoux, A.; Schulz, J.; Patin, H., Reduced transition metal colloids: a novel family of reusable catalysts? *Chemical Reviews* **2002,** 102, (10), 3757-3778.
15. Biffis, A.; Orlandi, N.; Corain, B., Microgel-stabilized metal nanoclusters: size control by microgel nanomorphology. *Advanced Materials* **2003,** 15, (18), 1551-1555.
16. Scott, R. W.; Wilson, O. M.; Crooks, R. M., Synthesis, characterization, and applications of dendrimer-encapsulated nanoparticles. *The Journal of Physical Chemistry B* **2005,** 109, (2), 692-704.
17. Lu, Y.; Spyra, P.; Mei, Y.; Ballauff, M.; Pich, A., Composite hydrogels: robust carriers for catalytic nanoparticles. *Macromolecular Chemistry and Physics* **2007,** 208, (3), 254-261.
18. Wang, C.; Flynn, N. T.; Langer, R., Controlled structure and properties of thermoresponsive nanoparticle–hydrogel composites. *Advanced Materials* **2004,** 16, (13), 1074-1079.
19. Liu, J.; Wang, J.; Wang, Y.; Liu, C.; Jin, M.; Xu, Y.; Li, L.; Guo, X.; Hu, A.; Liu, T., A thermosensitive hydrogel carrier for nickel nanoparticles. *Colloids and Interface Science Communications* **2015,** 4, 1-4.
20. Sahiner, N.; Butun, S.; Ozay, O.; Dibek, B., Utilization of smart hydrogel–metal composites as catalysis media. *Journal of colloid and interface science* **2012,** 373, (1), 122-128.
21. Senturk, H. B.; Ozdes, D.; Gundogdu, A.; Duran, C.; Soylak, M., Removal of phenol from aqueous solutions by adsorption onto organomodified Tirebolu bentonite: equilibrium, kinetic and thermodynamic study. *Journal of Hazardous Materials* **2009,** 172, (1), 353-362.
22. Busca, G.; Berardinelli, S.; Resini, C.; Arrighi, L., Technologies for the removal of phenol from fluid streams: a short review of recent developments. *Journal of Hazardous Materials* **2008,** 160, (2), 265-288.

23. Jana, S.; Pande, S.; Panigrahi, S.; Praharaj, S.; Basu, S.; Pal, A.; Pal, T., Exploitation of electrostatic field force for immobilization and catalytic reduction of o-nitrobenzoic acid to anthranilic acid on resin-bound silver nanocomposites. *Langmuir* **2006,** 22, (16), 7091-7095.
24. Patel, A. C.; Li, S.; Wang, C.; Zhang, W.; Wei, Y., Electrospinning of porous silica nanofibers containing silver nanoparticles for catalytic applications. *Chemistry of Materials* **2007,** 19, (6), 1231-1238.
25. Ghosh, S. K.; Mandal, M.; Kundu, S.; Nath, S.; Pal, T., Bimetallic Pt–Ni nanoparticles can catalyze reduction of aromatic nitro compounds by sodium borohydride in aqueous solution. *Applied Catalysis A: General* **2004,** 268, (1), 61-66.
26. Li, X.; Fields, L.; Way, G., Principles of fuel cells. *Platinum Metals Rev* **2006,** 50, (4), 200-1.
27. Ye, Y.-S.; Rick, J.; Hwang, B.-J., Water soluble polymers as proton exchange membranes for fuel cells. *Polymers* **2012,** 4, (2), 913-963.
28. Grove, W. R., On a small voltaic battery of great energy; some observations on voltaic combinations and forms of arrangement; and on the inactivity of a copper positive electrode in nitro-sulphuric acid. *Philosophical Magazine* **1839,** 15, 287–293.
29. Grove, W. R., On voltaic series and the combination of gases by platinum *Philosophical Magazine and Journal of Science* **1839,** 14, 127.
30. Merle, G.; Wessling, M.; Nijmeijer, K., Anion exchange membranes for alkaline fuel cells: A review. *Journal of membrane science* **2011,** 377, (1), 1-35.
31. Winter, M.; Brodd, R. J., What are batteries, fuel cells, and supercapacitors? *Chemical Reviews* **2004,** 104, (10), 4245-4270.
32. Yang, Y.; Shi, Z.; Holdcroft, S., Synthesis of Sulfonated Polysulfone-b lock-PVDF Copolymers: Enhancement of Proton Conductivity in Low Ion Exchange Capacity Membranes. *Macromolecules* **2004,** 37, (5), 1678-1681.
33. Glipa, X.; El Haddad, M.; Jones, D. J.; Rozière, J., Synthesis and characterisation of sulfonated polybenzimidazole: a highly conducting proton exchange polymer. *Solid State Ionics* **1997,** 97, (1), 323-331.

34. Kopitzke, R. W.; Linkous, C. A.; Anderson, H. R.; Nelson, G. L., Conductivity and water uptake of aromatic based proton exchange membrane electrolytes. *Journal of the Electrochemical Society* **2000,** 147, (5), 1677-1681.
35. Slade, S. C., S. A.; Ralph, T. R.; Walsh, F. C., Ionic Conductivity of an Extruded Nafion 1100 EW Series of Membranes. *J. Electrochem.Soc.* **2002,** 149, A1556.
36. St-Pierre, J.; Wilkinson, D. P., Fuel cells: a new, efficient and cleaner power source. *AIChE Journal* **2001,** 47, (7), 1482-1486.
37. Sumner, J.; Creager, S. E.; Ma, J.; DesMarteau, D., Proton conductivity in Nafion® 117 and in a novel bis [(perfluoroalkyl) sulfonyl] imide ionomer membrane. *Journal of the Electrochemical Society* **1998,** 145, (1), 107-110.
38. Dai, H.; Guan, R.; Li, C.; Liu, J., Development and characterization of sulfonated poly (ether sulfone) for proton exchange membrane materials. *Solid State Ionics* **2007,** 178, (5), 339-345.
39. Matsumoto, K.; Higashihara, T.; Ueda, M., Locally sulfonated poly (ether sulfone) with highly sulfonated units as proton exchange membrane. *Journal of Polymer Science Part A: Polymer Chemistry* **2009,** 47, (13), 3444-3453.
40. Miyatake, K.; Chikashige, Y.; Higuchi, E.; Watanabe, M., Tuned polymer electrolyte membranes based on aromatic polyethers for fuel cell applications. *Journal of the American Chemical Society* **2007,** 129, (13), 3879-3887.
41. Zhang, Y.; Wan, Y.; Zhao, C.; Shao, K.; Zhang, G.; Li, H.; Lin, H.; Na, H., Novel side-chain-type sulfonated poly (arylene ether ketone) with pendant sulfoalkyl g roups for direct methanol fuel cells. *Polymer* **2009,** 50, (19), 4471-4478.
42. Bae, B.; Hoshi, T.; Miyatake, K.; Watanabe, M., Sulfonated block poly (arylene ether sulfone) membranes for fuel cell applications via oligomeric sulfonation. *Macromolecules* **2011,** 44, (10), 3884-3892.
43. Zhong, S.; Cui, X.; Cai, H.; Fu, T.; Zhao, C.; Na, H., Crosslinked sulfonated poly (ether ether ketone) proton exchange membranes for direct methanol fuel cell applications. *Journal of Power Sources* **2007,** 164, (1), 65-72.
44. Liu, B.; Robertson, G. P.; Kim, D.-S.; Guiver, M. D.; Hu, W.; Jiang, Z., Aromatic poly (ether ketone) s with pendant sulfonic acid phenyl groups prepared by a mild

sulfonation method for proton exchange membranes. *Macromolecules* **2007,** 40, (6), 1934-1944.

45. Asano, N.; Aoki, M.; Suzuki, S.; Miyatake, K.; Uchida, H.; Watanabe, M., Aliphatic/aromatic polyimide ionomers as a proton conductive membrane for fuel cell applications. *Journal of the American Chemical Society* **2006,** 128, (5), 1762-1769.
46. Sun, F.; Wang, T.; Yang, S.; Fan, L., Synthesis and characterization of sulfonated polyimides bearing sulfonated aromatic pendant group for DMFC applications. *Polymer* **2010,** 51, (17), 3887-3898.
47. Li, Q.; Rudbeck, H. C.; Chromik, A.; Jensen, J. O.; Pan, C.; Steenberg, T.; Calverley, M.; Bjerrum, N.; Kerres, J., Properties, degradation and high temperature fuel cell test of different types of PBI and PBI blend membranes. *Journal of membrane science* **2010,** 347, (1), 260-270.
48. Jouanneau, J.; Mercier, R.; Gonon, L.; Gebel, G., Synthesis of sulfonated polybenzimidazoles from functionalized monomers: preparation of ionic conducting membranes. *Macromolecules* **2007,** 40, (4), 983-990.
49. Mader, J. A.; Benicewicz, B. C., Sulfonated polybenzimidazoles for high temperature PEM fuel cells. *Macromolecules* **2010,** 43, (16), 6706-6715.
50. Li, J.; Lee, C. H.; Park, H. B.; Lee, Y. M., Novel sulfonated poly (arylene ether ketone) containing benzoxazole membranes for proton exchange membrane fuel cell. *Macromolecular Research* **2006,** 14, (4), 438-442.
51. Tan, N.; Xiao, G.; Yan, D., Synthesis and hydrolytic stability of soluble sulfonated polybenzoxazoles derived from bis (3-sulfonate-4-carboxyphenyl) sulfone. *Polymer bulletin* **2009,** 62, (5), 593-604.
52. Tan, N.; Chen, Y.; Xiao, G.; Yan, D., Synthesis and properties of sulfonated polybenzothiazoles with benzimidazole moieties as proton exchange membranes. *Journal of membrane science* **2010,** 356, (1), 70-77.
53. Tan, N.; Xiao, G.; Yan, D., Sulfonated Polybenzothiazoles: A Novel Candidate for Proton Exchange Membranes†. *Chemistry of Materials* **2009,** 22, (3), 1022-1031.

54. Herranen, J.; Kinnunen, J.; Mattsson, B.; Rinne, H.; Sundholm, F.; Torell, L., Characterisation of poly (ethylene oxide) sulfonic acids. *Solid State Ionics* **1995,** 80, (3), 201-212.
55. Park, J. K.; Kang, Y. S.; Won, J., Characterization of deoxyribonucleic acid/poly (ethylene oxide) proton-conducting membranes. *Journal of membrane science* **2008,** 313, (1), 217-223.
56. Dashtimoghadam, E.; Hasani-Sadrabadi, M. M.; Moaddel, H., Structural modification of chitosan biopolymer as a novel polyelectrolyte membrane for green power generation. *Polymers for Advanced Technologies* **2010,** 21, (10), 726-734.
57. Smitha, B.; Sridhar, S.; Khan, A., Polyelectrolyte complexes of chitosan and poly (acrylic acid) as proton exchange membranes for fuel cells. *Macromolecules* **2004,** 37, (6), 2233-2239.
58. Smitha, B.; Sridhar, S.; Khan, A., Chitosan–sodium alginate polyion complexes as fuel cell membranes. *European Polymer Journal* **2005,** 41, (8), 1859-1866.
59. Mukoma, P.; Jooste, B.; Vosloo, H., A comparison of methanol permeability in Chitosan and Nafion 117 membranes at high to medium methanol concentrations. *Journal of membrane science* **2004,** 243, (1), 293-299.
60. Mukoma, P.; Jooste, B.; Vosloo, H., Synthesis and characterization of cross-linked chitosan membranes for application as alternative proton exchange membrane materials in fuel cells. *Journal of Power Sources* **2004,** 136, (1), 16-23.
61. Wu, H.; Zheng, B.; Zheng, X.; Wang, J.; Yuan, W.; Jiang, Z., Surface-modified Y zeolite-filled chitosan membrane for direct methanol fuel cell. *Journal of Power Sources* **2007,** 173, (2), 842-852.
62. Yuan, W.; Wu, H.; Zheng, B.; Zheng, X.; Jiang, Z.; Hao, X.; Wang, B., Sorbitol-plasticized chitosan/zeolite hybrid membrane for direct methanol fuel cell. *Journal of Power Sources* **2007,** 172, (2), 604-612.
63. Cui, Z.; Liu, C.; Lu, T.; Xing, W., Polyelectrolyte complexes of chitosan and phosphotungstic acid as proton-conducting membranes for direct methanol fuel cells. *Journal of Power Sources* **2007,** 167, (1), 94-99.

64. Wang, J.; Zheng, X.; Wu, H.; Zheng, B.; Jiang, Z.; Hao, X.; Wang, B., Effect of zeolites on chitosan/zeolite hybrid membranes for direct methanol fuel cell. *Journal of Power Sources* **2008,** 178, (1), 9-19.
65. Qiao, J.; Hamaya, T.; Okada, T., Chemically modified poly (vinyl alcohol)-poly (2-acrylamido-2-methyl-1-propanesulfonic acid) as a novel proton-conducting fuel cell membrane. *Chemistry of Materials* **2005,** 17, (9), 2413-2421.
66. Kang, M.-S.; Kim, J. H.; Won, J.; Moon, S.-H.; Kang, Y. S., Highly charged proton exchange membranes prepared by using water soluble polymer blends for fuel cells. *Journal of membrane science* **2005,** 247, (1), 127-135.
67. Hamaya, T.; Inoue, S.; Qiao, J.; Okada, T., Novel proton-conducting polymer electrolyte membranes based on PVA/PAMPS/PEG400 blend. *Journal of Power Sources,* **2006,** 156, (2), 311-314.
68. Won, J.; Ahn, S. M.; Cho, H. D.; Ryu, J. Y.; Ha, H. Y.; Kang, Y. S., Sulfonated dextran/poly (vinyl alcohol) polymer electrolyte membranes for direct methanol fuel cells. *Macromolecular Research* **2007,** 15, (5), 459-464.
69. Lin, C.; Huang, Y.; Kannan, A., Semi-interpenetrating network based on cross-linked poly (vinyl alcohol) and poly (styrene sulfonic acid-co-maleic anhydride) as proton exchange fuel cell membranes. *Journal of Power Sources* **2007,** 164, (2), 449-456.
70. Rhim, J.-W.; Park, H. B.; Lee, C.-S.; Jun, J.-H.; Kim, D. S.; Lee, Y. M., Crosslinked poly (vinyl alcohol) membranes containing sulfonic acid group: proton and methanol transport through membranes. *Journal of membrane science* **2004,** 238, (1), 143-151.
71. Lee, S.; Jang, W.; Choi, S.; Tharanikkarasu, K.; Shul, Y.; Han, H., Sulfonated polyimide and poly (ethylene glycol) diacrylate based semi-interpenetrating polymer network membranes for fuel cells. *Journal of Applied Polymer Science* **2007,** 104, (5), 2965-2972.
72. Seo, J.; Jang, W.; Lee, S.; Han, H., The stability of semi-interpenetrating polymer networks based on sulfonated polyimide and poly (ethylene glycol) diacrylate for fuel cell applications. *Polymer Degradation and stability* **2008,** 93, (1), 298-304.

73. Lu, J.; Nguyen, Q.; Zhou, J.; Ping, Z. H., Poly (vinyl alcohol)/poly (vinyl pyrrolidone) interpenetrating polymer network: Synthesis and pervaporation properties. *Journal of Applied Polymer Science* **2003,** 89, (10), 2808-2814.
74. Sahu, A.; Selvarani, G.; Bhat, S.; Pitchumani, S.; Sridhar, P.; Shukla, A.; Narayanan, N.; Banerjee, A.; Chandrakumar, N., Effect of varying poly (styrene sulfonic acid) content in poly (vinyl alcohol)–poly (styrene sulfonic acid) blend membrane and its ramification in hydrogen–oxygen polymer electrolyte fuel cells. *Journal of membrane science* **2008,** 319, (1), 298-305.
75. Wei, G.; Ma, P. X., Nanostructured biomaterials for regeneration. *Advanced Functional Materials* **2008,** 18, (22), 3568-3582.
76. Huang, Z.-M.; Zhang, Y.-Z.; Kotaki, M.; Ramakrishna, S., A review on polymer nanofibers by electrospinning and their applications in nanocomposites. *Composites science and technology* **2003,** 63, (15), 2223-2253.
77. Hong, K. H., Preparation and properties of electrospun poly (vinyl alcohol)/silver fiber web as wound dressings. *Polymer Engineering & Science* **2007,** 47, (1), 43-49.
78. Ondarcuhu, T.; Joachim, C., Drawing a single nanofibre over hundreds of microns. *EPL (Europhysics Letters)* **1998,** 42, (2), 215.
79. Harfenist, S. A.; Cambron, S. D.; Nelson, E. W.; Berry, S. M.; Isham, A. W.; Crain, M. M.; Walsh, K. M.; Keynton, R. S.; Cohn, R. W., Direct drawing of suspended f ilamentary micro-and nanostructures from liquid polymers. *Nano Letters* **2004,** 4, (10), 1931-1937.
80. Nain, A. S.; Wong, J. C.; Amon, C.; Sitti, M., Drawing suspended polymer micro-/nanofibers using glass micropipettes. *Applied physics letters* **2006,** 89, (18), 1 83105.
81. Feng, L.; Li, S.; Li, H.; Zhai, J.; Song, Y.; Jiang, L.; Zhu, D., Super-hydrophobic surface of aligned polyacrylonitrile nanofibers. *Angewandte Chemie* **2002,** 114, (7), 1269-1271.
82. Martin, C. R., Membrane-based synthesis of nanomaterials. *Chemistry of Materials* **1996,** 8, (8), 1739-1746.
83. Ma, P. X.; Zhang, R., Synthetic nano-scale fibrous extracellular matrix. **1999**.

84. Zhang, C.; Yuan, X.; Wu, L.; Han, Y.; Sheng, J., Study on morphology of electrospun poly (vinyl alcohol) mats. *European Polymer Journal* **2005,** 41, (3), 423-432.

85. McCann, J. T.; Li, D.; Xia, Y., Electrospinning of nanofibers with core-sheath, hollow, or porous structures. *Journal of Materials Chemistry* **2005,** 15, (7), 735-738.

86. Deitzel, J.; Kleinmeyer, J.; Harris, D.; Tan, N. B., The effect of processing variables on the morphology of electrospun nanofibers and textiles. *Polymer* **2001,** 42, (1), 261-272.

87. Koski, A.; Yim, K.; Shivkumar, S., Effect of molecular weight on fibrous PVA produced by electrospinning. *Materials Letters* **2004,** 58, (3), 493-497.

88. Tchounwou, P. B.; Ayensu, W. K.; Ninashvili, N.; Sutton, D., Review: Environmental exposure to mercury and its toxicopathologic implications for public health. *Environmental Toxicology* **2003,** 18, (3), 149-175.

89. De Silva, A. P.; Gunaratne, H. N.; Gunnlaugsson, T.; Huxley, A. J.; McCoy, C. P.; Rademacher, J. T.; Rice, T. E., Signaling recognition events with fluorescent sensors and switches. *Chemical Reviews* **1997,** 97, (5), 1515-1566.

90. Fan, Y.; Liu, Z.; Zhan, J., Synthesis of starch-stabilized Ag nanoparticles and Hg 2+ recognition in aqueous media. *Nanoscale research letters* **2009,** 4, (10), 1230.

91. Formo, E.; Lee, E.; Campbell, D.; Xia, Y., Functionalization of electrospun TiO2 nanofibers with Pt nanoparticles and nanowires for catalytic applications. *Nano Letters* **2008,** 8, (2), 668-672.

92. Jin, W. J.; Lee, H. K.; Jeong, E. H.; Park, W. H.; Youk, J. H., Preparation of Polymer Nanofibers Containing Silver Nanoparticles by Using Poly (N-vinylpyrrolidone). *Macromolecular rapid communications* **2005,** 26, (24), 1903-1907.

93. Wang, Y.; Li, Y.; Yang, S.; Zhang, G.; An, D.; Wang, C.; Yang, Q.; Chen, X.; Jing, X.; Wei, Y., A convenient route to polyvinyl pyrrolidone/silver nanocomposite by electrospinning. *Nanotechnology* **2006,** 17, (13), 3304.

94. Anton, F., Artificial thread and method of producing same. In US patent 1,975,504: 1940.

Scope and Objectives

Chapter – II

In the second chapter, we have discussed the scope and objectives of the thesis work.

Hydrogels continue to fascinate researchers throughout the world because of their inherent properties such as soft, flexible, hydrophilic, three dimensional (3D) network structure, stimuli responsiveness, and ease of preparation in different shapes and sizes. Because of these properties hydrogels have myriad of potential applications such as, drug delivery, gene carriers, scaffolds/implants in tissue engineering, molecular separations, sensors, actuators, robotics etc.[1-7] Extensive research has been done on the stimuli-responsive hydrogels where the properties of hydrogels such as swelling/shrinking, phase, colour, shape and actuation can be controlled in response to various external stimuli that include pH, temperature, light, electric and magnetic fields etc.

Besides the above mentioned applications of hydrogels, novel applications of hydrogels in catalysis, conducting hydrogel membranes for energy storage, sensors for toxic metal are emerging recently. Particularly, in catalytic applications hydrogels have been used as template for the preparation and protection of metal nanoparticles which are used as active catalysts in many reactions. Hydrogel carriers have helped in preventing undesired aggregations when the metal nanoparticles are incorporated in them for the catalytic applications. For example, Nickel nanoparticles embedded poly(2-acrylamido-2-methyl-1-propanesulfonic acid) (PAMPS) hydrogels have been used for the reduction of 4-nitrophenol to 4-aminophenol.[8] Hydrogels have also been used as nanoreactors for many chemical reactions in aqueous media.[9-12]

In the area of energy storage applications, hydrogels membranes are beginning to show great potential as proton exchange membranes in fuel cells. The water present in the hydrogel helps in proton conductivity. Currently, Nafion (DuPont), a poly (perfluorosulfonic acid) hydrated membrane is being successfully used as a proton exchange membrane (PEM) in fuel cell applications. However, very high cost of nafion and unsuitability to use at higher temperature and high methanol permeability [13-14] has hindered its complete utility. Therefore, alternate materials such as sulfonated polymers (sulfonated polysulfones, SPSU;[15-16] sulfonated polyphenyleneoxide, SPPO;[17] sulfonated polyether ether ketone, SPEEK[18-20]), polyphenylquinoxaline, (PPQ),[18] polybenzimidozoles (PBI)[21-24] have been looked at. Hence, there is a great demand and

scope for designing and developing more efficient hydrogel membranes for fuel cell applications.

Presently, nanoparticles in nanofibers are attracting lot of interest in the area of sensors for toxic metals, wound healing applications, controlled drug delivery, antibacterial scaffolds in tissue engineering applications etc. For example, Ag-NPs incorporated PVA nanofibers have been reported for catalytic applications.[25] Nanofibers provide very high surface area which helps in obtaining high sensitivity of sensors and efficient catalyst system.

The objectives of the thesis are:

- To design and synthesize silver nanoparticle (Ag-NPs) embedded hydrogel based on Poly(acrylamide) and Poly(aspartic acid) [PAm:PAS] for the catalytic reduction of 4-nitrophenol to 4-aminophenol.
- To synthesize and characterize Ag-NPs by "Green route" and incorporation into Sodium alginate and EHM-200 beads [SA/EHM-200] for the efficient catalyst system.
- Characterizations of nanoparticles by UV-Vis spectroscopy, TEM, XRD, XPS.
- To study the reduction reactions using nanoparticle embedded hydrogel systems.
- To study the catalyst efficiency and recyclability of the catalyst.
- To synthesize nanofibers based on Poly(vinyl alcohol) and Poly(aspartic acid) [PVA/PAS] with Ag-NPs for mercury sensing application.
- To study the antibacterial properties of the obtained Ag-NPs embedded hydrogels.
- To synthesize hydrogel membrane based on Poly(2-acrylamido-2-methyl-1-propanesulfonic acid) and Poly(vinyl alcohol) [PAMPS/PVA] and study its mechanical strength, proton conductivity with respect to humidity and temperature.

References

1. Zhu, J., Bioactive modification of poly (ethylene glycol) hydrogels for tissue engineering. *Biomaterials* **2010,** 31, (17), 4639-4656.
2. Patenaude, M.; Hoare, T., Injectable, mixed natural-synthetic polymer hydrogels with modular properties. *Biomacromolecules* **2012,** 13, (2), 369-378.
3. Censi, R.; Schuurman, W.; Malda, J.; Di Dato, G.; Burgisser, P. E.; Dhert, W. J.; Van Nostrum, C. F.; Di Martino, P.; Vermonden, T.; Hennink, W. E., A Printable Photopolymerizable Thermosensitive p (HPMAm-lactate)-PEG Hydrogel for Tissue Engineering. *Advanced Functional Materials* **2011,** 21, (10), 1833-1842.
4. Zuidema, J. M.; Pap, M. M.; Jaroch, D. B.; Morrison, F. A.; Gilbert, R. J., Fabrication and characterization of tunable polysaccharide hydrogel blends for neural repair. *Acta Biomaterialia* **2011,** 7, (4), 1634-1643.
5. Oh, J. K.; Siegwart, D. J.; Lee, H.-i.; Sherwood, G.; Peteanu, L.; Hollinger, J. O.; Kataoka, K.; Matyjaszewski, K., Biodegradable nanogels prepared by atom transfer radical polymerization as potential drug delivery carriers: synthesis, biodegradation, in vitro release, and bioconjugation. *Journal of the American Chemical Society* **2007,** 129, (18), 5939-5945.
6. Silan, C.; Akcali, A.; Otkun, M. T.; Ozbey, N.; Butun, S.; Ozay, O.; Sahiner, N., Novel hydrogel particles and their IPN films as drug delivery systems with antibacterial properties. *Colloids and Surfaces B: Biointerfaces* **2012,** 89, 248-253.
7. Teixeira, L. S. M.; Feijen, J.; van Blitterswijk, C. A.; Dijkstra, P. J.; Karperien, M., Enzyme-catalyzed crosslinkable hydrogels: emerging strategies for tissue engineering. *Biomaterials* **2012,** 33, (5), 1281-1290.
8. Sahiner, N.; Ozay, H.; Ozay, O.; Aktas, N., New catalytic route: hydrogels as templates and reactors for in situ Ni nanoparticle synthesis and usage in the reduction of 2-and 4-nitrophenols. *Applied Catalysis A: General* **2010,** 385, (1), 201-207.
9. Sahiner, N.; Ozay, O.; Inger, E.; Aktas, N., Controllable hydrogen generation by use smart hydrogel reactor containing Ru nano catalyst and magnetic iron nanoparticles. *Journal of Power Sources* **2011,** 196, (23), 10105-10111.

10. Sahiner, N.; Butun, S.; Turhan, T., p (AAGA) hydrogel reactor for in situ Co and Ni nanoparticle preparation and use in hydrogen generation from the hydrolysis of sodium borohydride. *Chemical Engineering Science* **2012,** 82, 114-120.
11. Seven, F.; Sahiner, N., Poly (acrylamide-co-vinyl sulfonic acid) p (AAm-co-VSA) hydrogel templates for Co and Ni metal nanoparticle preparation and their use in hydrogen production. *international journal of hydrogen energy* **2013,** 38, (2), 777-784.
12. Maity, M.; Maitra, U., An easily prepared palladium-hydrogel nanocomposite catalyst for C–C coupling reactions. *Journal of Materials Chemistry A* **2014,** 2, (44), 18952-18958.
13. Yang, Y.; Shi, Z.; Holdcroft, S., Synthesis of Sulfonated Polysulfone-b lock-PVDF Copolymers: Enhancement of Proton Conductivity in Low Ion Exchange Capacity Membranes. *Macromolecules* **2004,** 37, (5), 1678-1681.
14. Glipa, X.; El Haddad, M.; Jones, D. J.; Rozière, J., Synthesis and characterisation of sulfonated polybenzimidazole: a highly conducting proton exchange polymer. *Solid State Ionics* **1997,** 97, (1), 323-331.
15. Nolte, R.; Ledjeff, K.; Bauer, M.; Mülhaupt, R., Partially sulfonated poly (arylene ether sulfone)-A versatile proton conducting membrane material for modern energy conversion technologies. *Journal of membrane science* **1993,** 83, (2), 211-220.
16. Karlsson, L. E.; Jannasch, P., Polysulfone ionomers for proton-conducting fuel cell membranes: sulfoalkylated polysulfones. *Journal of membrane science* **2004,** 230, (1), 61-70.
17. Kerres, J.; Ullrich, A.; Meier, F.; Häring, T., Synthesis and characterization of novel acid–base polymer blends for application in membrane fuel cells. *Solid State Ionics* **1999,** 125, (1), 243-249.
18. Kopitzke, R. W.; Linkous, C. A.; Anderson, H. R.; Nelson, G. L., Conductivity and water uptake of aromatic-based proton exchange membrane electrolytes. *Journal of the Electrochemical Society* **2000,** 147, (5), 1677-1681.

19. Zhong, S.; Cui, X.; Cai, H.; Fu, T.; Zhao, C.; Na, H., Crosslinked sulfonated poly (ether ether ketone) proton exchange membranes for direct methanol fuel cell applications. *Journal of Power Sources* **2007,** 164, (1), 65-72.
20. Liu, B.; Robertson, G. P.; Kim, D.-S.; Guiver, M. D.; Hu, W.; Jiang, Z., Aromatic poly (ether ketone) s with pendant sulfonic acid phenyl groups prepared by a mild sulfonation method for proton exchange membranes. *Macromolecules* **2007,** 40, (6), 1934-1944.
21. Li, Q.; Rudbeck, H. C.; Chromik, A.; Jensen, J. O.; Pan, C.; Steenberg, T.; M; Bjerrum, N.; Kerres, J., Properties, degradation and high temperature fuel cell test of different types of PBI and PBI blend membranes. *Journal of membrane science* **2010,** 347, (1), 260-270.
22. Jouanneau, J.; Mercier, R.; Gonon, L.; Gebel, G., Synthesis of sulfonated polybenzimidazoles from functionalized monomers: preparation of ionic conducting membranes. *Macromolecules* **2007,** 40, (4), 983-990.
23. Mader, J. A.; Benicewicz, B. C., Sulfonated polybenzimidazoles for high temperature PEM fuel cells. *Macromolecules* **2010,** 43, (16), 6706-6715.
24. Deimede, V.; Voyiatzis, G.; Kallitsis, J.; Qingfeng, L.; Bjerrum, N., Miscibility behavior of polybenzimidazole/sulfonated polysulfone blends for use in fuel cell applications. *Macromolecules* **2000,** 33, (20), 7609-7617.
25. Meng, Y., A Sustainable Approach to Fabricating Ag Nanoparticles/PVA Hybrid Nanofiber and Its Catalytic Activity. *Nanomaterials* **2015,** 5, (2), 1124-1135.

An efficient Ag-NPs embedded Semi-IPN hydrogel for catalytic application

---

Chapter – III

In the third chapter, we report on the synthesis of Ag-NPs embedded Poly(acrylamide)/Poly(aspartic acid) (PAm:PAS) Semi-IPN hydrogel by free radical polymerization using MBA as a crosslinker and demonstrate its application in catalytic reduction of 4-nitrophenol to 4-aminophenol. The swelling of hydrogels could be controlled by varying the amount of PAS. The characterization techniques such as UV-Vis, XPS, XRD, TEM, EDAX for confirming nanoparticles formation, atomic composition, surface morphology were briefly explained.

RSC Advances 2015, 5, 7567-7574.

3.1. Introduction

Metal nanoparticles have been extensively investigated due to their unique physical and chemical properties that are markedly different from bulk properties.[1] Therefore, show potential applications in catalytic, controlled release technology, electronics, photonics and sensor fields.[2-10] Particularly, metal nanoparticles are found to be very efficient catalyst systems for large number of chemical reactions owing to their property of large surface area to volume ratio. For example, Witham etal. have reported on the design and synthesis of novel electrophilic Pt nanoparticles for homogenous catalytic reactions.[11] Olefinic hydrogenation and CO oxidation at low temperature by Au nanoparticles[12-13] and hydrosilylation reactions of olefins by Pd nanoparticles have been demonstrated.[14] A comprehensive review covering different methods of synthesis of metal nanoparticles and their catalytic applications is reported in the literature.[15] However, metallic nanoparticles have a tendency to aggregate and loose their important properties. Hence, metal nanoparticles need to be stabilized in solution to suit end applications.

In order to overcome the problem of aggregation in metal nanoparticles, many protective systems have been used to enhance the stability and dispersibility of these nanoparticles. For example, polysaccharides, polymeric latex particles,[16] micelles,[17] dendrimers,[18] hydrogels[19-21] have been used to stabilize metal nanoparticles. Amongst these, hydrogels are attracting increasing attention lately and are used as carrier systems for the in-situ synthesis of metal nanoparticles which prevent nanoparticles from aggregation.

Hydrogels with nanoparticles act like nanoreactors for chemical reactions. For example, reduction reaction of 4-nitrophenol to 4-aminophenol has been carried out using nanoparticles embedded hydrogels. Reduction of nitrophenol to valuable products is an important reaction since nitrophenols have several ecological and environmental issues. Further, the 4-aminophenol which is a reduced product of 4-nitrophenol is an important chemical used for the production of paraceatamol which is a analgesic and antipyretic drug.[22-23] It is also used as a corrosion inhibitor in paints and anticorrosion-lubricating agent in fuels for two-cycle engines. In the dye industry, 4-aminophenol is used as a

wood stain, imparting a rose like color to timber, and as a dyeing agent for fur and feathers.

Although hydrogels are useful resources, they have not been fully explored for dual action i.e., both as a template for metal nanoparticle synthesis and as a reactor in the reduction of various organic compounds. Therefore, in this work we report on the design and synthesis of Ag-NPs embedded Semi-IPN hydrogel based on the combination of Poly(acrylamide) and Poly(aspartic acid) and its applications in catalytic reduction of 4-nitrophenol to 4-aminophenol. The presence of Poly(aspartic acid) induces charges in the gel and enhances swelling and diffusion of more Ag^+ ions into the hydrogel through electrostatic interaction between $-COO^-$ groups of Poly(aspartic acid) and Ag^+ ions. The Ag-NPs embedded hydrogel was characterized by UV-Vis, X-ray photoelectron spectroscopy (XPS), X-ray diffraction (XRD) and Transmission electron microscopy (TEM).

3.2. Experimental

3.2.1. Materials

Acrylamide (Am), N,N´-Methylenebisacrylamide (MBA), N,N,N´,N´-Tetramethylethylenediamine (TEMED), ammonium persulfate (APS) were purchased from Aldrich (USA) and used as received. Poly(aspartic acid) (PAS) with an average molecular weight of 64 KDa was synthesized in our laboratory by polycondensation of L-aspartic acid reported earlier.[24] Silver nitrate ($AgNO_3$) was procured from S. D. Fine Chemicals Ltd. (India) and sodium borohydride ($NaBH_4$) was purchased from Merck (India).

3.2.2. Synthesis of Ag-NPs embedded Semi-IPN hydrogels

3.2.2.1 Synthesis of Poly(acrylamide)/Poly(aspartic acid) [PAm/PAS] Semi-IPN hydrogels

Poly(acrylamide)/Poly(aspartic acid) [PAm/PAS] Semi-IPN hydrogels were synthesized by free radical polymerization of acrylamide (Am) monomer in the presence of PAS polymer under nitrogen atmosphere. N, N'- methylenebisachrylamide (MBA)

was used as a crosslinker and ammonium persulfate (APS) and tetramethylethylenediamine (TEMED) were used as initiator and accelerator for the reaction respectively. In a typical reaction, known amount of acrylamide monomer and PAS were dissolved in distilled water. To the reaction mixture, MBA was added and dissolved completely. Upon complete dissolution, APS and TEMED were added and the polymerization was carried out at 30°C under N_2 atmosphere. The gelation took place in 10 minutes and polymerization was further carried out for 24 hours to complete the reaction. The obtained hydrogels were immersed in water to remove any unreacted monomers. Finally, hydrogels were sliced into discs of different diameter and thickness and dried to obtained xerogels. Semi-IPN hydrogels with different contents of PAS were prepared and stoichiometry for their preparation is given in **Table 3.1.**

Table 3.1: *Stoichiometry for the synthesis of Semi-IPN hydrogels*

Sr.No.	Samples (wt. ratio)	Am (g)	PAS (g)	MBA (g)	APS (g)	TEMED (µl)
1	PAm	1.0	0.0	0.027	0.01	10
2	PAm/PAS 80/20	1.0	0.25	0.027	0.01	10
3	PAm/PAS 60/40	1.0	0.66	0.027	0.01	10
4	PAm/PAS 50/50	1.0	1.0	0.027	0.01	10

3.2.2.2. Synthesis of Ag-NPs embedded Poly(acrylamide)/Poly(aspartic acid) Semi-IPN hydrogels

Discs, equilibrium swollen in water were immersed in a beaker containing 50 ml of 5mM $AgNO_3$ aqueous solution and allowed to equilibrate for 1 day. In this step, the silver ions diffuse into the gel network. Then, silver ion soaked gels (colorless) were immersed in 50 ml of 10mM $NaBH_4$ reducing agent and kept for 3 hrs. Upon reduction of silver ions to silver nanoparticles, the gels became dark brown in color which is an indication of the formation of Ag-NPs. The obtained hydrogels were denoted as Ag-NPs embedded Semi-IPN hydrogels.

3.3. Characterization

3.3.1. UV-Vis spectroscopy

UV-Visible absorption spectra of Ag-NPs embedded Semi-IPN hydrogels were recorded on a SHIMADZU 1610 PC UV-2450 UV-Vis spectrophotometer, Japan in the range 800-200 nm. For this, ground samples of Ag-NPs embedded hydrogels (10 mg/2 ml) were equilibrium swollen for 24 hours to leach out silver nanoparticles into water (medium). UV-Vis spectra were recorded for leached water.

3.3.2. X-ray diffraction (XRD)

Ag-NPs embedded samples were characterized by X-ray diffraction using Philips X'pert pro powder X-ray diffractometer operating with CuKα radiation (λ=0.15406 nm, Ni filter) generated at 40 kV and 30 mA X-ray diffractometer.

3.3.3. X-ray photoelectron spectroscopy (XPS)

XPS spectra were recorded on a VG Microtech Multilab ESCA3000 spectrometer equipped with non-monochromatised Mg-Kα X-ray source (h_n = 1253.6 eV).

3.3.4. Transmission electron microscopy (TEM)

The morphology of nanoparticles was investigated using a high-resolution transmission electron microscope (HR-TEM) at 300 kV (Cs = 0.6 mm, resolution 1.7Å), Technai-FEI 3010. Samples were prepared by dropping 5-10 μl of finely ground and sonicated dispersion of Ag-NPs embedded hydrogel on copper grid. Grid was then allowed to dry in air and stored in desiccators before taking for microscopy measurements.

3.3.5. Energy dispersive X-ray analysis (EDAX)

The elemental analysis was performed using EDAX, to confirm the formation of Ag-NPs which is an attachment to the scanning electron microscopy. The powder sample of Ag-NPs embedded hydrogels were analysed by EDAX spectrum.

3.3.6. Swelling measurements and Kinetics of swelling

Fully dried Ag-NPs embedded Semi-IPN gels were accurately weighed and equilibrated in distilled water at 30°C for 3 days. The equilibrium swelling ratio (Q) of the hydrogel was calculated using the following equation 1.

$$Q = \frac{W_s - W_d}{W_d} \times 100 \qquad (1)$$

Where, W_s = mass of the equilibrium swollen hydrogel, W_d = mass of xerogel

Further, the kinetics of swelling was studied by measuring the swelling of gels at different time intervals. The fractional uptake of water, 'F' at pre determined time, 't' was determined using equation of Korsmeyer and Peppas,[25]

$$F = \frac{W_t}{W_s} = kt^n \qquad (2)$$

Where, W_t and W_s are mass of swollen gel at time 't' and at equilibrium respectively. k is constant and 'n' is the diffusion exponent which provides information on swelling kinetics. Further, the Q values of Ag-NPs embedded hydrogels in 4-NP/$NaBH_4$ which was the reaction medium of catalysis, were investigated similarly.

3.3.7. Catalytic activity

The catalytic activity of the Ag-NPs embedded Semi-IPN hydrogel was evaluated for the reduction reaction of 4-nitrophenol (4-NP) to 4-aminophenol (4-AP) by $NaBH_4$ by monitoring the electronic absorption of reaction mixture as a function of time. In a typical experiment, 1.4 ml of water, 0.3 ml of 2 mM 4-NP was taken in a quartz cell and 1 ml of 0.03M $NaBH_4$ was added. To this reaction mixture, 10 mg of Ag-NPs embedded Semi-IPN gel was added. The progress of reaction was monitored by recording the time-dependent absorbance using UV-Vis spectrophotometer in the scanning range of 800-200 nm at 30°C.

3.3.8. Reusability of the catalyst

After the first cycle of reaction, the Ag-NPs embedded Semi-IPN hydrogel was separated and washed 2-3 times with 50 ml distilled water. The washed hydrogel catalyst

was dried and subsequently taken for further cycles of reaction and evaluated using the above mentioned procedure.

3.3.9. Antibacterial activity

Antibacterial studies of Semi-IPN hydrogel and Ag-NPs embedded hydrogel were tested by bore well method using E.coil and S.aureus. 5 ml of nutrient agar (NA) medium (pH 6.8) was poured into the sterilized plates and allowed to solidify. The plates were inoculated with spore suspensions of E.coli and S.aureus. The hydrogels were equilibrium swollen and leached out nanoparticle in solutions (20 µl) was added to the bore as test solution and the plates were incubated at 37°C for 24 h. The inhibition zone appeared around the disc was measured and recorded as the antibacterial effect of Ag-NPs.

3.4. Results and Discussion

3.4.1. Synthesis of Ag-NPs embedded Semi-IPN Hydrogels

Unprotected nanoparticles in general are unstable and hence coagulation or aggregation is unavoidable during the catalytic reactions. Hydrogels with embedded metal nanoparticles combine the versatility of former with interesting catalytic properties of the later. In this work, we have synthesized Ag-NPs embedded Semi-IPN hydrogel based on Poly(acrylamide) (PAm) and Poly(aspartic acid) (PAS). The hydrogel synthesis is performed in the presence of PAS, where in this PAS is physically entangled in the 3D structure of PAm resulting into Semi-IPN hydrogel. The advantage with this combination of polymers is that, the PAm has an excellent hydrogel forming property with ease of formation of 3D network structure. Whereas, PAS is a biocompatible, biodegradable, non-toxic polymer and has protecting and nucleating nature for metal nanoparticles. The gelation takes place at room temperature. Furthermore, PAS has ionizable -COOH groups which helps in absorbing more silver ions through electrostatic interactions between COO^- and Ag^+ ions resulting into more Ag-NPs. The Semi-IPN hydrogels swollen in aqueous $AgNO_3$ solution were subjected to reduction reaction in the presence of $NaBH_4$ to form Ag-NPs embedded Semi-IPN hydrogels. The schematic representation of the formation of Ag-NPs in Semi-IPN hydrogel is shown in **Scheme 3.1.**

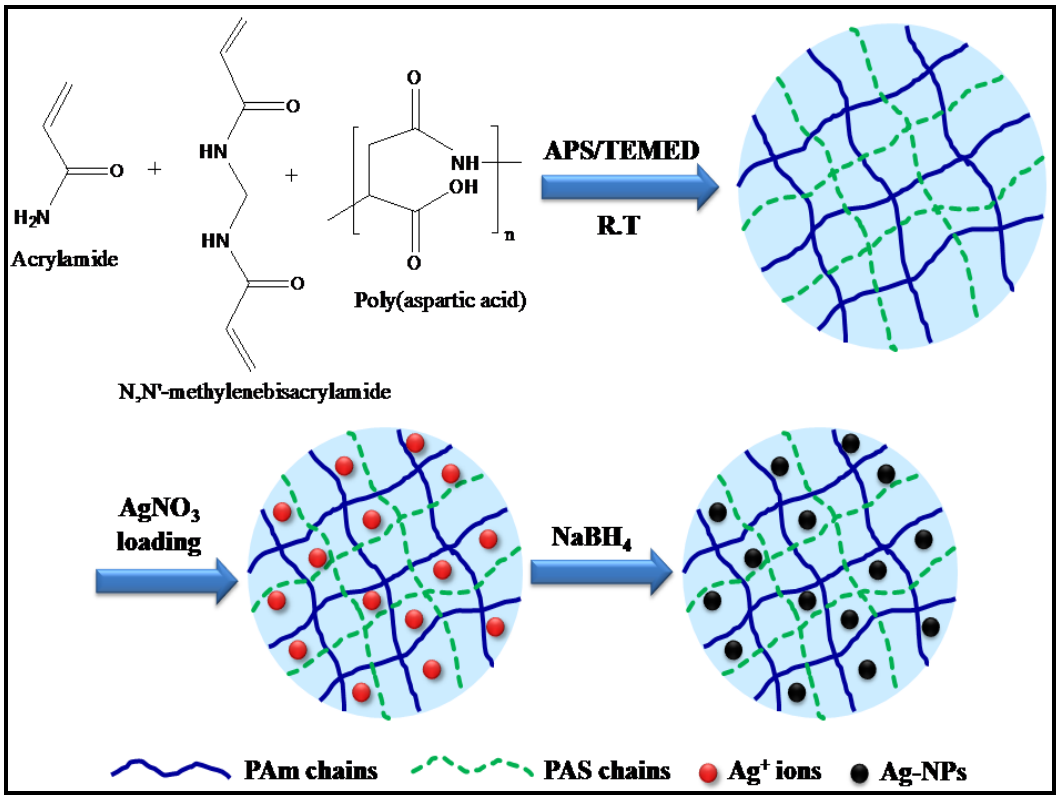

Scheme 3.1: *Schematic representation of formation of Ag-NPs in Semi-IPN hydrogel*

3.4.2. Swelling measurements

Figure 3.1 (a) shows the influence of PAS content on the equilibrium swelling ratios (Q) of Semi-IPN hydrogels. It can be readily seen that, with the same degree of crosslinking, PAm hydrogel without any PAS swells the least because of its non-ionic nature. However, as the PAS content increases, the Q value increases significantly. This could be attributed to the fact that, PAS contains ionizable -COOH groups and the Semi-IPN hydrogel become more ionic in nature and increases the hydrophilicity of the hydrogel. This results in enhancing the swelling ratios of hydrogels.

Figure 3.1 (b) shows the swelling kinetics of Semi-IPN hydrogels. The *n* values of all ratios (100:0, 80:20, 60:40, 50:50) of PAm:PAS Semi-IPN hydrogels were calculated from the slopes of lines of log (F) against log (t) and found to be 0.625, 0.664, 0.734, 0.839 respectively. This clearly indicated the transport in all the Semi- IPN hydrogels is Non-Fickian and dominated by diffusion.

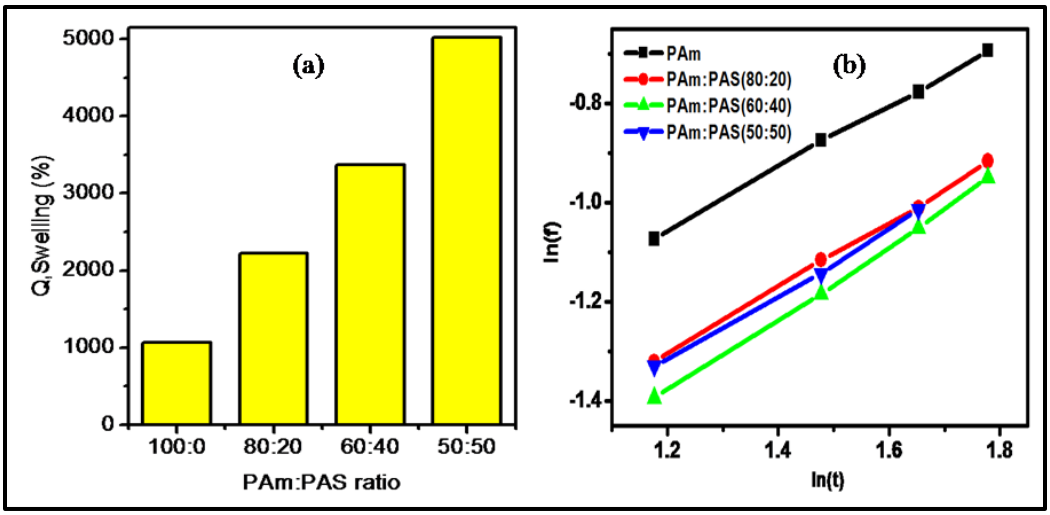

Figure 3.1: *(a) Equilibrium swelling ratio (Q) of Semi-IPN hydrogels in water (b) Plot of ln(F) vs ln(t)*

In order to check the influence of pH on the swelling ratios of Semi-IPN hydrogels, the swelling ratios were determined in different pH solutions and the results are shown in **Figure 3.2.** It is observed that the equilibrium swelling ratio is maximum in the pH range of 6-10 and exhibits lower values in the acidic pH range due to the unionized carboxylic groups of PAS. With increase in pH; the ionization of -COOH groups in PAS occurs and the electrostatic repulsive forces between ionized -COO^- groups in PAS leads to increased swelling ratios. However, at very high pH value, the electrostatic repulsive forces are screened and the swelling ratio decreases.

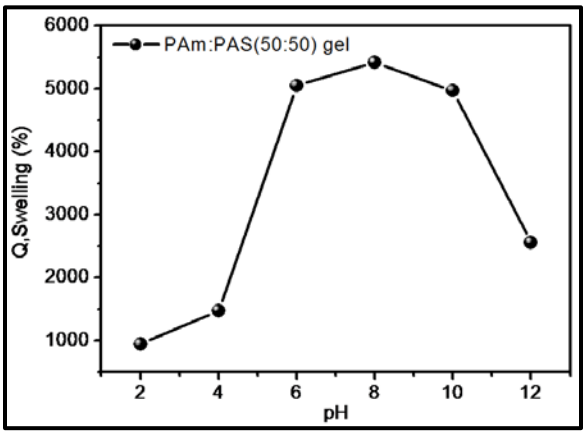

Figure 3.2: *Equilibrium swelling ratio (Q) of PAm:PAS (50:50) sample as an example in different pH solution*

Figure 3.3 (a) compares equilibrium swelling of Semi-IPN hydrogel and Ag-NPs embedded hydrogel in water and 4-NP/$NaBH_4$ solution. For this study we only selected PAm and PAm:PAS (50:50) ratio. It is clear from the figure that Ag-NPs embedded hydrogel has lower equilibrium swelling ratio in water than the pure hydrogel. This may be attributed due to the fact that the pores in 3D network of hydrogel present in case of Ag-NPs embedded hydrogel network are more easily occupied by Ag-NPs which reduces the water volume hence decrease in swelling was seen.

Figure 3.3 (b) shows the swelling ratios of Ag-NPs embedded PAm and PAm:PAS (50:50) hydrogel in 4-NP/$NaBH_4$ (alkaline medium of pH-10.2) which was a reaction medium of catalysis. It is clear from figure that swelling of Ag-NPs embedded PAm hydrogel is less compare to pure PAm:PAS (50:50) hydrogel. This may be due to the ionization of -COOH groups of PAS in basic medium results into increased swelling due to the electrostatic repulsive forces between ionized -COO^- groups.

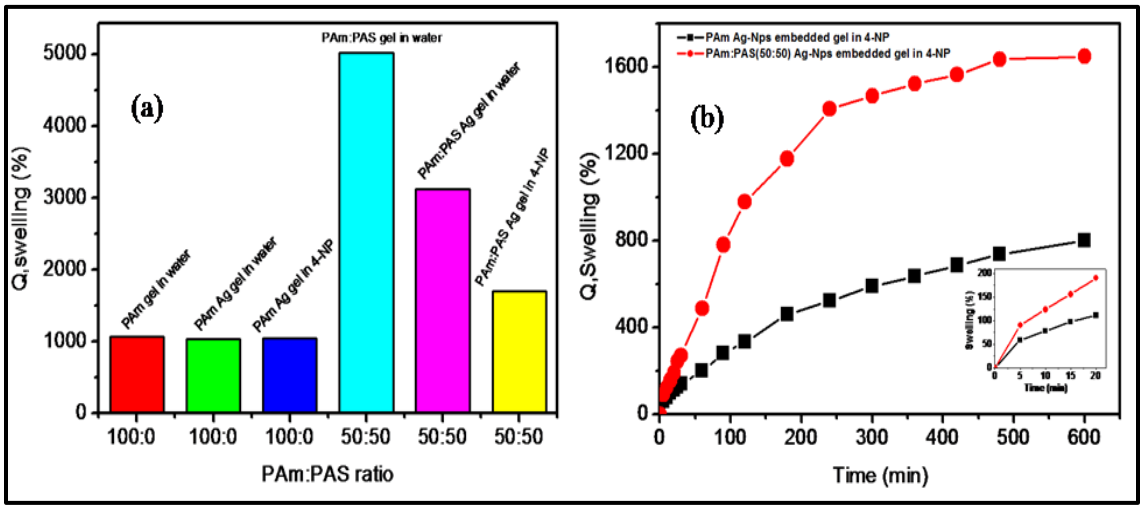

Figure 3.3: *(a) Comparison of Equilibrium swelling ratios (Q) of PAm and PAm:PAS (50:50) hydrogel with and without Ag-NPs in water and 4-NP/$NaBH_4$ [- PAm gel in water, - PAm Ag-NPs embedded gel in water, - PAm Ag-NPs embedded gel in 4-NP/$NaBH_4$, - PAm:PAS(50:50) gel in water, - PAm:PAS (50:50) Ag-NPs embedded gel in water, - PAm:PAS (50:50) Ag-NPs embedded gel in 4-NP/$NaBH_4$] (b) comparison of swelling ratio of PAm and PAm:PAS (50:50) Ag-NPs embedded gel in 4-NP/$NaBH_4$*

3.4.3. UV-Vis spectroscopy

The presence of embedded Ag-NPs in the Semi-IPN hydrogel network was confirmed by UV-Vis spectroscopy. The Semi-IPN hydrogels swollen in $AgNO_3$ solution were readily reduced using $NaBH_4$ which was indicated by the change in the colour of the hydrogel from colourless to dark brown. **Figure 3.4** shows the distinct absorption peak of Ag-NPs embedded Semi-IPN hydrogels at 410 nm due to the characteristics Surface Plasmon Resonance effect of Ag-NPs in the hydrogel. It was observed that with increase in PAS content in the hydrogel, the loading of silver salt in the hydrogel also increased which resulted in the formation of more Ag-NPs in the hydrogel. This is clearly seen in the intense absorption peaks of silver in the UV spectra of samples containing more PAS content. Further, the absence of peaks at 335 nm and 560 nm indicates that there is no aggregation of Ag-NPs in the hydrogel and the Ag-NPs are stable and well dispersed in the Semi-IPN hydrogel matrix. This is confirmed by TEM which will be discussed in the later section.

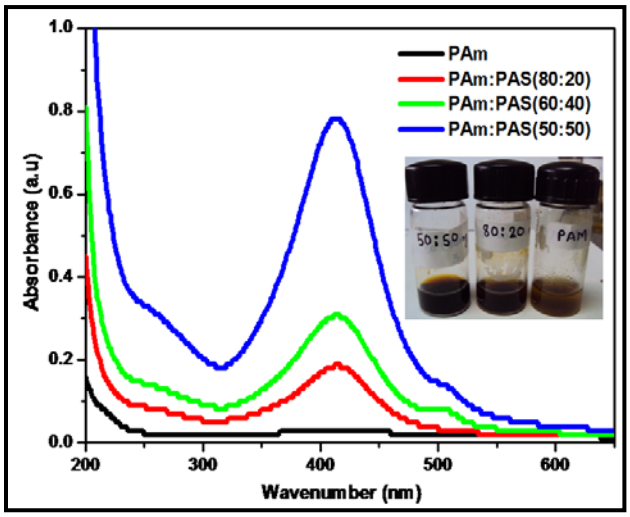

Figure 3.4: *UV-Vis spectra of Ag -NPs embedded Semi-IPN hydrogels*

3.4.4. X-ray diffraction

The presence of Ag-NPs in the hydrogel was investigated by X-ray diffraction. The X-ray diffraction patterns of pure Semi-IPN hydrogel and Ag-NPs embedded hydrogel are shown in **Figure 3.5.** The diffractogram of Ag-NPs embedded hydrogel exhibits the presence of reflection peaks typical of a face centered cubic (fcc) structure of

silver nanoparticles, with 2θ values of about 38.4° and 64.5° assigned to the lattice planes of face centered cubic (fcc) structure of Ag-NPs.

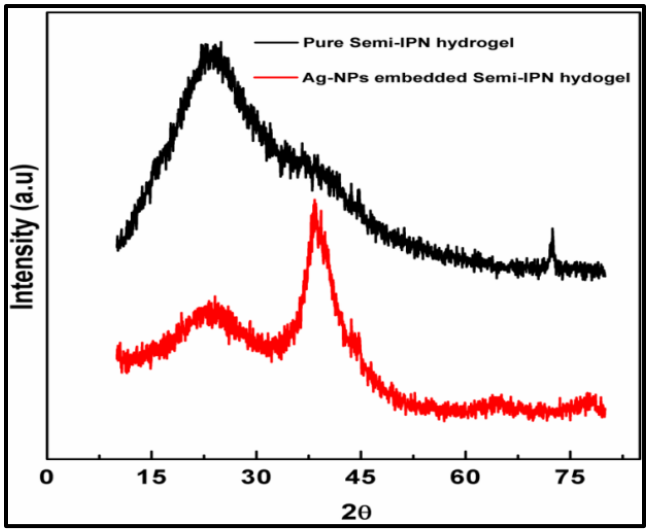

Figure 3.5: *XRD diffractogram of pure Semi-IPN hydrogel and Ag-NPs embedded Semi-IPN hydrogel (50:50)*

These peaks represent the crystalline nature of Ag-NPs embedded in the Semi-IPN hydrogel matrix. Further, the absence of these peaks in the pure Semi-IPN gel clearly indicates the amorphous nature of the hydrogel.

3.4.5. X-ray photoelectron spectroscopy (XPS)

To obtain further information on the Ag-NPs in the hydrogel matrix, we performed XPS measurements on the sample PAm:PAS (50:50) with Ag-NPs embedded into it. Ag 3d and C 1s core level spectra of Ag-NPs embedded gel are shown in **Figure 3.6.** Ag $3d_{5/2}$ and $3d_{3/2}$ spin-orbit coupled core levels are observed at 368 eV and 374 eV respectively. Ag $3d_{5/2}$ peak at 367.5 ± 0.2 eV corresponds to metallic Ag (Ag^0). This confirms the presence of Ag in metallic state.

C 1s core level spectra are shown in **Figure 3.6 (b).** It can be readily seen that peak at 285 eV is a typical feature of alkyl carbon. The peak at 285.6 eV corresponds to carbon attached to nitrogen (C-N) and the peak at 288.2 eV can be attributed to the carbonyl group. The above observations clearly indicate the presence of Ag-NPs in the gel matrix.

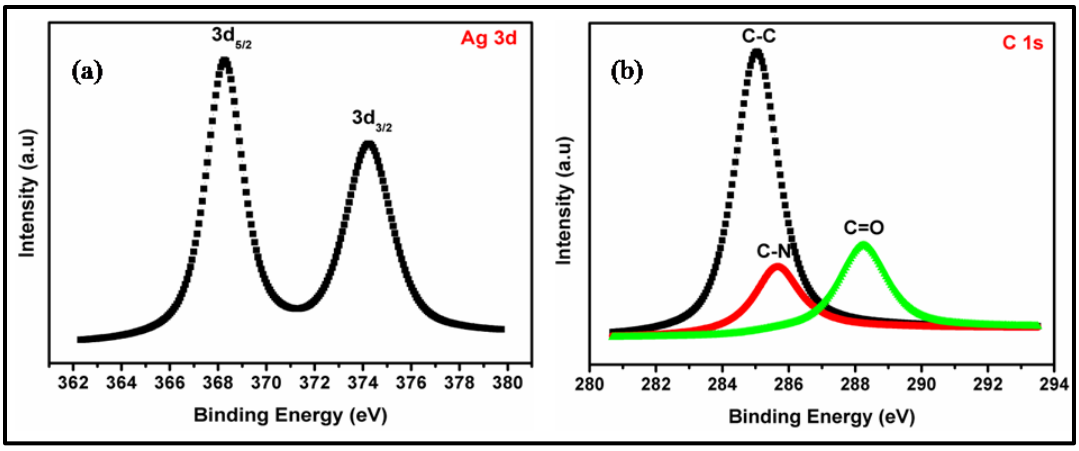

Figure 3.6: *Core level XPS spectra of (a) Ag 3d (b) C 1s of PAm:PAS (50:50) hydrogel*

3.4.6. Transmission electron microscopy (TEM)

To further confirm the formation of Ag-NPs and their morphology in the Semi-IPN hydrogel, the samples were analyzed using Transmission electron microscopy (TEM). We show in **Figure 3.7,** the TEM images of Ag-NPs embedded PAm:PAS (50:50) and PAm hydrogel and **Figure 3.7 (c)** shows picture of Ag-NPs embedded PAm and PAm:PAS (50:50) hydrogel for visual observations. It can be readily seen that, the Ag-NPs are uniformly dispersed in the hydrogel matrix with a size of 10-20 nm. The Ag-NPs are found to be spherical in shape and the selective area electron diffraction (SAED) pattern of Ag-NPs is clearly observed as diffraction ring which is attributed to the face-centered cubic (fcc) structure of Ag-NPs.

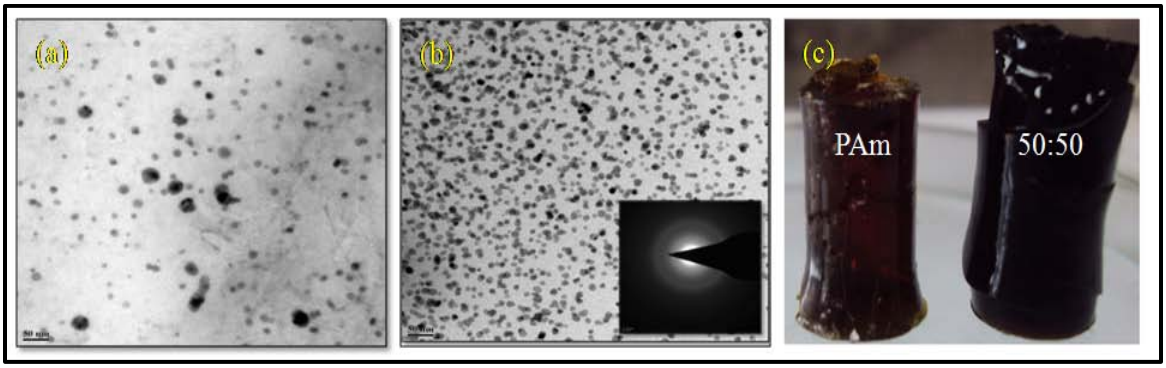

Figure 3.7: *TEM images of Ag-NPs in (a) PAm and (b) PAm:PAS (50:50) hydrogel with SAED pattern inset (c) picture of Ag-NPs embedded PAm and PAm:PAS (50:50) hydrogel*

The formation of Ag-NPs in the PAm gel can also be seen in the TEM micrograph of PAm hydrogel. However, the number of Ag-NPs formed in the PAm hydrogel is very less which could be due to the less absorption of silver salt in the PAm hydrogel. This observation is clearly supported by our UV-absorption study of Ag-NPs embedded PAm hydrogel, in which the intensity of absorption peak is very weak. However, with the incorporation of PAS into PAm hydrogel, more absorption of silver salt into hydrogel takes place resulting into more number of Ag-NPs. PAS helps in anchoring more Ag-NPs into the hydrogel matrix.

3.4.7. Energy dispersive X-ray analysis (EDAX)

To confirm the formation of Ag-NPs and % of Ag present in hydrogel, the samples were analyzed by energy dispersive X-ray analysis (EDAX). Metallic silver nanocrystals generally show typical optical absorption peak approximately at 3 keV due to Surface Plasmon Resonance. **Figure 3.8 (a)** shows that in the case of PAm hydrogel, there is very less number of Ag-NPs formed which is insensitive to be detected by EDAX. However, in the case of PAm:PAS (50:50) **[Figure 3.8 (b)]** we could see a strong signal in the Ag region confirming the presence of Ag-NPs in the gel. We also show in **Table 3.2**, the composition of each element (wt %) present as determined by EDAX measurement. The results clearly show that the amount of silver is more in Semi-IPN hydrogel of PAm:PAS (50:50).

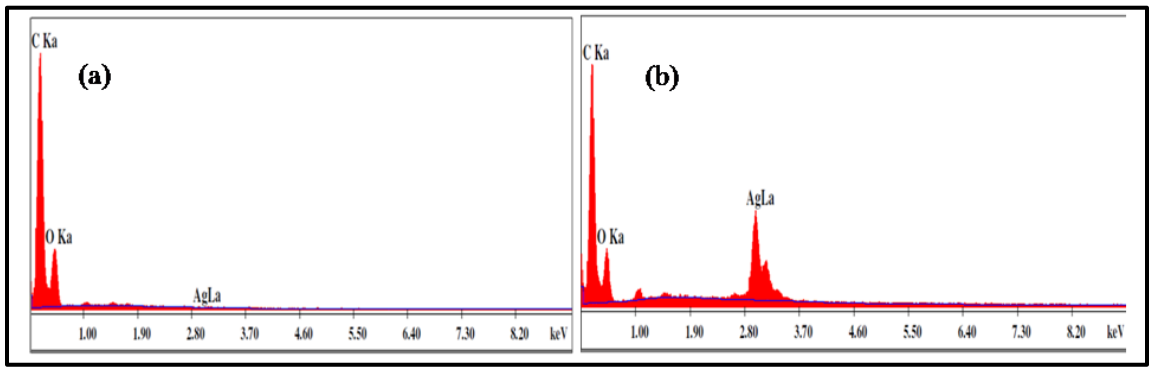

Figure 3.8: *EDAX images of (a) Ag-NPs embedded PAm hydrogel and (b) Ag-NPs embedded PAm:PAS (50:50) hydrogel*

Table 3.2: *Weight % of each element by EDAX*

Element	Ag-NPs embedded PAm Hydrogel (Wt %)	Ag-NPs embedded PAm:PAS (50:50) Hydrogel (Wt %)
C (K)	73.83	61.61
O (K)	26.17	21.59
Ag (L)	0	16.79
Total	100.00	100.00

3.4.8. Catalytic activity of Ag-NPs embedded Semi-IPN hydrogel

The catalytic reduction of 4-NP to 4-AP was performed using Ag-NPs embedded Semi-IPN hydrogel. The reduction of 4-NP by sodium borohydride ($NaBH_4$) over a Ag catalyst is important for practical application. Silver has drawn great interest because of its high catalytic activity for various chemical reactions. The product 4-AP is an important chemical which has wide range of application in analgesic and antipyretic drugs, photographic developers, corrosion inhibitors, and anticorrosion lubricants etc.

Although the reduction of 4-NP to 4-AP using $NaBH_4$ is thermodynamically favourable, the reaction rate is very low and sluggish. However, in the presence of Ag-NPs, which acts as catalyst, the reaction proceeds very fast and the reaction time reduces significantly. The conversion of 4-NP to 4-AP occurs via an intermediate, 4-nitrophenolate ion formation. As shown in **Figure 3.9**, 4-NP exhibits a strong absorption peak @ 317 nm, which shifts to 400 nm upon addition of $NaBH_4$ due to formation of 4-nitrophenolate ion in the alkaline medium. It is important to note that, although the shift has occurred, the absorption intensity has remained more or less same even after the 60 minutes, indicating that the reduction of 4-NP to 4-AP did not proceed in the absence of catalyst **[see Figure 3.9 (b)].** We also show that just by the addition of precursor Semi-IPN hydrogel without Ag-NPs to reaction medium, there was no reduction of 4-NP to 4-AP **[see Figure 3.9 (c)].**

However, upon addition of Ag-NPs embedded Semi-IPN hydrogel [(PAm:PAS (50:50)] to the reaction medium, there was a gradual decrease in the intensity of absorption peak at 400 nm with time and simultaneously, there was an appearance of new absorption peak at 298 nm indicating the reduction of 4-NP and the formation of 4-AP as shown in **Figure 3.9 (d).**

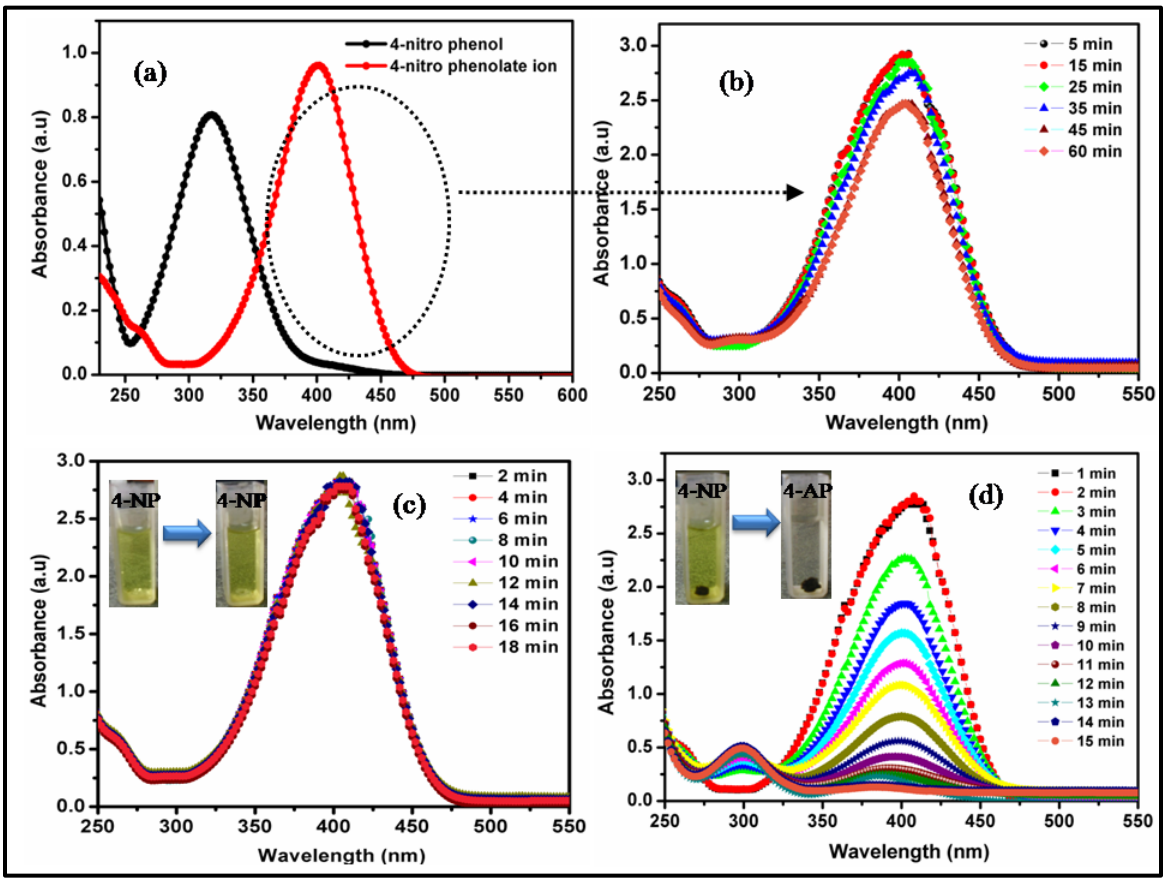

Figure 3.9: *UV spectra of (a) 4-NP and 4-nitro phenolate ion (b) reduction of 4-NP using sodium borohydride without catalyst as a function of time (c) reduction reaction of 4-NP using only precursor Semi-IPN hydrogel without Ag-NPs (d) Catalytic effect of Ag-NPs embedded gel on reduction of 4-NP*

The completion of reaction, which happened in ≈ 16 minutes, was indicated by the slow fading of yellow colour of the reaction mixture. In order to understand the kinetics of the reaction, the decrease in the concentration of reactant w.r.t time was measured. The kinetics of reaction could be described by equation,

$$\ln(C/C_0) = -kt \qquad (3)$$

Where 'k' is the first order rate constant (since the concentration of $NaBH_4$ is in large excess), 't' is the reaction time, 'C' and 'C_0' are the concentration of 4-NP at time 't' and '0' respectively. **Figure 3.10** shows the linear plot between ln (C/C_0) and reaction time 't' for the reduction of 4-NP to 4-AP using Ag-NPs embedded Semi-IPN hydrogel as catalyst. It can be readily seen from the figure that the reaction followed pseudo first order reaction kinetics with the rate constant determined from the slope of liner plot which was found to be 0.374 min^{-1}. The correlation coefficient of the linear plot was very good with the value =0.997.

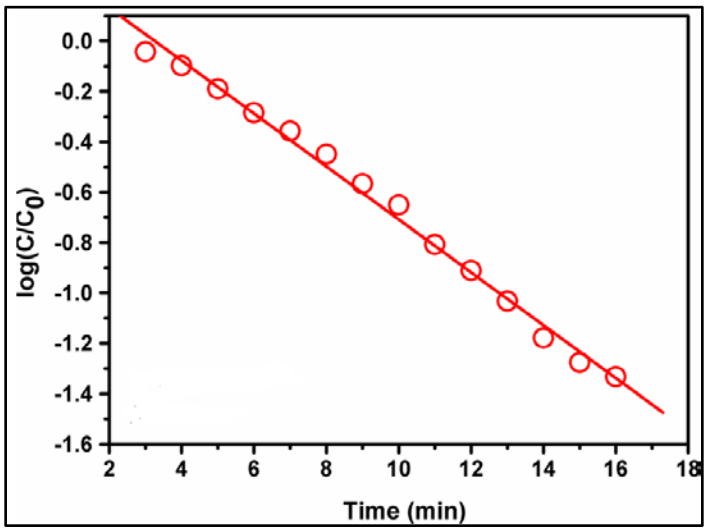

Figure 3.10: *Plot of ln(C/C_0) against the reaction time for the reduction of 4-NP by $NaBH_4$ using catalyst*

3.4.8.1. Effect of concentration of PAS on catalytic activity

In order to study the effect of concentration of PAS on the catalytic activity, we performed the reduction of 4-NP to 4-AP using different ratios of PAm:PAS Ag-NPs embedded hydrogels. **Figure 3.11** shows that, as the PAS content increases, the catalytic activity of hydrogel also increases. It reveals that 50:50 ratio has more number of Ag-NPs and also has more swelling ratio (Q) which increases rate of reaction as compared to PAm and 80:20 hydrogel. These results are again in agreement with our UV and TEM studies discussed in earlier sections.

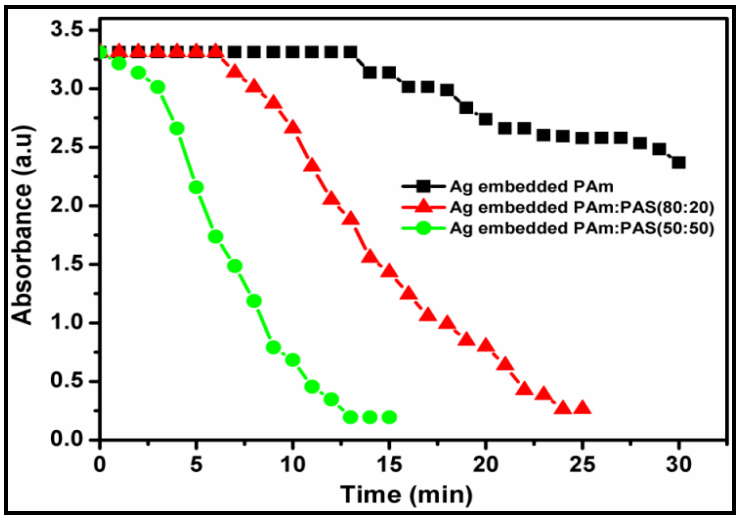

Figure 3.11: *Catalytic effect of Ag-NPs embedded hydrogel with different ratio of PAm:PAS*

The mechanism of catalytic reduction of 4-NP by Ag-NPs involved slow diffusion of BH_4^- and 4-NP into the hydrogel matrix from aqueous solution to the surface of the Ag-NPs. Therefore, swelling of hydrogels is very important factor in catalytic applications for diffusion of reactants. BH_4^- ion reacts with surface of Ag-NPs and transfer hydride ion. Ag-NPs accept this electron with hydride ion and transfer to 4-NP, thus helping to catalyze the reaction by facilitating electron relay from donor BH_4^- to acceptor 4-NP which is shown in **Figure 3.12.**

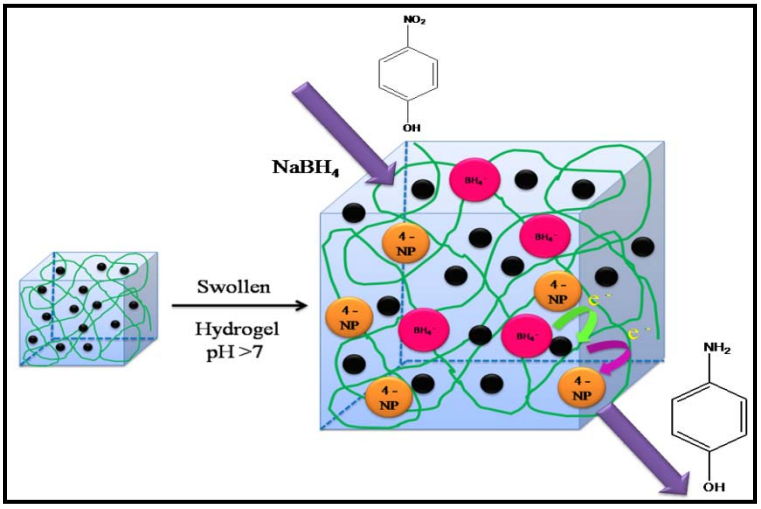

Figure 3.12: *Mechanism of reduction of 4-NP to 4-AP using Ag-NPs embedded hydrogel*

3.4.9. Catalyst recycling

After completion of the first run of reaction, we also explored the repeated use of the same catalyst in successive multiple reaction runs. The Ag-NPs embedded Semi-IPN hydrogel could be easily separated from each cycle and washed with Milli Q water and dried under vacuum before taking it for the next reaction. We show in **Figure 3.13**, the plots of C/C_0 versus reaction time for successive 3 cycles of reduction of 4-NP to 4-AP using the same reaction conditions. It can be readily seen that the Ag-NPs embedded Semi-IPN hydrogel can be successfully reused for 3 cycles without the loss of catalytic activity. However, there is slight decrease in the rate constants for successive cycles shown in **Figure 3.13 (c)** which may be attributed to the loss of Ag- NPs while washing in the intermittent stage. Nevertheless, these observations clearly indicate that the catalyst can be recycled for 3-4 cycles.

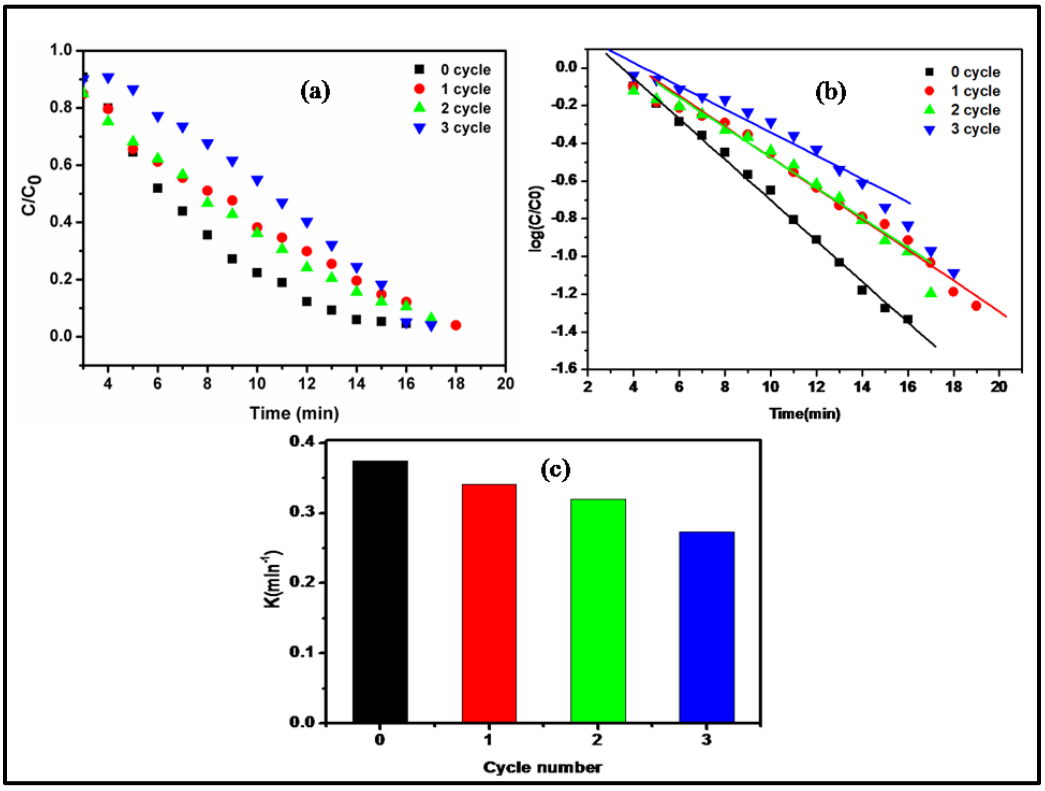

Figure 3.13: *Plot of (a) C/C_0 (b) log C/C_0 against the reaction time for successive three cycle reactions using catalyst (c) Value of rate constant k for each cycle with the Ag-NPs embedded hydrogel as catalyst*

3.4.10. Antibacterial activity

In order to see the efficacy of these hydrogels in bio-medical applications also, we were interested in knowing their antibacterial properties. Therefore, we undertook the study of antibacterial properties of Ag-NPs embedded hydrogels. This effect mostly depends on the size of nanoparticles and the swelling ratios of hydrogels, which have a direct interaction with the bacteria. The silver nanoparticles which are uniformly distributed throughout the hydrogel network come out with the time in aqueous medium and interact with the bacteria. Antibacterial studies of pure Semi-IPN hydrogel and Ag-NPs embedded hydrogels were tested by bore well method using E.Coil and S.aureus as shown in **Figure 3.14**. The results suggest that PAm:PAS (50:50) hydrogel show good antibacterial activity in case of S.aureus (Gram +ve bacteria), while pure hydrogel didn't show any activity. The inhibition area for AgNPs embedded hydrogels follows the order PAm:PAS (50:50) > PAm:PAS (80:20) > PAm. This result clearly indicate that because of more concentration of Ag-NPs due to higher swelling ratio of 50:50 and, they easily come out and interact with lipid layer of cell membrane, there by attaching with microbial DNA to preventing bacterial replication, which are responsible for inhibition of bacterial growth. Therefore, we conclude that the Ag-NPs embedded Semi-IPN hydrogels are having good antibacterial properties.

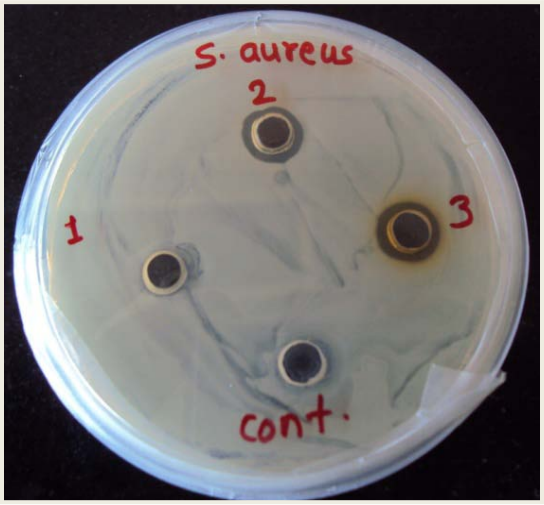

Figure 3.14: *Antibacterial activity of Ag-NPs embedded 1-PAm, 2- PAm:PAS (80:20), 3-PAm:PAS (50:50) compared with Control- Pure hydrogel*

3.5. Conclusions

In summary, in this chapter we have reported on the synthesis and characterization of Ag-NPs embedded hydrogel based on combination of Poly(acrylamide) and Poly(aspartic acid) for catalytic applications. The formation of Ag-NPs was confirmed by using variety of analytical methods, such as UV-Vis spectroscopy, which gave a Surface Plasmon Resonance in the range of 400-420 nm. The TEM images indicated the size of nanoparticles in the range of 10-20 nm. We demonstrated the use of these Ag-NPs embedded hydrogel in the catalytic application of reduction of 4-NP to 4-AP. More importantly, the Ag-embedded hydrogel could be easily separated and reused for subsequent repeated cycles without losing the catalytic activity which is the most desired aspects. These hydrogels also showed good antibacterial properties which can have other bio-medical applications.

3.6. References

1. Burda, C.; Chen, X.; Narayanan, R.; El-Sayed, M. A., Chemistry and properties of nanocrystals of different shapes. *Chemical Reviews* **2005,** 105, (4), 1025-1102.
2. Liz-Marzán, L. M., Tailoring surface plasmons through the morphology and assembly of metal nanoparticles. *Langmuir* **2006,** 22, (1), 32-41.
3. Makiura, R.; Yonemura, T.; Yamada, T.; Yamauchi, M.; Ikeda, R.; Kitagawa, H.; Kato, K.; Takata, M., Size-controlled stabilization of the superionic phase to room temperature in polymer-coated AgI nanoparticles. *Nature materials* **2009,** 8, (6), 476-480.
4. Xu, S.; Zhang, J.; Paquet, C.; Lin, Y.; Kumacheva, E., From hybrid microgels to photonic crystals. *Advanced Functional Materials* **2003,** 13, (6), 468-472.
5. Shipway, A. N.; Willner, I., Nanoparticles as structural and functional units in surface-confined architectures. *Chemical Communications* **2001**, (20), 2035-2045.
6. Luo, X.; Morrin, A.; Killard, A. J.; Smyth, M. R., Application of nanoparticles in electrochemical sensors and biosensors. *Electroanalysis* **2006,** 18, (4), 319-326.
7. Brigger, I.; Dubernet, C.; Couvreur, P., Nanoparticles in cancer therapy and diagnosis. *Advanced Drug Delivery Reviews* **2012,** 64, 24-36.
8. Alivisatos, A. P., Semiconductor clusters, nanocrystals, and quantum dots. *Science* **1996,** 271, (5251), 933.
9. Biswas, A.; Aktas, O.; Schürmann, U.; Saeed, U.; Zaporojtchenko, V.; Faupel, F.; Strunskus, T., Tunable multiple plasmon resonance wavelengths response from multicomponent polymer-metal nanocomposite systems. *Applied physics letters* **2004,** 84, (14), 2655-2657.
10. Ajayan, P. M.; Schadler, L. S.; Braun, P. V., *Nanocomposite science and technology*. John Wiley & Sons: 2006.
11. Witham, C. A.; Huang, W.; Tsung, C.-K.; Kuhn, J. N.; Somorjai, G. A.; Toste, F. D., Converting homogeneous to heterogeneous in electrophilic catalysis using monodisperse metal nanoparticles. *Nature Chemistry* **2010,** 2, (1), 36-41.
12. Hutchings, G. J., Heterogeneous catalysts—discovery and design. *Journal of Materials Chemistry* **2009,** 19, (9), 1222-1235.

13. Haruta, M., When gold is not noble: catalysis by nanoparticles. *The Chemical Record* **2003,** 3, (2), 75-87.
14. Lewis, L. N.; Lewis, N., Platinum-catalyzed hydrosilylation-colloid formation as the essential step. *Journal of the American Chemical Society* **1986,** 108, (23), 7228-7231.
15. Roucoux, A.; Schulz, J.; Patin, H., Reduced transition metal colloids: a novel family of reusable catalysts? *Chemical Reviews* **2002,** 102, (10), 3757-3778.
16. Biffis, A.; Orlandi, N.; Corain, B., Microgel-stabilized metal nanoclusters: size control by microgel nanomorphology. *Advanced Materials* **2003,** 15, (18), 1551-1555.
17. Sakai, T.; Alexandridis, P., Single-step synthesis and stabilization of metal nanoparticles in aqueous pluronic block copolymer solutions at ambient temperature. *Langmuir* **2004,** 20, (20), 8426-8430.
18. Scott, R. W.; Wilson, O. M.; Crooks, R. M., Synthesis, characterization, and applications of dendrimer-encapsulated nanoparticles. *The Journal of Physical Chemistry B* **2005,** 109, (2), 692-704.
19. Lu, Y.; Spyra, P.; Mei, Y.; Ballauff, M.; Pich, A., Composite hydrogels: robust carriers for catalytic nanoparticles. *Macromolecular Chemistry and Physics* **2007,** 208, (3), 254-261.
20. Wang, C.; Flynn, N. T.; Langer, R., Controlled structure and properties of thermoresponsive nanoparticle–hydrogel composites. *Advanced Materials* **2004,** 16, (13), 1074-1079.
21. Zhao, X.; Ding, X.; Deng, Z.; Zheng, Z.; Peng, Y.; Long, X., Thermoswitchable electronic properties of a gold nanoparticle/hydrogel composite. *Macromolecular rapid communications* **2005,** 26, (22), 1784-1787.
22. Vaidya, M. J.; Kulkarni, S. M.; Chaudhari, R. V., Synthesis of p-aminophenol by catalytic hydrogenation of p-nitrophenol. *Organic Process Research & Development* **2003,** 7, (2), 202-208.
23. Rode, C.; Vaidya, M.; Jaganathan, R.; Chaudhari, R., Hydrogenation of nitrobenzene to p-aminophenol in a four-phase reactor: reaction kinetics and mass transfer effects. *Chemical Engineering Science* **2001,** 56, (4), 1299-1304.

24. Tomida, M.; Nakato, T.; Matsunami, S.; Kakuchi, T., Convenient synthesis of high molecular weight poly (succinimide) by acid-catalysed polycondensation of L-aspartic acid. *Polymer* **1997,** 38, (18), 4733-4736.
25. Peppas, N.; Korsmeyer, R., Dynamically swelling hydrogels in controlled release applications. *Hydrogels in medicine and pharmacy* **1987,** 3, 109-136.

Green Synthesis of Ag-NPs embedded in Sodium alginate/Hydrophobically modified ethyl hydroxyethyl cellulose blend beads as highly active catalyst for reduction of 4-nitrophenol

---

Chapter – IV

In the fourth chapter, we have reported on the environmentally friendly route for the synthesis of Ag-NPs incorporated in Sodium alginate (SA) and hydrophobically modified ethyl hydroxy ethyl cellulose (EHM-200) hydrogel beads and used them for the catalytic reduction reaction of 4-NP to 4-AP. The isolation of catalyst after the reaction was quite easy and the catalyst could be reused for 2-3 cycles. The characterization techniques such as, UV-Vis, SEM, TEM for confirming nanoparticles formation, surface morphology were briefly explained.

4.1. Introduction

As mentioned earlier, metal nanoparticles exhibit unique physical and chemical properties and hence show great promise in controlled drug delivery, biomedical, catalysis, sensors etc. applications. Particularly, gold (Au) and silver (Ag) nanoparticles have attracted great attention due to their biocompatibility, non-toxicity and ease of synthesis. A variety of techniques have been reported in the literature for the preparation of metallic nanoparticles[1-3] which includes using reducing agents,[4-5] electrochemical techniques,[6-10] photochemical reduction,[11] irradiation[12-14] and laser ablation [15-16] etc. Amongst all, the chemical reduction method is widely practiced to prepare metal nanoparticles using reducing agents such as, hydrazine hydrate, sodium borohydride etc. However, reducing agents like sodium borohydride and hydrazine hydrate are toxic and pose environmental concern. Therefore, alternate and environmentally friendly reducing agents are continuously under search and nanoparticles preparation by green route is preferred. In this context, polysaccharides have become promising reducing agents in the preparation of metal nanoparticles. For example, Bankura etal.,[17] have reported on the simple one-step synthesis of Ag-NPs using aqueous dextran solution as both reducing and capping agent. El- Rafie etal.,[18] have used a polysaccharide from marine macroalgae. Due to the advantages of polysaccharides such as biocompatibility, non-toxicity, environmental sustainability and low cost, they have attracted major attention as “green” carriers for immobilization of metal nanoparticles. In addition, polysaccharides contain various functionalities which help in more interactions with metal through electrostatic and non-covalent binding (e.g. H-bonding). This also helps in stabilizing the metal nanoparticles.

In this chapter, we report on the synthesis and characterization of hydrogel blend from two polysaccharides namely, Sodium Alginate (SA) and Hydrophobically modified Ethyl Hydroxy Ethyl Cellulose (HM-EHEC) (EHM-200) for making Ag-NPs via green route. Sodium alginate acts as both reducing as well as end-capping agent for Ag-NPs. On the other hand, EHM-200 with long alkyl phenol helps in stabilizing the nanoparticles. EHM-200 also helps in enhancing the swelling of the hydrogel as a result, there can be better diffusion of reactants through the hydrogel. The obtained Ag-NPs in

the hydrogel were characterized by XRD, TEM, UV-Vis etc. Finally, we have demonstrated the use of this Ag-NPs embedded hydrogel blend for the same catalytic reduction reaction of 4-NP to 4-AP.

4.2. Experimental

4.2.1. Materials

Sodium Alginate (SA), EHM-200 was received as a gift sample from Akzo Nobel, Sweden. Calcium chloride used as crosslinker procured from Merck. Silver nitrate ($AgNO_3$) was procured from S. D. Fine Chemicals Ltd. (India).

4.2.2. Synthesis of Ag-NPs embedded beads

4.2.2.1. Synthesis of Sodium alginate (SA) capped Ag-NPs

A 50 ml solution of 0.08 wt% silver nitrate ($AgNO_3$) and 1 wt % SA was prepared by adding 40 mg of $AgNO_3$ and 0.5 g of SA. Whole solution was stirred at room temperature for 4 hours and then kept standing for 2 days. The appearance of a dark brown colour indicated the formation of Ag-NPs (i.e. reduction of Ag^{+1} to Ag^0). Further confirmation was done by UV-Vis spectroscopy.

4.2.2.2. Synthesis of Ag-NPs embedded sodium alginate (SA)/EHM-200 beads [SA/EHM-200 Ag-NPs beads]

To the above prepared SA capped Ag-NPs solution (50 ml), 1 wt% solution (20 ml) of EHM-200 was slowly added and stirred well to make homogenous blend solution. The prepared blend solution was added drop by drop into 150 ml of $CaCl_2$ solution (3 wt %) with the help of syringe to get uniform size beads. The brown colour gel beads were immediately formed and further kept in solution for 30 min. After that, the gel beads were separated from the solution, washed with distilled water twice (100 ml) and dried. Ag-NPs embedded SA beads (SA Ag-NPs beads) were also obtained using same procedure. The schematic representation of the formation of Ag-NPs embedded beads is shown in **Scheme 4.1**.

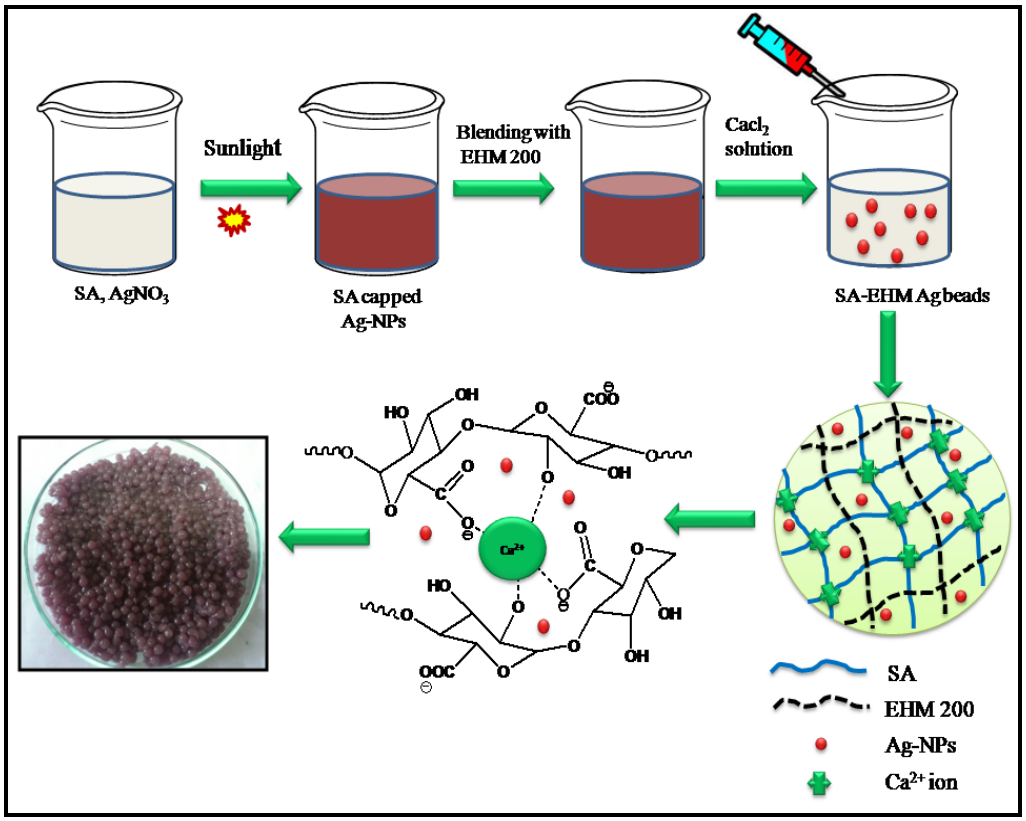

Scheme 4.1: *Schematic representation of formation of Ag-NPs embedded SA/EHM-200 hydrogel beads*

4.3. Characterization

4.3.1. UV-Vis spectroscopy

UV-visible absorption spectra of Ag-NPs were recorded on a SHIMADZU 1610 PC UV-2450 UV-Vis spectrophotometer, Japan in the range 800-200 nm. Samples kept for 24 hrs and 48 hrs were taken for the measurements.

4.3.2. Transmission electron microscopy (TEM)

The morphology of nanoparticles was investigated using a high-resolution transmission electron microscope (HR-TEM) at 300 kV (Cs = 0.6 mm, resolution 1.7Å), Technai- FEI 3010. For TEM measurements, samples were prepared by dropping 5-10 µl SA capped Ag-NPs solution on copper grid. Grid was then allowed to dry in air and stored in desiccators before taking for microscopy.

4.3.3. Scanning electron microscopy (SEM)

The surface morphology of the beads was investigated using a scanning electron microscope (SEM). Quanta 200 3D dual beam ESEM (FEI, Finland). The electron source was a tungsten filament with thermionic emission at a resolution of 3 nm (30 kV) in high vacuum. The beads were mounted on an appropriate stub and then coated with a thin layer of gold by sputtering in a vacuum evaporator in an argon atmosphere. The coated samples were then observed under a scanning electron microscope.

4.3.4. Swelling measurements

Fully dried Ag-NPs embedded beads were accurately weighed and immersed in liquid and kept to reach equilibrium swelling. The swollen beads were then separated, wiped with filter paper and weight was measured. The equilibrium swelling ratio (Q) was calculated according to the following equation 1,

$$Q = \frac{W_s - W_d}{W_d} \times 100 \qquad (1)$$

Where, W_s and W_d are the weights of the dry and the swollen beads samples respectively.

Further, the Q values in 4-NP/$NaBH_4$ which was the reaction medium of catalysis were determined similarly.

4.3.5. Catalytic activity

The catalytic activity of the Ag-NPs embedded beads was evaluated for reduction reaction of 4-nitrophenol (4-NP) to 4-aminophenol (4-AP) by $NaBH_4$ by monitoring the electronic absorption of reaction mixture as a function of time. Detailed procedure is discussed in **Chapter III (3.3.7).**

4.3.6. Reusability of the catalyst

After the first cycle of reaction, the Ag-NPs embedded beads were separated and washed 2-3 times with 50 ml distilled water. The washed beads were dried and subsequently taken for further cycles of reaction.

4.4. Results and Discussion

4.4.1. Synthesis of Ag-NPs

Although the chemical reduction method is widely used method for the preparation of Ag-NPs, the toxicity of reducing agents and their environmental impacts are of great concern. Therefore, the present study was focused on the use of biopolymer, sodium alginate hydrogel as a green and effective reducing agent for the synthesis of Ag-NPs. Silver nitrate was used as a salt precursor and sodium alginate was used as a reducing and capping agent.

Sodium alginate is a naturally occurring poly-anionic polysaccharide derived from brown marine algae and composed of 1, 4-linked beta-D-mannuronic and alpha-L-guluronic residues in varying proportions. It is cheap, biocompatible polysaccharide with numerous applications in biotechnology industry. It has -COOH and -OH functionalities which help to act as both reducing and stabilizing agent. These groups facilitate the formation of complexes with silver ion. Subsequently, these silver ions are reduced to silver nanoparticles (Ag^0). Thus, these oxygen-containing groups on the surface of alginate have a remarkable reducing ability for the in-situ synthesis of metal nanoparticles as shown in **Scheme 4.2.**

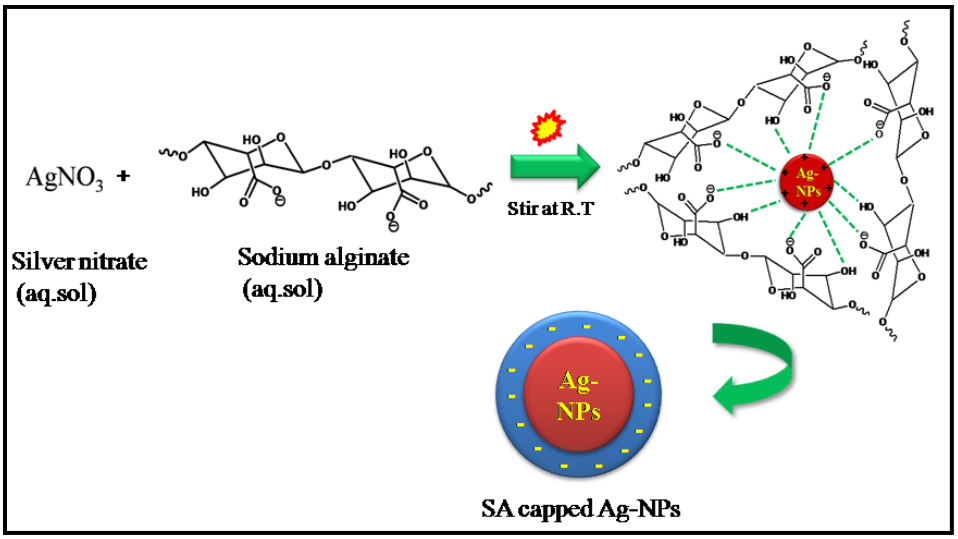

Scheme 4.2: *Schematic representation of formation of SA capped Ag-NPs having interactions with -COOH and -OH groups*

4.4.2. Synthesis of Ag-NPs embedded SA/EHM-200 beads

The alginate is known to form hydrogel beads with divalent cations such as Ca^{2+}, Ba^{2+}, Sr^{2+} etc. This 3D crosslinked network structure occurs via ionic interaction of carboxylic groups of the alginate polymer and divalent cations in the presence of EHM-200, where in this EHM-200 is physically entangled in the 3D structure of SA resulting into Semi-IPN hydrogel beads. These hydrogel beads have been demonstrated as "Green" material for incorporation of nanoparticles. Entrapment of metallic nanoparticles by alginate beads is very safe and simple process obtained by just dropping the SA capped Ag-NPs solution blended with EHM-200 into the crosslinker solution ($CaCl_2$).

4.4.3. UV-Vis spectroscopy

The formation of sodium alginate capped Ag-NPs was confirmed by UV-Vis spectroscopy. **Figure 4.1** shows the distinct absorption peaks of Ag-NPs capped with SA at ≈ 425 nm and there is a complete disappearance of absorption peak of $AgNO_3$ solution at ≈ 300 nm. This clearly indicates the formation of Ag-NPs. The observation of brown color also further confirms the formation of Ag-NPs. It can be seen from **Figure 4.1** that the intensity of absorption peak at 425 nm increased with time with no significant difference in the peak position or shift in SPR (at 425 nm), indicating a continuous reduction of the silver ions.

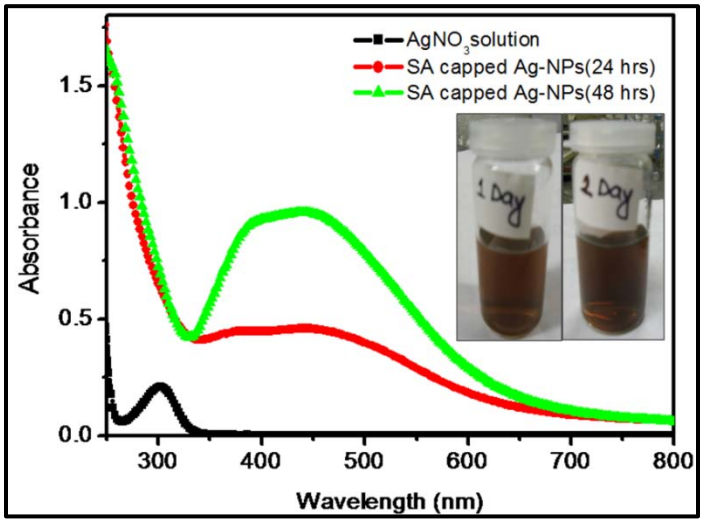

Figure 4.1: *UV-Vis spectra of Ag -NPs capped with SA at different times*

4.4.4. Transmission electron microscopy (TEM)

Figure 4.2 shows the TEM images of as synthesized SA Ag-NPs. It can be readily seen that the nanoparticles are more or less spherical in shape with sizes in the range of 15-30 nm. The selective area electron diffraction (SAED) pattern of Ag-NPs is clearly observed as diffraction ring, which is attributed to the face-centered cubic (fcc) structure of Ag-NPs shown in **Figure 4.2 (b)**

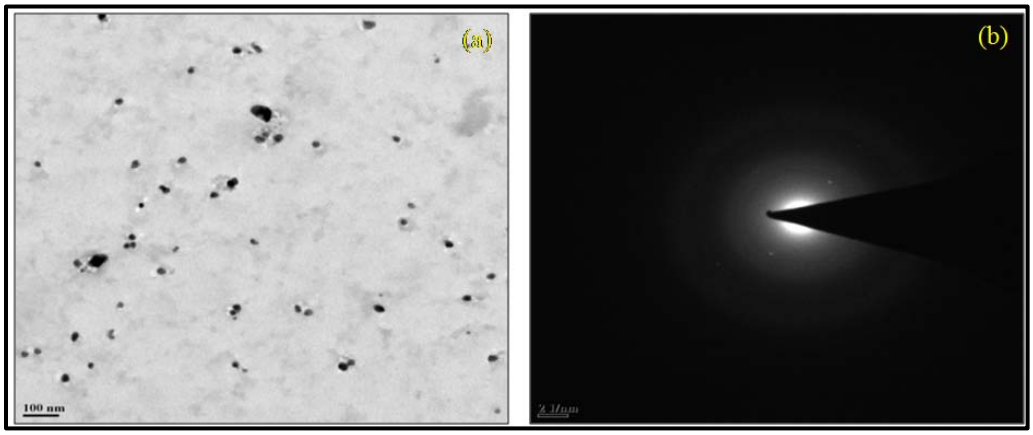

Figure 4.2*: TEM images of a) SA Ag-NPs b) SAED pattern of Ag-NPs*

4.4.5. Scanning electron microscopy (SEM)

The morphology of SA Ag-NPs and SA/EHM-200 Ag-NPs beads was studied by SEM. The results are shown in **Figure 4.3**. From the SEM images, it is observed that the beads in both the cases are more or less spherical in nature.

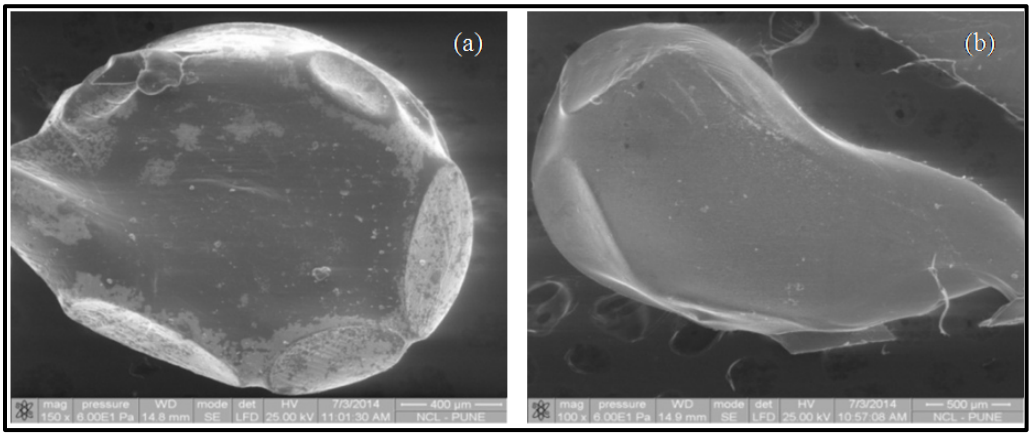

Figure 4.3: *SEM images of a) SA Ag-NPs beads, b) SA/EHM-200 Ag-NPs beads*

4.4.6. Swelling measurements

Figure 4.4 shows the equilibrium swelling ratios of SA Ag-NPs beads and SA/EHM-200 Ag-NPs beads in water as well as in 4-NP/$NaBH_4$ solution (basic). It is observed that SA Ag-NPs beads swell least in water and 4-NP/$NaBH_4$ solution. However, in the case of SA/EHM-200 Ag-NPs beads equilibrium swelling ratio (Q) increased in both water as well as in 4-NP/$NaBH_4$. The Q value increased significantly in 4-NP/$NaBH_4$ solution. This could be attributed to the fact that EHM-200 is a hydrophobically modified polymer with long alkyl phenol chains. In the basic solution, these phenolic -OH groups ionize and hydrogel become more ionic in nature which results in the enhanced swelling.

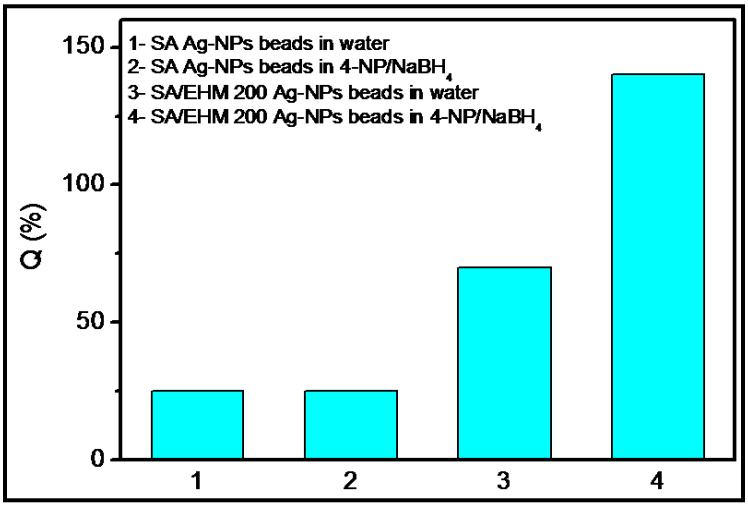

Figure 4.4: *Swelling studies of SA Ag-NPs and SA/EHM-200 Ag-NPs beads in water and 4-NP/$NaBH_4$ solution*

4.4.7. Catalytic activity of Ag-NPs beads

The catalytic efficiency of Ag-NPs beads was evaluated for a model reduction reaction of 4-nitrophenol (4-NP) to 4-aminophenol (4-AP). Although the reduction of 4-NP to 4-AP is thermodynamically favorable but the reaction proceeded very slowly in the absence of catalyst. Normally, 4-NP exhibit strong absorption peak @317 nm, which has a red shift to 400 nm after the addition of $NaBH_4$ due to formation of intermediate 4-nitrophenolate ion discussed in **Chapter III**, **3.4.8. Section** and shown in **Figure 3.9 (a)**. The reduction of 4-NP to 4-AP can be performed with only $NaBH_4$. However, the

reaction is very slow and show only 5% conversion after 6-8 hrs. In the presence of Ag catalyst, the reaction goes very fast with 90% conversion in 8-9 minutes. This is demonstrated below.

Upon addition of SA/EHM-200 Ag-NPs beads to the reaction medium, there was a gradual decrease in the intensity of absorption peak at 400 nm with time and simultaneously, there was an appearance of new absorption peak at 298 nm indicating the reduction of 4-NP and the formation of 4-AP as shown in **Figure 4.5 (a).** The completion of reaction with SA/EHM-200 Ag-NPs beads, which happened in ≈ 8-9 minutes, was indicated by the slow fading of yellow colour of the reaction mixture**.**

We also show that just by the addition of SA Ag-NPs beads to reaction medium did not reduce 4-NP to 4-AP even in 60 minutes [**See Figure 4.5 (b)].** This could be attributed to the fact that SA/EHM-200 Ag-NPs beads have more swelling ratio compare to plain SA Ag-NPs beads and this enhanced swelling helps in easy diffusion of reactants resulting into more products.

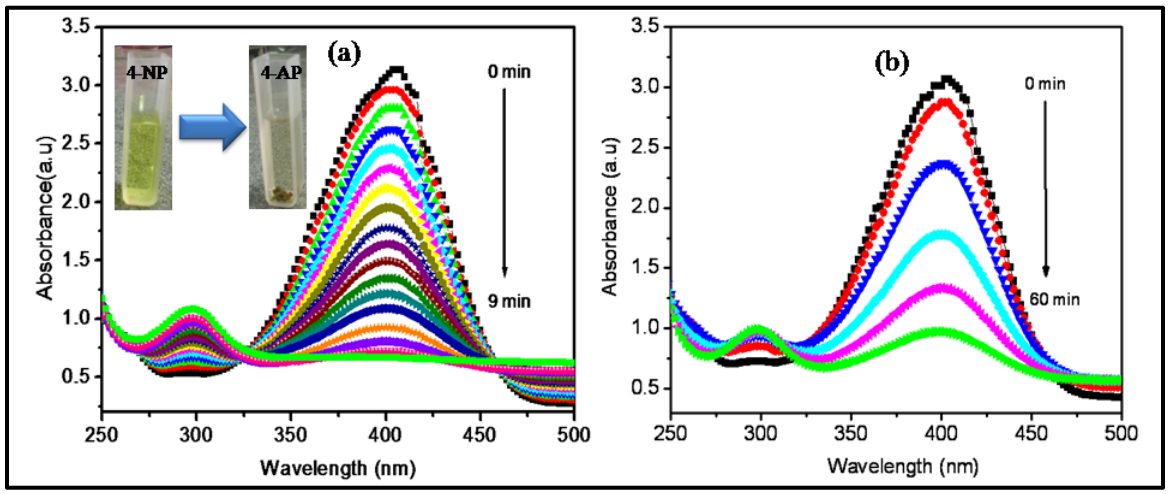

Figure 4.5: *Catalytic effect of (a) SA/EHM-200 Ag-NPs beads (b) SA Ag-NPs beads on reduction of 4-NP to 4-AP*

Due to the large excess of $NaBH_4$ in the reaction medium, the reduction reaction can be regarded as a pseudo-first-order reaction based on the evaluation of the rate constant with regard to 4-NP. Therefore, the reaction kinetics can be described as,

$$ln\,(C/C_0) = -kt \qquad (1)$$

Where 'k' is the first order rate constant (since the concentration of $NaBH_4$ is in large excess), 't' is the reaction time, 'C' and 'C_0' are the concentration of 4-NP at time 't' and '0' respectively.

Figure 4.6 (a) shows the linear plot between ln (C/C_0) and reaction time 't' for the reduction of 4-NP to 4-AP using SA/EHM-200 Ag-NPs beads. It can be readily seen from the figure that the reaction follows pseudo first order reaction kinetics with the rate constant obtained from the slope of liner plot which was found to be 0.204 min^{-1}. The correlation coefficient of the linear plot was very good with the value =0.997.

We have also compared the catalytic activity of reaction with only $NaBH_4$, with the SA/EHM-200 Ag-NPs beads for cycle 0, 1, 2 and with the SA Ag-NPs beads which can be shown in **Figure 4.6 (b).**

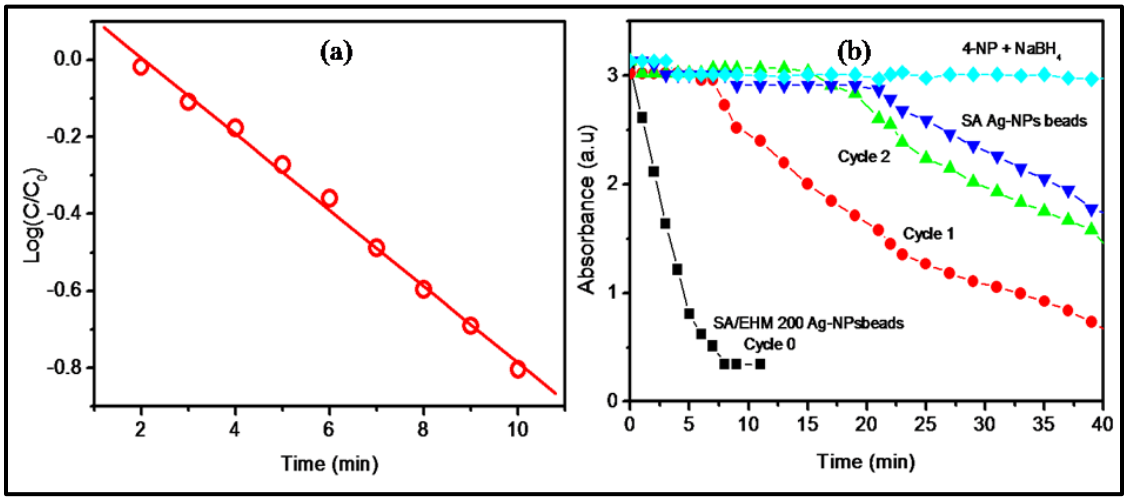

Figure 4.6: (a) *Linear plot between ln (C/C_0) and reaction time't' for the reduction of 4-NP to 4-AP using SA/EHM-200 Ag-NPs beads (b) comparsion of the catalytic acitivity with only $NaBH_4$, SA Ag-NPs beads, SA/EHM-200 Ag-NPs beads*

4.4.8. Catalyst recycling

Stability and recyclability is of great importance for the practical applications of catalysts. After completion of the first run of reaction, we also explored the repeated use

of the same catalyst in successive multiple reaction runs. The SA/EHM-200 Ag-NPs beads could be easily separated from each cycle and washed with Milli Q water and dried under vacuum before taking it for the next reaction. We have observed that beads can be recycled for atleast two times as shown in **Figure 4.6 (b).** However, the second and third cycle required 43, 80 minutes respectively for complete conversion which may be attributed to adsorption of reactants and products on Ag-NPs surface which block active sites for catalysis. The mechanism of catalytic reduction of 4-NP by Ag-NPs is already discussed in the previous chapter. The reduction in the catalytic activity may be attributed to the surface adsorption of catalyst which can hinder the catalyst sites.

4.5. Conclusions

In summary, we report on the environmentally friendly route for the synthesis of Ag-NPs incorporated in Sodium alginate (SA) and hydrophobically modified ethyl hydroxy ethyl cellulose (EHM-200) hydrogel beads and used them for the catalytic reduction reaction of 4-NP to 4-AP. Sodium alginate could act as both reducing agent and capping agent for Ag-NPs. The formation of Ag-NPs in the hydrogel beads was confirmed by UV-Vis spectroscopy, and TEM. In the absence of Ag-NPs and with only $NaBH_4$, the reduction reaction of 4-NP to 4-AP was very slow and the conversion was very low. However, in the presence of SA/EHM-200 Ag-NPs beads as catalyst, the reaction rate was faster with high conversion upto $\approx$ 90 %. The isolation of catalyst after the reaction was quite easy and the catalyst could be reused for 2-3 cycles.

4.6. References

1. Rycenga, M.; Cobley, C. M.; Zeng, J.; Li, W.; Moran, C. H.; Zhang, Q.; Qin, D.; Xia, Y., Controlling the synthesis and assembly of silver nanostructures for plasmonic applications. *Chemical Reviews* **2011,** 111, (6), 3669-3712.
2. Sun, Y., Controlled synthesis of colloidal silver nanoparticles in organic solutions: empirical rules for nucleation engineering. *Chemical Society Reviews* **2013,** 42, (7), 2497-2511.
3. Sakamoto, M.; Fujistuka, M.; Majima, T., Light as a construction tool of metal nanoparticles: synthesis and mechanism. *Journal of Photochemistry and Photobiology C: Photochemistry Reviews* **2009,** 10, (1), 33-56.
4. Yu, D.-G., Formation of colloidal silver nanoparticles stabilized by Na+–poly (γ-glutamic acid)–silver nitrate complex via chemical reduction process. *Colloids and Surfaces B: Biointerfaces* **2007,** 59, (2), 171-178.
5. Šileikaitė, A.; Prosyčevas, I.; Puišo, J.; Juraitis, A.; Guobienė, A., Analysis of silver nanoparticles produced by chemical reduction of silver salt solution. *Mater. Sci.-Medzg* **2006,** 12, 287-291.
6. Liu, Y.-C.; Lin, L.-H., New pathway for the synthesis of ultrafine silver nanoparticles from bulk silver substrates in aqueous solutions by sonoelectrochemical methods. *Electrochemistry communications* **2004,** 6, (11), 1163-1168.
7. Khaydarov, R. A.; Khaydarov, R. R.; Gapurova, O.; Estrin, Y.; Scheper, T., Electrochemical method for the synthesis of silver nanoparticles. *Journal of Nanoparticle Research* **2009,** 11, (5), 1193-1200.
8. Rodriguez-Sanchez, L.; Blanco, M.; Lopez-Quintela, M., Electrochemical synthesis of silver nanoparticles. *The Journal of Physical Chemistry B* **2000,** 104, (41), 9683-9688.
9. Ma, H.; Yin, B.; Wang, S.; Jiao, Y.; Pan, W.; Huang, S.; Chen, S.; Meng, F., Synthesis of silver and gold nanoparticles by a novel electrochemical method. *ChemPhysChem* **2004,** 5, (1), 68-75.
10. Starowicz, M.; Stypuła, B.; Banaś, J., Electrochemical synthesis of silver nanoparticles. *Electrochemistry communications* **2006,** 8, (2), 227-230.

11. Henglein, A., Colloidal silver nanoparticles: photochemical preparation and interaction with O_2, CCl_4, and some metal ions. *Chemistry of Materials* **1998,** 10, (1), 444-450.
12. Chen, P.; Song, L.; Liu, Y.; Fang, Y.-e., Synthesis of silver nanoparticles by γ-ray irradiation in acetic water solution containing chitosan. *Radiation Physics and Chemistry* **2007,** 76, (7), 1165-1168.
13. Mostafavi, M.; Dey, G.; Francois, L.; Belloni, J., Transient and stable silver clusters induced by radiolysis in methanol. *The Journal of Physical Chemistry A* **2002,** 106, (43), 10184-10194.
14. Remita, H.; Lampre, I.; Mostafavi, M.; Balanzat, E.; Bouffard, S., Comparative study of metal clusters induced in aqueous solutions by γ-rays, electron or C 6+ ion beam irradiation. *Radiation Physics and Chemistry* **2005,** 72, (5), 575-586.
15. Amendola, V.; Meneghetti, M., Laser ablation synthesis in solution and size manipulation of noble metal nanoparticles. *Physical Chemistry Chemical Physics* **2009,** 11, (20), 3805-3821.
16. Murray, P.; Shin, E., Formation of silver nanoparticles by through thin film ablation. *Materials Letters* **2008,** 62, (28), 4336-4338.
17. Bankura, K.; Maity, D.; Mollick, M. M.; Mondal, D.; Bhowmick, B.; Bain, M.; Chakraborty, A.; Sarkar, J.; Acharya, K.; Chattopadhyay, D., Synthesis, characterization and antimicrobial activity of dextran stabilized silver nanoparticles in aqueous medium. *Carbohydrate Polymers* **2012,** 89, (4), 1159-1165.
18. El-Rafie, H.; El-Rafie, M.; Zahran, M., Green synthesis of silver nanoparticles using polysaccharides extracted from marine macro algae. *Carbohydrate Polymers* **2013,** 96, (2), 403-410.

Electrospun Ag-NPs embedded Poly(vinyl alcohol)/Poly(aspartic acid) nanofibers used as mercury sensor

---

Chapter – V

In the fifth chapter, we have worked on incorporating Ag-NPs into Poly(vinyl alcohol)/Poly(aspartic acid) (PVA/PAS) nanofibers and studied their applications in detecting toxic metal namely mercury (Hg). Ag-NPs were synthesized by green route in the PVA/PAS nanofibers and their formation is confirmed by UV and TEM analysis. Low-cost, linear response, easy synthesis are some of the prominent features of these nanofibers as sensors.

5.1. Introduction

Homogeneous distribution of nanoparticles in a polymer matrix is still considered as an important challenge in material science today, especially at a low volume fraction.[1] Amongst the nanoparticles, silver nanoparticles (Ag-NPs) have become important and applied in many hygienic and medical fields.[2-3] Their predominant antimicrobial activity can be attributed to a strong interaction with bacterial cells,[4] but relatively low toxicity to human cells.[5] Nevertheless, such dispersed metallic nanoparticles often tend to con-gregate and become unstable, and lose their desired properties. Moreover, the size and size distribution are two crucial factors for Ag-NPs induced toxicity and biological responses.[6-7] Thus, many efforts are being made to design and synthesize stable Ag-NPs of a smaller size.

Besides these applications, Ag-NPs are now attracting increasing attention in the area of sensors also. They can be used as selective chemosensors for heavy metal ions which have toxic issues in the environment.[8-9]Amongst them, mercury (Hg) is considered as one of the most toxic metal for environment. Therefore, environmental monitoring of mercury becomes very important. Currently, methods of detecting mercury such as colorimetric methods[10-12] atomic absorption spectrometry[13-14] inductively coupled plasma mass spectrometry[15], mercury sensors with gold nanorods,[16] and gold nanoparticles[17] have been reported. Although these methods have good sensitivity and selectivity, they are costly and time consuming. Therefore, it has become necessary to develop a simple and rapid method to detect Hg. Ag-NPs have been used for colorimetric sensors for Hg where in, silver forms amalgam with Hg and influence the surface plasmon resonance extinction of Ag-NPs.

Since, these NPs are susceptible to oxidation and degradation, embedding nanoparticles in the polymer matrix can resolve these problems to a great extent.[18-19] Further, packing of these sensors in general is cumbersome. Therefore, incorporation of Ag-NPs into electrospun fibers is gaining interest and the electrospinning is a simple approach to prepare polymer nanofibers embedded with Ag-NPs having high porosity and large specific surface area.

The electrospinning technique has been widely used in filtration membranes, catalysis reaction, protective clothing, molecular templates, tissue scaffolds, wound dressings and this procedure is easy-to-handle and cost-effective to fabricate man-made fibers with Ag-NPs.

In this chapter, we have worked on incorporating Ag-NPs into Poly(vinyl alcohol)/Poly(aspartic acid) (PVA/PAS) nanofibers and studied their applications in detecting toxic metal, mercury (Hg).

5.2. Experimental

5.2.1. Materials

PVA (99% hydrolyzed, Mw = 1,15000) was procured from Loba chemicals. Poly(aspartic acid) (PAS) was synthesized in the laboratory. Silver nitrate ($AgNO_3$) was procured from S. D. Fine Chemicals Ltd. (India).

5.2.2. Synthesis Ag-NPs embedded nanofibers

5.2.2.1. Synthesis of PAS capped Ag-NPs

PAS capped Ag-NPs were synthesized by dissolving PAS in aqueous $AgNO_3$ solution (3 mM and 5mM) with polymer concentration 0.5 wt %. The solution was stirred at 80°C for 8 hr. The change in colour of solution to yellow/dark brown indicates the formations of Ag-NPs which were analyzed by UV- Vis spectroscopy.

5.2.2.2. Synthesis of Ag-NPs embedded PVA/PAS electrospun nanofibers

To the above Ag-NPs solution, PVA was added and dissolved to make 10 wt% solution and fibers were formed by electrospinning using the conditions, 0.5 ml/hr flow rate, 25 KV voltage and 15 cm distance between the nozzle and collector. These nanofibers were later crosslinked by glutaraldehyde vapours for different times (24, 48 h).

5.3. Characterization

5.3.1. UV-Vis spectroscopy

UV-visible absorption spectra of Ag-NPs were recorded on a SHIMADZU 1610 PC UV-2450 UV-Vis spectrophotometer, Japan in the range of 800-200 nm. A solution of PAS capped Ag-NPs were taken for measurements.

5.3.2. X-ray diffraction (XRD)

Ag-NPs were characterized by X-ray diffraction using Philips X'pert pro powder X-ray diffractometer operating with CuKά radiation

5.3.3. Transmission electron microscopy (TEM)

The morphology of nanoparticles in the solution as well as in nanofibers were investigated using a high-resolution transmission electron microscope (HR-TEM) at 300 kV (Cs = 0.6 mm, resolution 1.7Å), Technai- FEI 3010. For TEM measurements, samples were prepared by dropping 5-10 µl PAS capped Ag-NPs solution on copper grid and then allowed to dry in air and stored in desiccators before taking for microscopy. Ag-NPs embedded nanofibers were directly electrospun on TEM grid for measurements.

5.3.4. FT-IR spectroscopy

The FT-IR spectra of all the nanofiber samples were recorded on a FT-IR spectrum Perkin Elmer Spectrometer, UK in a diffused reflectance mode between 400 to 4000 cm^{-1}.

5.3.5. Scanning electron microscopy (SEM)

The surface morphology of nanofibers was investigated using a scanning electron microscope (SEM), a Quanta 200 3D dual beam ESEM (FEI, Finland). The electron source was a tungsten filament with thermionic emission at a resolution of 3 nm (30 kV) in high vacuum. The nanofibers were mounted on an appropriate stub and then coated with a thin layer of gold by sputtering in a vacuum evaporator in an argon atmosphere. The coated samples were then observed under a scanning electron microscope.

5.3.6. General procedure for the colorimetric determination of Hg

For colorimetric detection of mercury ion, 4-5 mg of Ag-NPs embedded crosslinked nanofibers were taken in 2 ml of DI-water. The Ag-NPs were leached out and solution becomes orange in color. 10 ppm solution of Hg^{2+} was added subsequently into

Ag-NPs solution. The assays and the changes in the UV-Vis absorption spectra were performed and monitored at room temperature. The photographs were taken with a digital camera after 2 min of mixing.

5.4. Results and Discussion

5.4.1. Synthesis of Ag-NPs embedded PVA/PAS nanofibers

The formation of Ag-NPs in the PAS solution was easily confirmed by the color change to yellowish brown, and the strong surface plasmon resonance (SPR) peak in the range of 425 nm. It is now established that PAS acts as reducing agent to form Ag-NPs. When $AgNO_3$ was mixed with PAS solution, Ag^+ ions could bind to PAS chains via electrostatic interactions, forming PAS-Ag^+ complex. Under certain conditions (heating, irradiation), reduction from Ag^+ to Ag^0 could take place. PVA acts as a supporting template for polymer nanofibers-Ag-NPs composites. Further, PVA has good fiber forming property and stabilize the PAS capped Ag-NPs in the nanofibers to prevent from aggregation and oxidation. These Ag-NPs embedded nanofibers were found to be stable for several months. The process of making Ag-NPs in PAS and subsequent electrospinning with PVA is shown in **Scheme 5.1.** The obtained nanofibers were later crosslinked by glutaraldehyde vapours for 24 and 48 hrs.

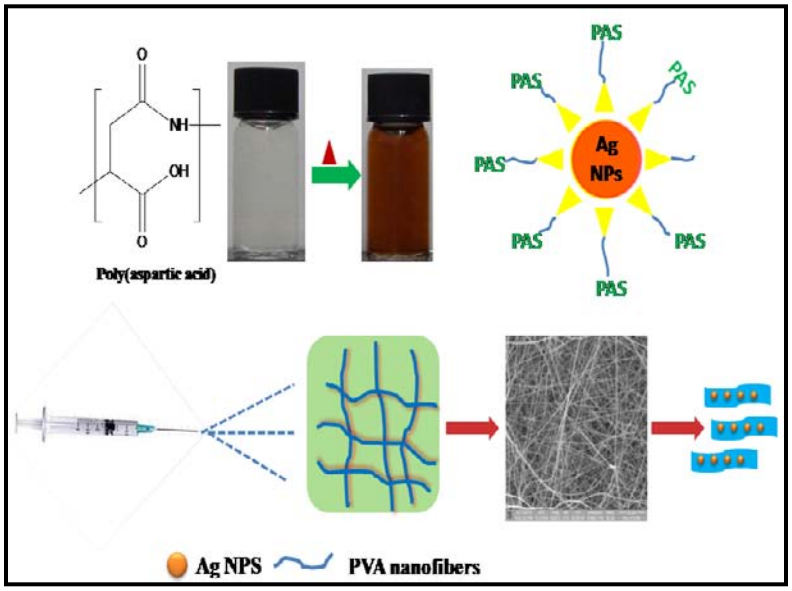

Scheme 5.1: *Formation of Ag-NPs in PAS and subsequent Electrospinning with PVA*

5.4.2. UV-Vis spectroscopy

We have shown in **Figure 5.1** the distinct absorption peaks of Ag-NPs at 415 nm due to the characteristics Surface Plasmon Resonance effect in UV spectroscopy. As silver nitrate concentration increases, number of nanoparticles also increase which can be seen in the intensity of the peak.

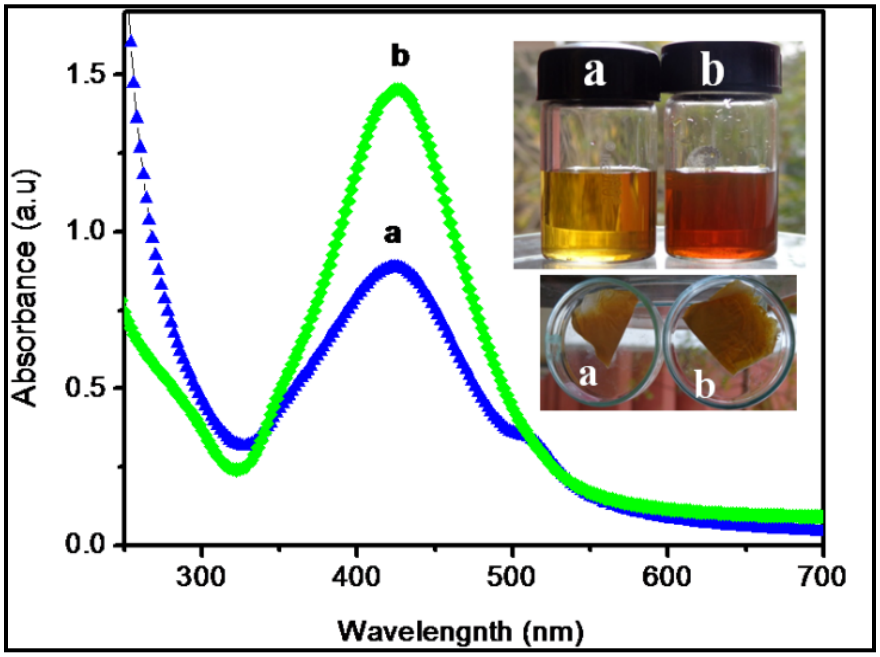

Figure 5.1: *UV spectra of PAS capped Ag-NPs with two different concentration of $AgNO_3$ (a) 3mM $AgNO_3$ (b) 5 mM $AgNO_3$*

5.4.3. X-ray diffraction (XRD)

Figure 5.2 shows X-ray diffraction pattern of plain PVA/PAS nanofibers and Ag-NPs embedded nanofibers. Ag-NPs embedded nanofibers exhibit the presence of reflection peaks typical of a face centered cubic (fcc) structure of silver nanoparticles, with 2θ values of about 38.4° and 46.5° assigned to the lattice planes of face centered cubic (fcc) structure of silver.

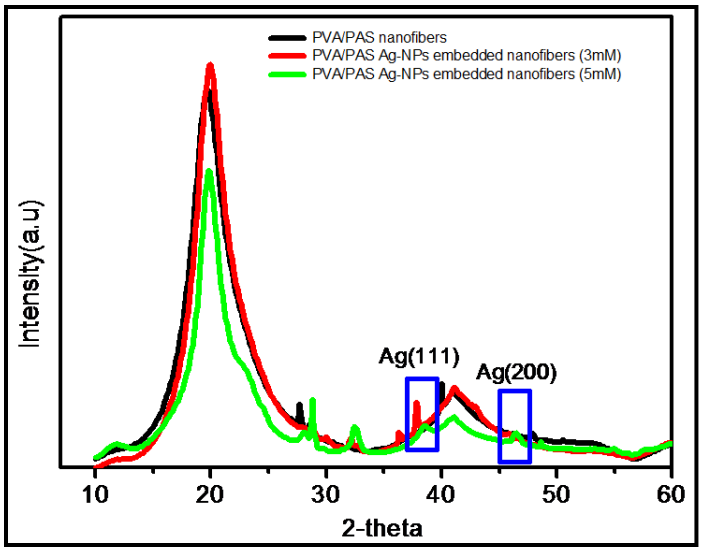

Figure 5.2: *XRD patterns of plain PVA/PAS and Ag-NPs embedded PVA/PAS nanofibers*

5.4.4. Transmission electron microscopy (TEM)

To further confirm the formation of Ag-NPs in PAS solution as well as trapped nanoparticles into nanofibers, TEM was performed on the samples and the results are shown in **Figure 5.3.** It can be readily seen that the nanoparticles are more or less spherical in shape with sizes in the range of 10-35 nm. Higher density of Ag-NPs was observed in sample with higher concentration of $AgNO_3$ (5 mM) **(see Figure 5.3 b).** We have also shown the Ag-NPs into the nanofibers **(see Figure 5.3 a-1, b-1)**. The Ag-NPs were located preferentially on the edges of nanofibers. Thus, it can be confirmed that Ag-NPs were trapped in nanofibers which prevent them from agglomerization and found to be stable for several months in dry state.

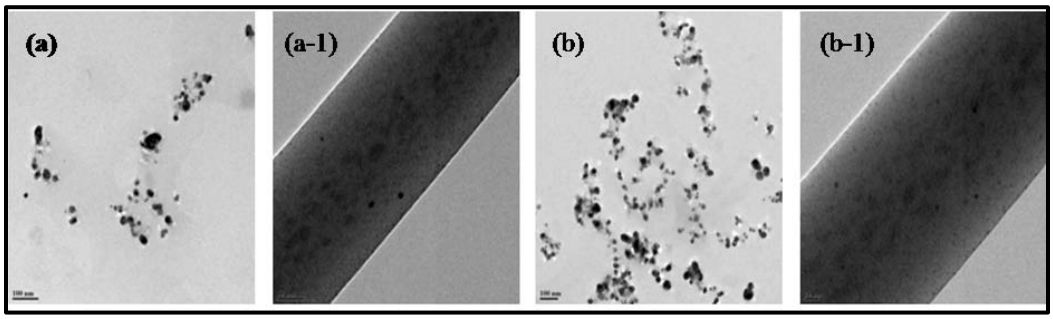

Figure 5.3: *TEM of Ag-NPs in PAS solution as well as in the nanofibers containing different concentration of $AgNO_3$, (a, a-1) 3mM, (b, b-1) 5mM respectively*

5.4.5. FT-IR spectroscopy

The Ag-NPs embedded PVA/PAS nanofibers were crosslinked using glutaraldehyde vapours. To confirm the crosslinking of Ag-NPs embedded PVA/PAS nanofibers by glutaraldehyde, the IR spectra were recorded for the samples.

We show in **Figure 5.4**, the IR spectra of neat Ag-NPs embedded nanofibers and crosslinked nanofibers by reacting with glutaraldehyde vapours for 24 hrs and 48 hrs. It is seen from the figure that the -OH stretching vibration band at 3340 cm^{-1} is observed in all spectra of samples. However, the intensity of the -OH peak decreased as the crosslinking with glutaraldehyde increased. This indicate that, -OH group are involved in the crosslinking to form acetal bridges. The two vibrational bands observed between 2943 and 2907 cm^{-1} refer to the stretching vibration of C-H from alkyl and O=C-H from the aldehyde and the bands between 1700-1720 cm^{-1} are due to the -C=O stretching of the unreacted end of the aldehyde in the vapor crosslinked PVA. The band observed at 1093 cm^{-1} with gradual broadening of the peak width w.r.t increase in crosslinking is attributed to O-C-O vibration of the acetal group.

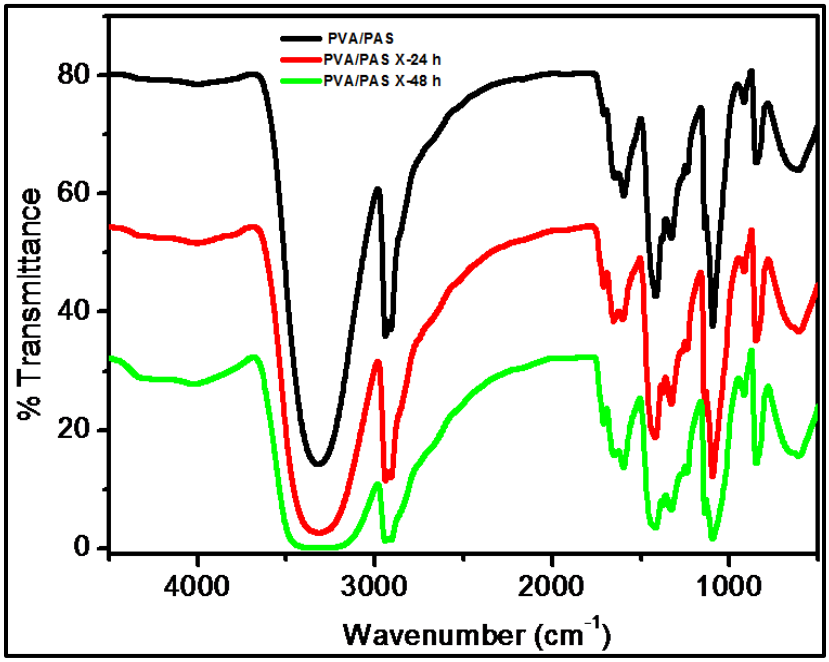

Figure 5.4: *FT-IR spectra of neat Ag-NPs embedded PVA/PAS and glutaraldehyde vapours crosslinked nanofibers*

5.4.6. Scanning electron microscopy (SEM)

The morphology of PVA/PAS nanofibers with 3mM and 5mM $AgNO_3$ was studied by SEM and micrographs are shown in **Figure 5.5**. The average diameter of Ag-NPs embedded PVA/PAS nanofibers with 3mM and 5mM $AgNO_3$ were 283 ± 25 nm, 195 ± 22 nm respectively. The diameters of nanofibers slightly decreased with the increasing concentration of $AgNO_3$. This might be because of the influence of $AgNO_3$ concentration on the viscosity and conductivity of the electrospinning solutions. It is obvious that the viscosity and conductivity will increase with the increase of $AgNO_3$. The increase of Ag^+ concentration evidently induced the increase in conductivity. In addition, the interaction between PAS and Ag^+/Ag-NPs lead to chelation which may induce an increase in viscosity. The morphology of nanofibers was affected by the viscosity and conductivity of solution mixture which resulted into decrease in diameter of nanofibers with increase in concentration of $AgNO_3$.

To confirm the formation of Ag-NPs, the nanofibers with Ag-NPs were analyzed by energy dispersive X-ray analysis (EDAX) shown in **Figure 5.5 a-1 and b-1.** Metallic silver nanocrystals generally show typical optical absorption peak approximately at 3 keV due to Surface Plasmon Resonance. We could see a signal in the Ag region confirming the presence of Ag-NPs in the nanofibers.

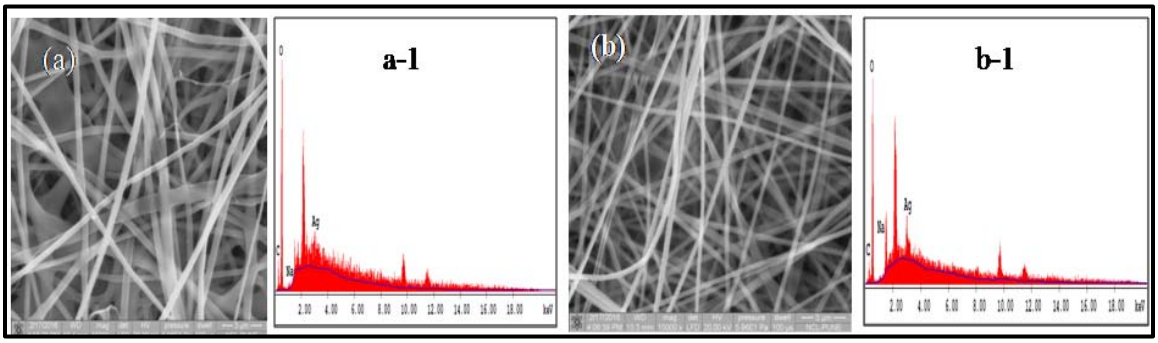

Figure 5.5: *SEM and EDAX images of PVA/PAS nanofibers containing different content of $AgNO_3$ (a, a-1) 3mM, (b, b-1) 5mM respectively*

5.4.7. Hg metal sensing experiments

The response in optical properties of the Ag-NPs embedded PVA/PAS nanofibers to mercury metal ions was investigated as shown in **Figure 5.6.**

Interestingly, the addition of Hg^{2+} solution into Ag-NPs decolorized the solution from dark orange and demonstrated the sensing of Hg^{2+} ions. Initial addition of Hg^{2+} ions (50 µl of 10 ppm solution) slightly blue shifted λ_{max} with reduction of absorption intensity during subsequent additions (100, 150, 200, 250 µl of 10 ppm solution). The clear decay and blue shift of absorption peak were completely disappeared after adding 10 µl of 500 ppm Hg^{2+} solution as shown in **Figure 5.6 (b).**

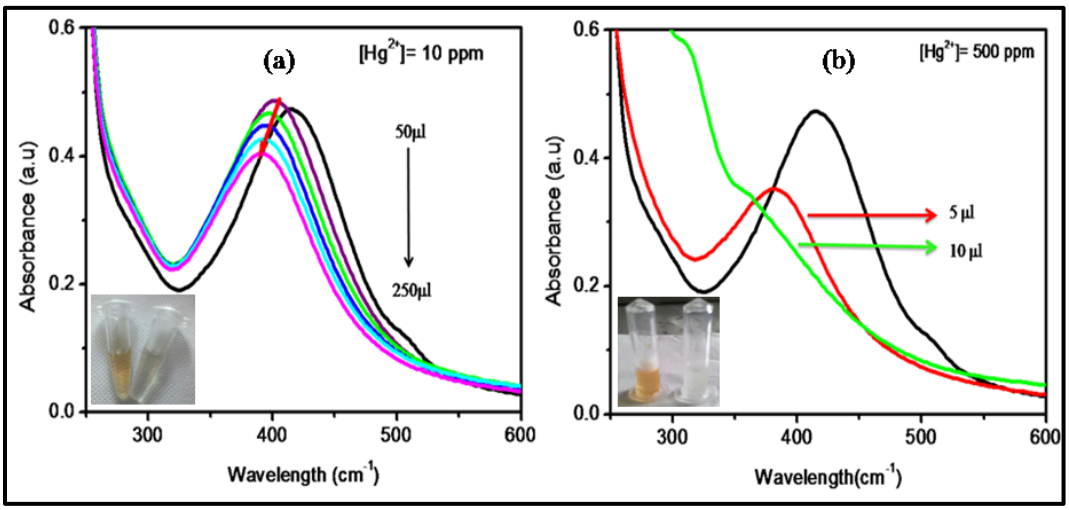

Figure 5.6: *Variation of the SPR spectra of Ag-PVA/PAS nanofibers in different concentrations of* Hg^{2+}

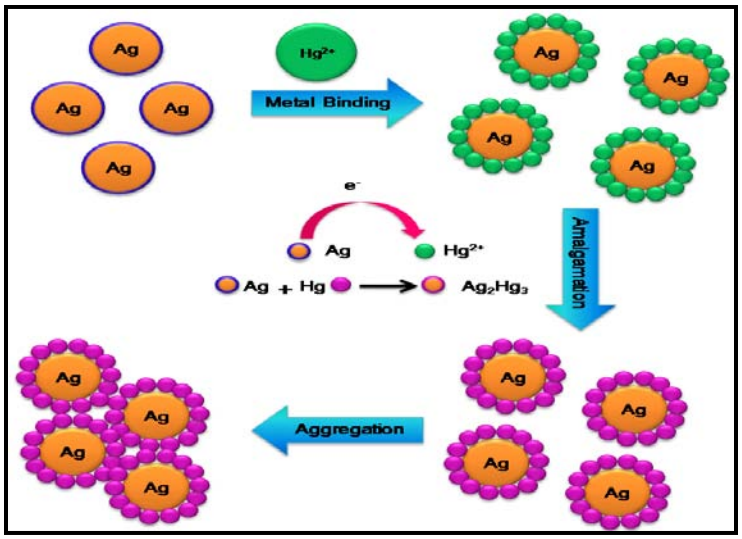

Figure 5.7: *Schematic representation of mechanism* Hg^{2+} *sensing by Ag-NPs embedded PVA/PAS nanofibers*

The mechanism of Hg^{2+} sensing could be explained based on the electrochemical differences of Ag^{+} and Hg^{2+} ions. The standard reduction potential for Ag is +0.80V whereas for Hg^{2+} it is +0.92 V and according to the electrochemical series, metals with a higher reduction potential act as better oxidizing agents. Hg^{2+} reduces to Hg^{0} and deposits on Ag-NPs surface to form silver- amalgam complex. Because of this complex formation, aggregation in Ag-NPs occur leading to a color change from dark orange to colourless which causes blue shift in UV-absorption as shown in **Figure 5.6**. The mechanism Hg^{2+} sensing is shown in **Figure 5.7.**

5.5. Conclusions

In summary, we have reported on the synthesis of Ag-NPs embedded PVA/PAS nanofibers which could sense Hg^{2+} metal ions in solution. Ag-NPs were synthesized by green route and the formation of nanoparticles confirmed by UV-Vis and TEM. PVA/PAS nanofibers were used to stabilize Ag-NPs and prevent them from degradation and oxidation. Characteristic blue shift of the SPR spectrum upon interaction with mercury was observed. Low-cost, linear response, easy synthesis are the main features of these nanofibers as sensor.

5.6. References

1. Wan, Y.; Guo, Z.; Jiang, X.; Fang, K.; Lu, X.; Zhang, Y.; Gu, N., Quasi-spherical silver nanoparticles: Aqueous synthesis and size control by the seed-mediated Lee–Meisel method. *Journal of colloid and interface science* **2013,** 394, 263-268.
2. Sun, Y.; Gates, B.; Mayers, B.; Xia, Y., Crystalline silver nanowires by soft solution processing. *Nano Letters* **2002,** 2, (2), 165-168.
3. Chen, S.-C.; Zhang, Z.-H.; Chen, Q.; Wang, L.-Q.; Xu, J.; He, M.-Y.; Du, M.; Yang, X.-P.; Jones, R. A., An efficient strategy to achieve hydrophilic polymeric silver (I) materials with exceptional antibacterial activity. *Chemical Communications* **2013,** 49, (13), 1270-1272.
4. Ray, S.; Mohan, R.; Singh, J. K.; Samantaray, M. K.; Shaikh, M. M.; Panda, D.; Ghosh, P., Anticancer and antimicrobial metallopharmaceutical agents based on palladium, gold, and silver N-heterocyclic carbene complexes. *Journal of the American Chemical Society* **2007,** 129, (48), 15042-15053.
5. Clement, J. L.; Jarrett, P. S., Antibacterial silver. *Met Based Drugs* **1994,** 1, (5-6), 467-482.
6. Nel, A.; Xia, T.; Mädler, L.; Li, N., Toxic potential of materials at the nanolevel. *Science* **2006,** 311, (5761), 622-627.
7. Marambio-Jones, C.; Hoek, E. M., A review of the antibacterial effects of silver nanomaterials and potential implications for human health and the environment. *Journal of Nanoparticle Research* **2010,** 12, (5), 1531-1551.
8. Tchounwou, P. B.; Ayensu, W. K.; Ninashvili, N.; Sutton, D., Review: Environmental exposure to mercury and its toxicopathologic implications for public health. *Environmental Toxicology* **2003,** 18, (3), 149-175.
9. De Silva, A. P.; Gunaratne, H. N.; Gunnlaugsson, T.; Huxley, A. J.; McCoy, C. P.; Rademacher, J. T.; Rice, T. E., Signaling recognition events with fluorescent sensors and switches. *Chemical Reviews* **1997,** 97, (5), 1515-1566.
10. Lee, J.-S.; Mirkin, C. A., Chip-based scanometric detection of mercuric ion using DNA-functionalized gold nanoparticles. *Analytical chemistry* **2008,** 80, (17), 6805-6808.

11. Xu, X.; Wang, J.; Jiao, K.; Yang, X., Colorimetric detection of mercury ion (Hg 2+) based on DNA oligonucleotides and unmodified gold nanoparticles sensing system with a tunable detection range. *Biosensors and Bioelectronics* **2009,** 24, (10), 3153-3158.
12. Li, D.; Wieckowska, A.; Willner, I., Optical analysis of Hg2+ ions by oligonucleotide–gold-nanoparticle hybrids and DNA-based machines. *Angewandte Chemie* **2008,** 120, (21), 3991-3995.
13. Kim, I.-B.; Bunz, U. H., Modulating the sensory response of a conjugated polymer by proteins: an agglutination assay for mercury ions in water. *Journal of the American Chemical Society* **2006,** 128, (9), 2818-2819.
14. Leermakers, M.; Baeyens, W.; Quevauviller, P.; Horvat, M., Mercury in environmental samples: speciation, artifacts and validation. *TrAC Trends in Analytical Chemistry* **2005,** 24, (5), 383-393.
15. Ugo, P.; Zampieri, S.; Moretto, L. M.; Paolucci, D., Determination of mercury in process and lagoon waters by inductively coupled plasma-mass spectrometric analysis after electrochemical preconcentration: comparison with anodic stripping at gold and polymer coated electrodes. *Analytica chimica acta* **2001,** 434, (2), 291-300.
16. Rex, M.; Hernandez, F. E.; Campiglia, A. D., Pushing the limits of mercury sensors with gold nanorods. *Analytical chemistry* **2006,** 78, (2), 445-451.
17. Lin, C.-Y.; Yu, C.-J.; Lin, Y.-H.; Tseng, W.-L., Colorimetric sensing of silver (I) and mercury (II) ions based on an assembly of Tween 20-stabilized gold nanoparticles. *Analytical chemistry* **2010,** 82, (16), 6830-6837.
18. Wang, Y.; Yang, F.; Yang, X., Colorimetric detection of mercury (II) ion using unmodified silver nanoparticles and mercury-specific oligonucleotides. *Acs Applied Materials & Interfaces* **2010,** 2, (2), 339-342.
19. Wei, H.; Chen, C.; Han, B.; Wang, E., Enzyme colorimetric assay using unmodified silver nanoparticles. *Analytical chemistry* **2008,** 80, (18), 7051-7055.

Poly(2-acrylamido-2-methyl-1-propanesulfonic acid)/sultone modified Poly(vinyl alcohol) hydrogel as a proton conducting membrane

Chapter – VI

In the sixth chapter, we have synthesized and evaluated Poly(2-acrylamido-2-methyl-1-propanesulfonic acid)/sultone modified Poly(vinyl alcohol) Semi-IPNs hydrogel as a proton conducting membrane. Non-ionic PVA was modified by reacting it with 1, 3 propane sultone which partially introduced -SO_3H groups on PVA backbone chain. The -SO_3H groups gave proton conductivity property to PVA. The in-situ crosslinking of the membranes were effected using methylene bis acrylamide (MBA) as a crosslinker. The obtained membranes were characterized in terms of swelling, mechanical strength, and evaluated for conductivity with respect to humidity and temperature.

6.1. Introduction

Proton exchange membrane fuel cells (PEMFCs) are considered as one of the most promising energy conversion systems for powering all kinds of vehicles.[1] Therefore, currently major efforts are being made to develop efficient fuel cells for technological applications. The key component of a fuel cell is the proton conducting polymer membrane and the membrane is expected to have good conductivity and selectivity for proton transport, good chemical, thermal and mechanical stability. The most used PEM membrane is Nafion which is perfluorinated ionomer developed by DuPont, USA having high proton conductivity. However, its applications are restricted due to its high cost, high methanol permeability (~10^{-6} cm^2/s) and difficulty in synthesis and processing.[2-7] To overcome these drawbacks, major efforts are now undertaken to synthesize new proton conducting membranes based on sulfonated aromatic polymers like sulfonated poly(ether ether ketone),[8] sulfonated polyimide,[9] polybenzimidazoles,[10] and sulfonated polyposphazene.[11] Other strategies like acid base blends,[12] irradiation graft polymers,[13-14] crosslinked[15] and polymer blends,[16] have been studied.

Currently, more focus is given to relatively cheaper poly(2-acryalmido-2-methyl-1-propanesulfonic acid) (PAMPS) polymers which contain sulfonic acid groups. PAMPS polymers are expected to give high conductivity due to high dissociation constant, both in polar organic solvents and in water. There are literature reports on linear and crosslinked copolymers of AMPS monomer with acrylamide,[17] n-tert-butylacrylamide,[18] 2-hydroxyethylmethacrylate[19-20] which show potential as PEM for fuel cell applications.

In this chapter, we report on the synthesis of PAMPS/sultone modified PVA Semi-IPNs hydrogel as a proton conducting membrane. PAMPS exhibits good proton conducting properties and PVA shows an excellent film forming property. PVA itself does not have any ionic groups, and hence acts as a poor proton conducting material. However, several functional groups like amine, carboxylate, sulfonate can be incorporated into PVA to impart hydrophilicity and ionic property. In this work, a non-ionic PVA is modified by reacting it with 1, 3-propane sultone which partially introduce -SO_3H groups on PVA backbone chain. The -SO_3H groups give proton conductivity property to PVA. Proton exchange membranes were prepared using the combination of PAMPS and sultone modified PVA. The obtained

membranes were characterized in terms of swelling, mechanical strength, and evaluated for conductivity in fuel cell applications.

6.2. Experimental

6.2.1. Materials

2-Acrylamido-2-methyl-1-propanesulfonic acid (AMPS), N,N-Methylenebisacryl-amide (MBA), potassium per sulphate (KPS) , 1, 3-propane sultone, potassium tert-butoxide were procured from Aldrich (USA) and used as received. PVA (99% hydrolyzed, average MW 1,86,000 $gmol^{-1}$) was procured from Loba chemicals, India.

6.2.2. Synthesis

6.2.2.1. Synthesis of sultone modified PVA (1, 3-propane sultone grafting on PVA-OH) [PVA $(OH)_x$ $(SO_3H)_y$]

Into a 250 ml three necked round bottom flask equipped with an addition funnel, weighed quantities of PVA and NMP were added. The dissolution was carried out at 120°C under nitrogen atmosphere. After complete dissolution, the temperature was decreased to 50°C and 1, 3-propane sultone dissolved in 20 ml NMP was added. The solution of t-BuOK dissolved in 20 ml NMP was added dropwise through the addition funnel. The reaction was continued at 60°C for 3 hrs. Then the obtained polymer was precipitated in acetone to get dry powder. Further, the polymer was dissolved in water and packed in dialysis bag and dialyzed for 5 days and then lyophilized. The obtained polymers were denoted as, PVA $(OH)_{93}$ $(SO_3H)_7$ as [PVA-1b], PVA $(OH)_{87}$ $(SO_3H)_{13}$ as [PVA-1c] and the precursor polymer PVA $(OH)_{100}$ $(SO_3H)_0$ as [PVA-1a]. Stoichiometry for the PVA and sultone reaction and the nomenclature of the samples are given in **Table 6.1.**

Table 6.1: *Stoichiometry for the synthesis of sultone modified PVA*

Sr.No	Polymer	% of grafting	PVA (mmol)	1,3-propane sultone (mmol)	t-BuOk (mmol)
1	PVA-1b	10	111.63	11.63	11.63
2	PVA -1c	25	111.63	28.32	28.32

6.2.2.2. Synthesis of PAMPS/sultone modified PVA hydrogel membranes

PAMPS/PVA-1a, PVA-1b, PVA-1c Semi-IPN hydrogels were synthesized by free radical polymerization using AMPS as monomer in the presence of PVA. N, N'-methylenebisacrylamide (MBA) was used as a crosslinker, ammonium persulfate as an initiator. In a typical reaction, known amount of PVA/sultone modified PVA dissolved in distilled water at 80°C. Solution was allowed to attain the room temperature. To this, AMPS, MBA were added and dissolved completely. Upon complete dissolution, KPS was added and solution was poured in Petra dish. Polymerization was carried out at 60°C for 4 hrs. After polymerization, films were dried in oven at 40°C. Stoichiometry of reactants and the nomenclature of the samples are given in **Table 6.2.**

Table 6.2: *Stoichiometry for the synthesis of Semi-IPN hydrogel membranes*

Sr. No.	Samples (50:50) ratio	AMPS (g)	PVA (g)	PVA(OH)x(SO_3H)y (g)	MBA (g)	KPS (g)
1	PAMPS	0.5	-	-	0.015	0.013
2	PAMPS/PVA-1a	0.5	0.5	-	0.015	0.013
3	PAMPS/PVA-1b	0.5	-	0.5	0.015	0.013
4	PAMPS/PVA-1c	0.5	-	0.5	0.015	0.013

6.3. Characterization

6.3.1. FT-IR spectroscopy

The FT-IR spectra of sultone modified PVA samples were recorded on a FT-IR spectrum Perkin Elmer Spectrometer, UK in a diffused reflectance mode. The samples were mulled with KBr and the frequency range used was from 400 to 4000 cm^{-1}.

6.3.2. NMR spectroscopy

The ^{1}H-NMR of sultone modified PVA samples were recorded using a 5 mm QNP probe in Bruker DRX-500 spectrometer operating at a proton frequency of 500 MHz. The samples were made in DMSO-d_6 and TMS used as a reference for chemical shifts (0 ppm).

6.3.3. Zeta potential measurements

The surface charge of PVA before and after modification was determined by measuring zeta potential. The electrode probe was dipped in a dilute polymer solution. Electric field of 7.0 V/cm was applied across two electrodes. Zeta potential was determined with input of pH. For each measurement, 10 runs were averaged with each run employing 10 cycles. The data was analyzed using zeta pals software of Brookhaven instruments.

6.3.4. Energy dispersive X-ray analysis (EDAX)

The elemental analysis was performed using EDAX, to confirm the presence sulfur and % of sulfur in sultone modified PVA samples. The powder samples of polymer were analyzed by EDAX spectra.

6.3.5. Swelling measurements

An accurately weighed membrane was swollen in water for a day, then the surface water was carefully wiped with a filter paper, and weighed immediately. The equilibrium swelling ratio (Q) of the hydrogel was calculated using the following equation 1.

$$Q = \frac{W_s - W_d}{W_d} \times 100 \qquad (1)$$

Where, W_s = mass of the equilibrium swollen hydrogel membrane, W_d = mass of dry hydrogel membrane

6.3.6. Ion exchange capacity (IEC)

The ion exchange capacity (IEC; mequiv g^{-1}) of the membranes was determined titrimetrically. Square (1cm x 1cm) pieces of each membrane were soaked in 15 ml of a 2 M NaCl solution and equilibrated for at least 24 h to replace the protons by sodium ions. The remaining solution was then titrated with a 0.1 M NaOH solution using phenolphthalein as an indicator.

6.3.7. Dynamic mechanical analysis (DMA)

Mechanical strength of the membranes was determined by Uniaxial Tension using RSA III (TA Instrument). Tensile tests were carried out with a load cell of 1 kN, at room

temperature with an elongation rate of 1mm/min. Films with fixed dimensions of 3 mm (width) x 0.15-0.2 mm (thickness) were used.

6.3.8. Proton conductivity

Impedance spectroscopy was used for measuring the proton conductivity in the temperature range of 30 to 60°C and in the humidity range of 30-95% RH. The samples were sandwiched between the stainless steel blocking electrodes and placed in humidity and temperature controlled chamber (ESPEC). The impedance measurements were carried out on a Bio-Logic VMP-3 instrument in the frequency range of 1MHz to 0.1Hz against the open circuit potential with AC amplitude of 10 mV. Proton conductivity was obtained from following equation 2.

$$\sigma = \frac{l}{RA} \qquad (2)$$

Where σ is the proton conductivity (Scm^{-1}), R is the bulk resistance or ohmic resistance of the membrane sample, l is the thickness of the membrane (cm) and A is the cross-sectional area of the membranes sample (cm^2).

6.4. Results and Discussion

6.4.1. Synthesis of sultone modified PVA and PAMPS/sultone modified PVA hydrogel membranes

In order to enhance the proton conductivity of PVA, the $-SO_3H$ groups were introduced by reacting PVA with 1, 3-propane sultone. Then, the Semi-IPN hydrogel membranes were prepared using the combination of sultone modified PVA and PAMPS polymers. Synthetic pathway is shown in **Scheme 6.1.**

Free radical polymerization of AMPS monomer was carried out in the presence of sultone modified PVA using MBA as crosslinker. The polymerization could be initiated using standard initiators like KPS, APS or by photoinitiators such as AIBN-hydrochloride (V_{50}). The photo initiation can be important since proton conducting membrane can be directly obtained between two electrodes. Since the hydrogel synthesis is performed in the

presence of sultone modified PVA, it is physically entangled in the 3D structure of PAMPS resulting into Semi-IPN hydrogel. The synthetic pathway for making Semi-IPN hydrogel is shown in **Scheme 6.2.** and pictorial representation is shown in **Figure 6.1.**

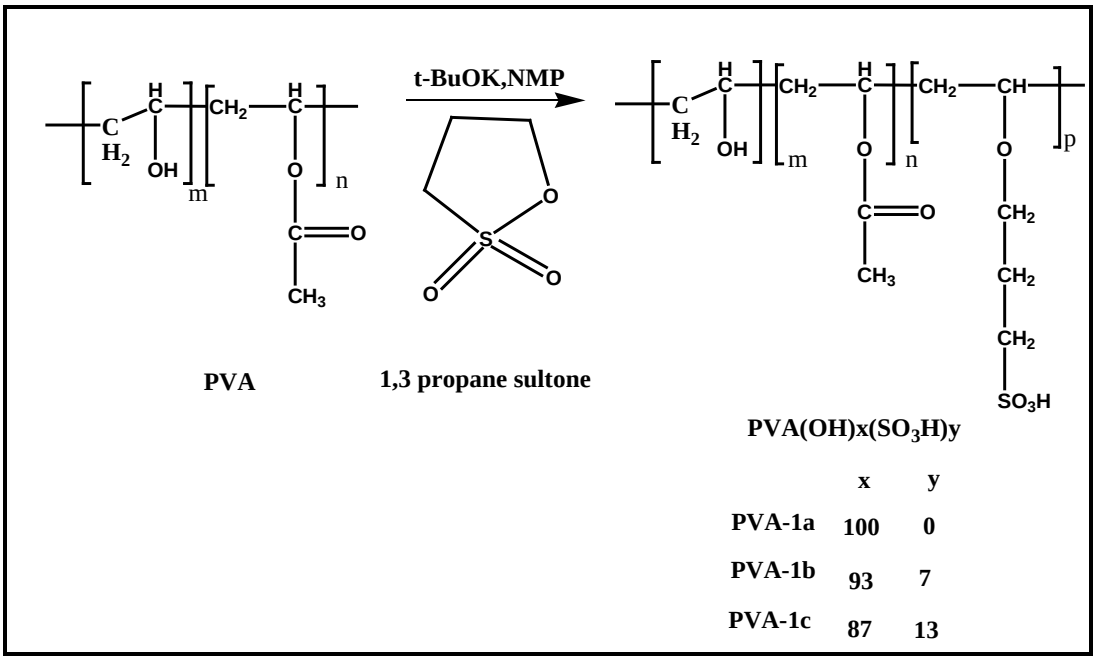

	x	y
PVA-1a	100	0
PVA-1b	93	7
PVA-1c	87	13

Scheme 6.1: *Synthesis of sultone modified PVA by grafting 1, 3-propane sultone*

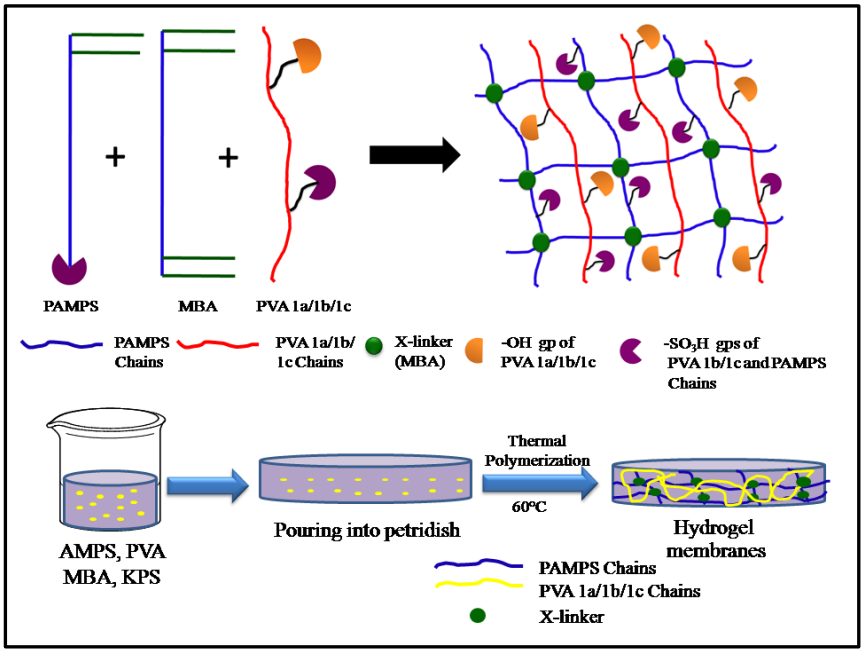

Figure 6.1: *Pictorial representation for making Semi-IPN hydrogel membrane*

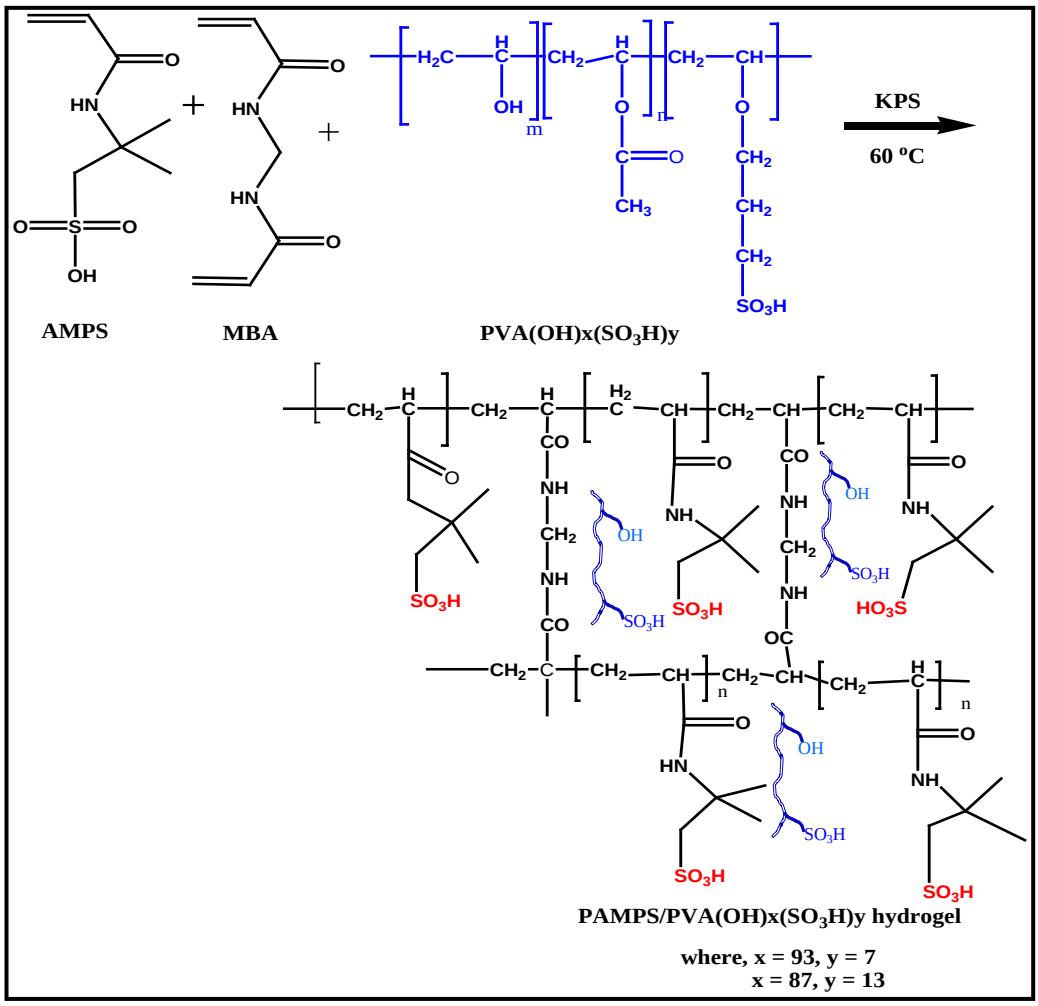

Scheme 6.2: *Synthesis of PAMPS/sultone modified PVA Semi-IPN hydrogel membranes*

6.4.2. FT-IR spectroscopy

We show the FT-IR spectra of PVA-1a, PVA-1b, PVA-1c polymers in **Figure 6.2.** It is clear from the figure that the absorption band at 3390 cm^{-1} arises from -OH stretching. The C-H methylene stretch appeared at 2934 cm^{-1}, the absorption band at 1635 cm^{-1} corresponds to the carbonyl functional groups due to the residual acetate groups remaining after obtaining PVA from hydrolysis of polyvinyl acetate.

Further, the absorption bands at 1415 cm^{-1} and 1132 cm^{-1} corresponds to $-SO_2$ asymmetric and symmetric stretch respectively, which indicated the presence of sulfonic acid groups in PVA chains.

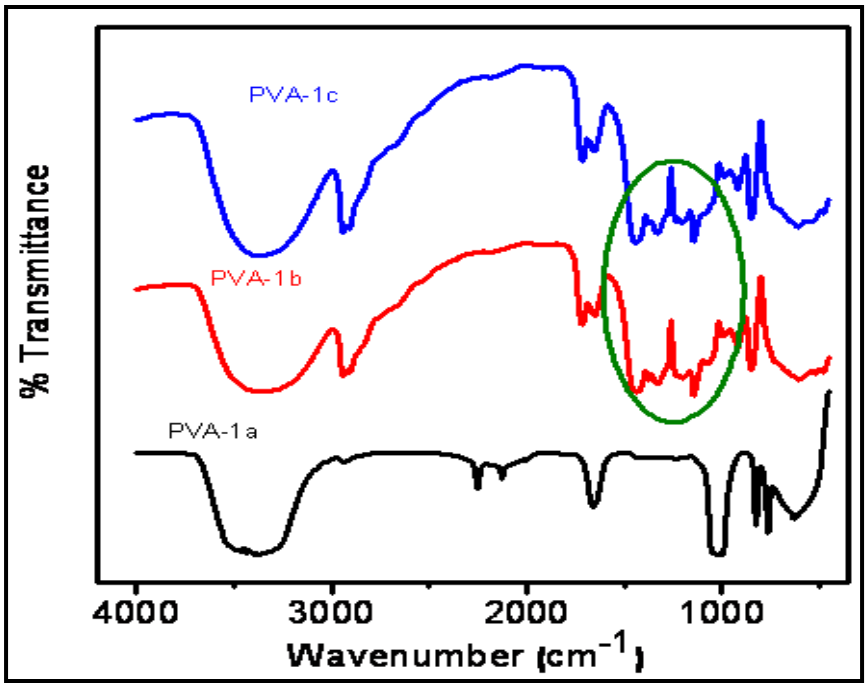

Figure 6.2: *FT-IR spectra of PVA-1a, PVA-1b, PVA-1c*

6.4.3. NMR spectroscopy

The structural characterizations of the sultone modified PVA-1b and PVA-1c were also done by ^{1}H NMR spectroscopy.

We show in **Figure 6.3**, the stacked plots of ^{1}H NMR spectra of PVA-1a, PVA-1b, and PVA-1c recorded in DMSO-d_6. In the case of PVA and sultone modified PVA, the methylene protons of the backbone (-CH_2) appeared in the range of 1.36-1.94 ppm and methine (-CH) protons attached to carbon to which -OH and -$OCOCH_3$ groups are attached appeared at 3.35 and 3.83 ppm, respectively. The -OH protons appeared at 4.25/4.49/4.68 ppm (atactic) because of the formation of intermolecular H-bonding in the polymer. Protons which appeared at 3.40 ppm corresponds to the methylene group (-CH_2) attached to -SO_3H group and ether group (-OCH_2) which is overlapping with protons attached to carbon to which -OH group is attached. Therefore, the quantitative NMR was difficult.

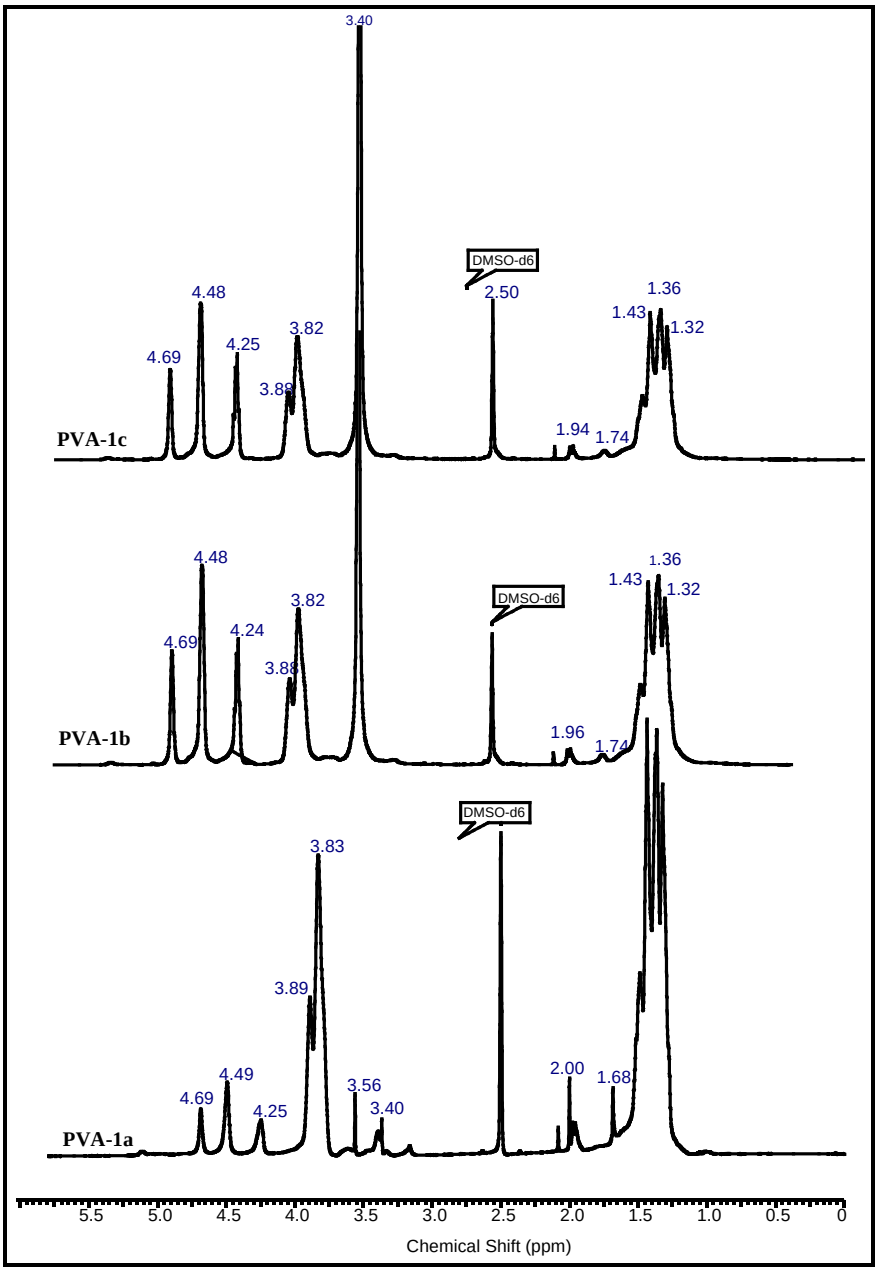

Figure 6.3: *^{1}H NMR spectra of PVA-1a, PVA-1b, PVA-1c*

6.4.4. Zeta potential analysis

To determine the Zeta Potential and mobility measurements of polymer PVA-1a, PVA-1b, PVA-1c, Smoluchowski's Equation was used to determine the electrophoretic mobility and zeta potential of the particle.

The Zeta Potential of the polymers was measured at 0.3 wt% concentration of the polymer. The pH of polymers was in the range of 6.3 to 6.5. Zeta potential measurements gave negative values and lower negative value was obtained in the case of PVA-1a and higher negative values were observed for PVA-1b and PVA-1c. These results clearly indicate the presence of -SO_3H groups in polymers.

Table 6.3: *Zeta potential values of PVA-1a, PVA-1b, PVA-1c*

Samples	pH	Zeta potential
PVA-1a	6.4	-10.6
PVA-1b	6.5	-19.4
PVA-1c	6.4	-22.4

6.4.5. Energy dispersive X-ray analysis (EDAX)

To confirm the presence of sulfur and % of sulfur after reacting PVA with different amount of 1, 3-propane sultone, polymers were analyzed by energy dispersive X-ray analysis (EDAX). The results are shown in **Figure 6.4**. A strong signal in the sulfur region of PVA-1b and PVA-1c samples confirm the presence of -SO_3H group in polymers. We also show in **Table 6.4**, the composition of each element (wt %) present in the polymer.

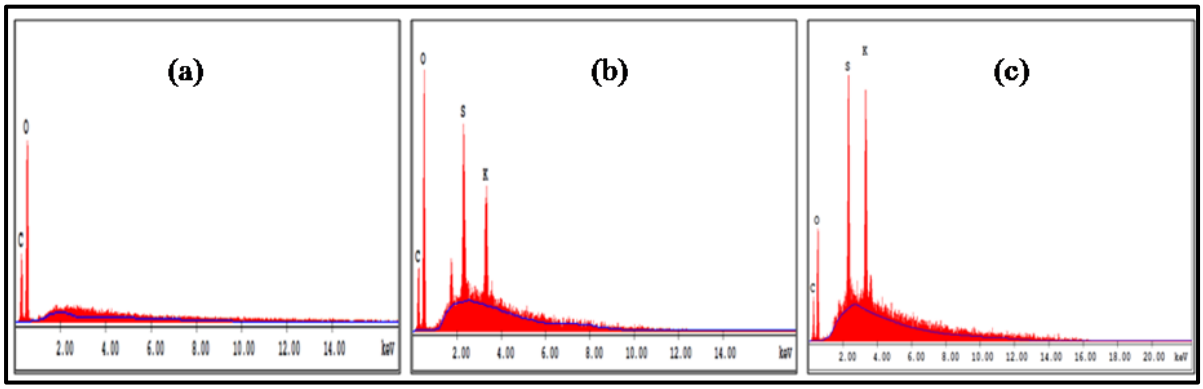

Figure 6.4: *EDAX images of (a) PVA-1a (b) PVA -1b (c) PVA-1c*

Table 6.4: *Weight % of each element by EDAX measurements*

Element	PVA-1a (Wt %)	PVA-1b (Wt %)	PVA-1c (Wt %)
C (K)	36.7	29.7	27.9
O (K)	63.3	55.6	42.3
S (L)	0	7.5	13.3
K (L)	0	7.2	16.5
Total	100.00	100.00	100.00

6.4.6. Swelling measurements of hydrogel membranes

Figure 6.5 shows the equilibrium swelling ratios (Q) of Semi-IPN hydrogels membranes. Swelling is in the order of PAMPS/PVA-1c > PAMPS/PVA-1b > PAMPS/PVA-1a. The swelling of PAMPS/PVA-1c hydrogel membrane was more compared to PAMPS/PVA-1b and PAMPS/PVA-1a. This could be attributed to the fact that, PAMPS/PVA-1c contains more -SO_3H groups compared to others which make hydrogel more ionic in nature and increase the hydrophilicity of the hydrogel. As a result, more swelling of the hydrogel membrane was observed.

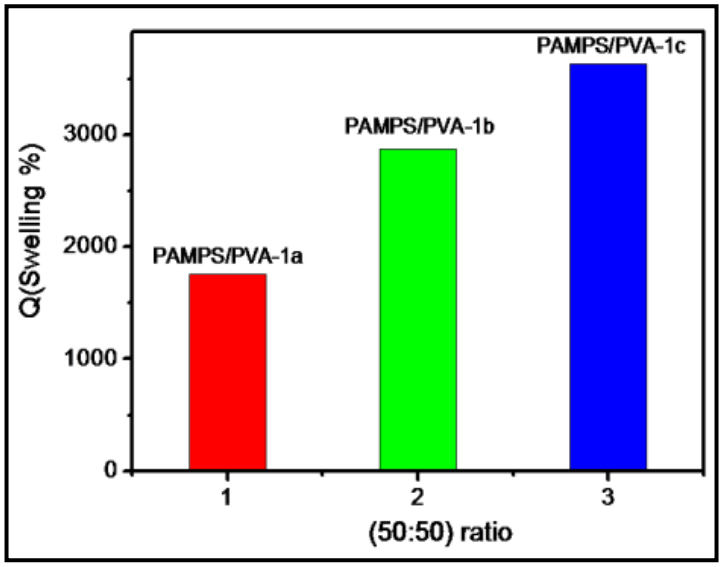

Figure 6.5: *Equilibrium swelling ratio (Q) of PAMPS/PVA 1a, 1b, 1c Semi-IPN hydrogel membranes in water*

6.4.7. Ion exchange capacity (IEC)

In general, proton conductivity increases with increase in swelling of the hydrogel membrane because of the larger free volume which contributes to the high mobility of free ions. Also, the proton conductivity increases with increase in IEC because of the high charge density of the membranes.

Table 6.5 shows swelling of membrane (g g^{-1}) with IEC and proton conductivity (Scm^{-1}). IEC and the swelling of membrane increased with increase in sultone modified PVA content as a result of high charge density. Despite their high ion exchange capacity (IEC) and high water uptake compare to nafion, the membranes showed good stability/strength at even 95% RH. IEC were both higher than that of Nafion 117 (swelling = 0.34 g g^{-1} and IEC = 0.94 mequiv g^{-1})

Table 6.5: *IEC values of hydrogel membranes*

Ratio	Swelling (g $g^{-1)}$	IEC (mequiv g^{-1})	σ (10^{-2} Scm^{-1})
PAMPS/PVA-1a	17.5	1.98	0.59
PAMPS/PVA-1b	28.7	2.10	2.48
PAMPS/PVA-1c	36.3	2.15	4.31

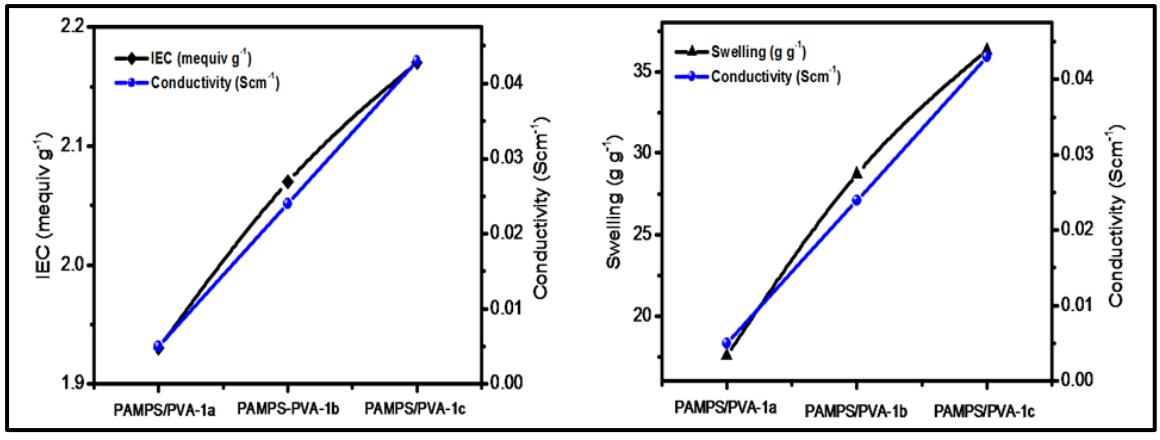

Figure 6.6: *Proton conductivity (●), swelling (▲), and IEC (■) of PAMPS/PVA-1a, PAMPS/PVA-1b, PAMPS/PVA-1c*

6.4.8. Dynamic mechanical analysis (DMA)

The mechanical properties of hydrogel membranes were determined using uniaxial extension experiments. **Figure 6.7** shows the tensile stress-strain curve for hydrogel membrane at R.T, at 95% relative humidity (RH). Sample PAMPS/PVA-1a at R.T. showed the tensile strength of 30 MPa with a percent elongation of 220%. Whereas, sample PAMPS/PVA-1b showed tensile strength of 22.8 MPa with a percent elongation of 360% and sample PAMPS/PVA-1c showed tensile strength of 19.9 MPa with a percent elongation of 420%. This clearly indicates that sulfonated PVA gives considerable flexibility to membranes because of pendant alkyl chain which contributes to the relaxation of chains.

However at 60°C and 95% RH, there is a decrease in tensile strength and elongation in all hydrogel membranes which are shown in **Table 6.6** and **Figure 6.7**. This could be attributed to fact that hydrogel membranes are in a swollen state at 95% RH and decrease the mechanical strength. Nevertheless, even in the hydrated state all the membranes showed good elongation properties which could help in easy handling of the membranes.

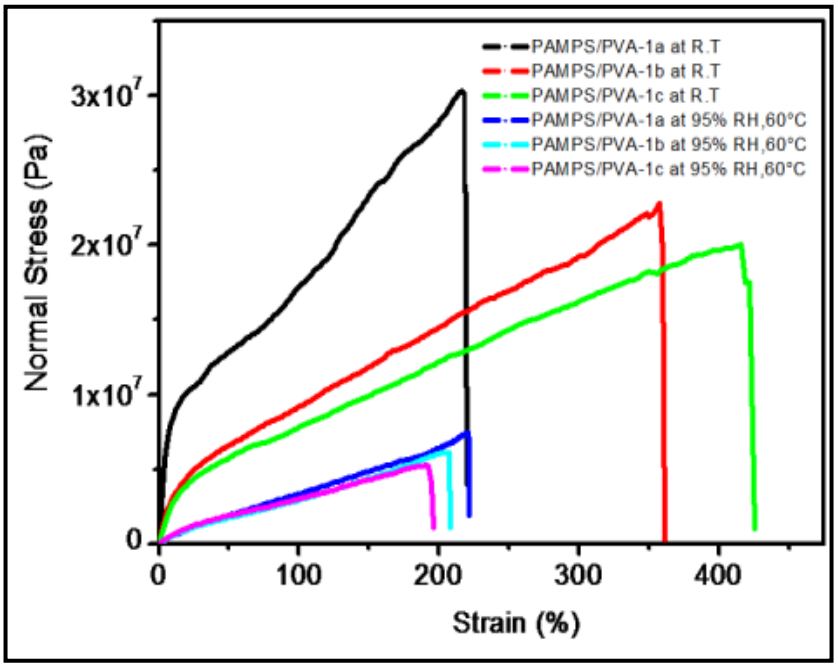

Figure 6.7: *Uniaxial extension of PAMPS/PVA-1a, PAMPS/PVA-1b, PAMPS/PVA-1c hydrogel membranes at RT and at 95% RH, 60°C*

Table 6.6.: *Tensile strength and % elongation of hydrogel membranes*

Samples	Tensile Strength (MPa)	Elongation (%)
PAMPS/PVA-1a at R.T	30.0	220
PAMPS/PVA-1b at R.T	22.8	360
PAMPS/PVA-1c at R.T	19.9	420
PAMPS/PVA-1a at 95% RH, 60°C	7.4	215
PAMPS/PVA-1b at 95% RH, 60°C	6.1	205
PAMPS/PVA-1c at 95% RH, 60°C	5.2	190

6.4.9. Proton Conductivity

We show in **Figure 6.8** the proton conductivities (σ) of hydrogel membranes measured at constant humidity and temperature (95% RH, 60°C). It can be seen from the figure that conductivity has increased significantly in the case of PAMPS/PVA-1c due to higher swelling and high ion exchange capacity (IEC) as a result of the presence of sulfonic acid groups.

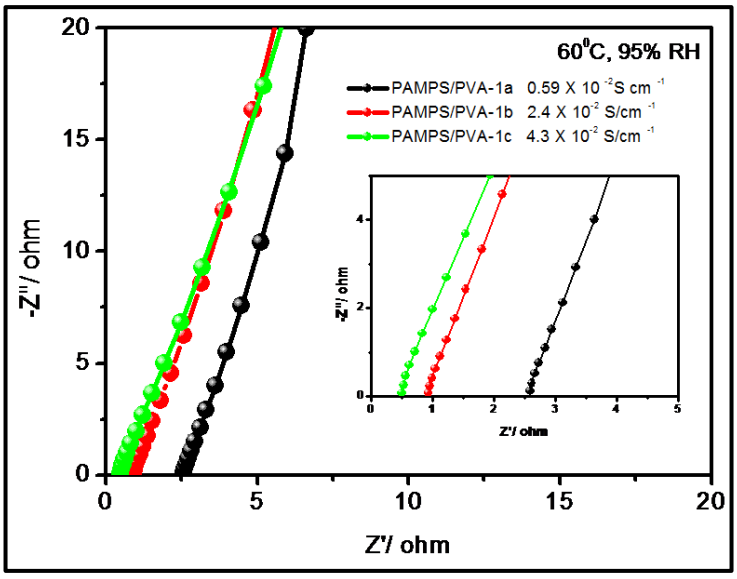

Figure 6.8: *Nyquist plot of a) PAMPS/ PVA-1a, b) PAMPS/PVA-1b, PAMPS/PVA-1c at 95% relative humidity and 60°C temperature*

Swelling in the hydrogel membranes enhances the mobility of free ions and increase the number of charge carriers in the system. It can be noted that, PAMPS/PVA-1a showed the least proton conductivity (**See Table 6.7**) mainly due to the less number of sulfonic acid groups.

Table 6.7: *Proton conductivities of hydrogel membranes at 95% RH and 60°C*

Samples	Humidity (%)	Conductivity at 60°C (10^{-2} Scm^{-1})
PAMPS/PVA-1a	95	0.59
PAMPS/PVA-1b	95	2.48
PAMPS/PVA-1c	95	4.31

6.4.10. Effect of humidity on proton conductivity of hydrogel membranes

In order to understand the influence of humidity on the proton conductivity of hydrogel membranes, the proton conductivity of PAMPS/PVA-1b and PAMPS/PVA-1c hydrogel membranes was measured at three different humidity conditions e.g. 30%, 60% and 95% humidity. **Figure 6.9** shows the Nyquist plots for PAMPS/PVA-1b and PAMPS/PVa-1c for three different values of humidity. The resistance values were determined from the impedance of real and imaginary plots and the point of resistance is where the imaginary part is zero.

From the figure, it is clear that both the samples showed decrease in resistance with increase in relative humidity (RH) which implies higher proton conductivity at higher humidity. Particularly, the hydrogel membrane PAMPS/PVA-1c showed higher proton conductivity compared to PAMPS/PVA-1b membrane at 95% RH. This can be attributed to the fact that former membrane contained more number of $-SO_3H$ groups compared to the later and hence exhibited higher proton conductivity. However, at low RH (i.e. 30% and 60 %) PAMPS/PVA-1c showed lower proton conductivity which may be due to low coordination of H_3O^+ ion with sultone and groups at low water contents.

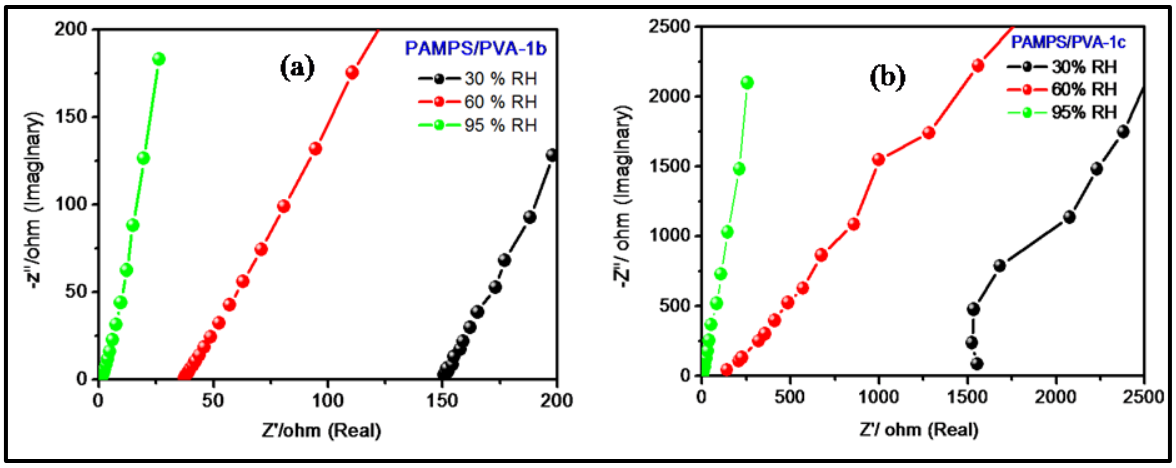

Figure 6.9: *Nyquist plot for effect of humidity on proton conductivity of a) PAMPS/PVA-1b, b) PAMPS/PVA-1c hydrogel membranes*

6.4.11. Effect of temperature on proton conductivity of hydrogel membranes

To determine the activation energy (E_a) required for the proton conduction of hydrogel membranes, the temperature dependent proton conductivities were measured at constant relative humidity (95% RH) in the temperature range of 25-60°C. The results are shown in **Figure 6.10.** It is observed from the figure that, the change in conductivities of hydrogel membranes followed the Arrhenius behaviour. The activation energies were calculated from the slopes of log σ vs 1000/T liner plots and found to be 7.5 KJ/mol and 3.5 KJ/mol for PAMPS/PVA-1b and PAMPS/PVA-1c respectively. These values are slightly lower than the activation energy (E_a) of Nafion 117, which has the E_a of 12 KJ/mol. From these results, it can be inferred that higher amount of $-SO_3H$ groups improves the proton transport in the hydrogel membranes. Further, the water molecules form H-bonding network with $-SO_3H$ and -OH groups through which protons can "hop" along via the Grotthuss mechanism.

Alternatively, the proton (from $-SO_3H$ group) can migrate to solvent molecules like water to form hydrated ions such as H_3O^+, $H_5O_2^+$, etc. and the proton transfer can occur by diffusion of these hydrated ions. This is known as vehicle mechanism. The high water content in the membranes can influence and enhances the diffusion of hydrated ions. Both

the mechanisms are represented in **Figure 6.11.** In our hydrogel membranes, the possibility of both mechanisms could be operative and can contribute to proton conductivity.

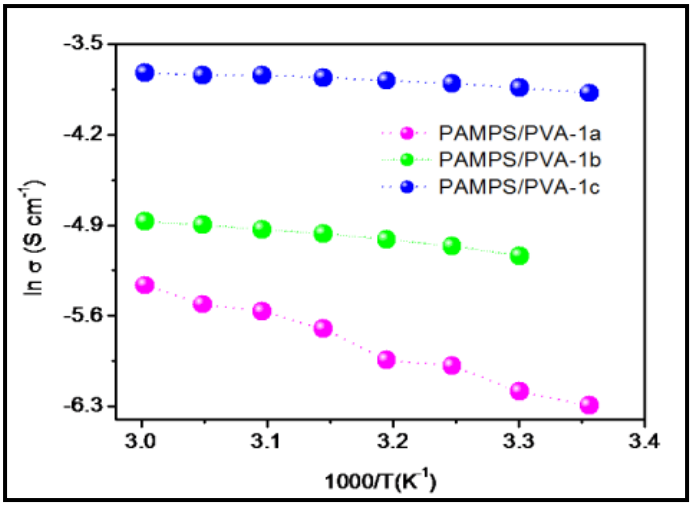

Figure 6.10: *Temperature dependences of the proton conductivity for PAMPS/PVA-1a, PAMPS/PVA-1b, PAMPS/PVA-1c hydrogel membranes*

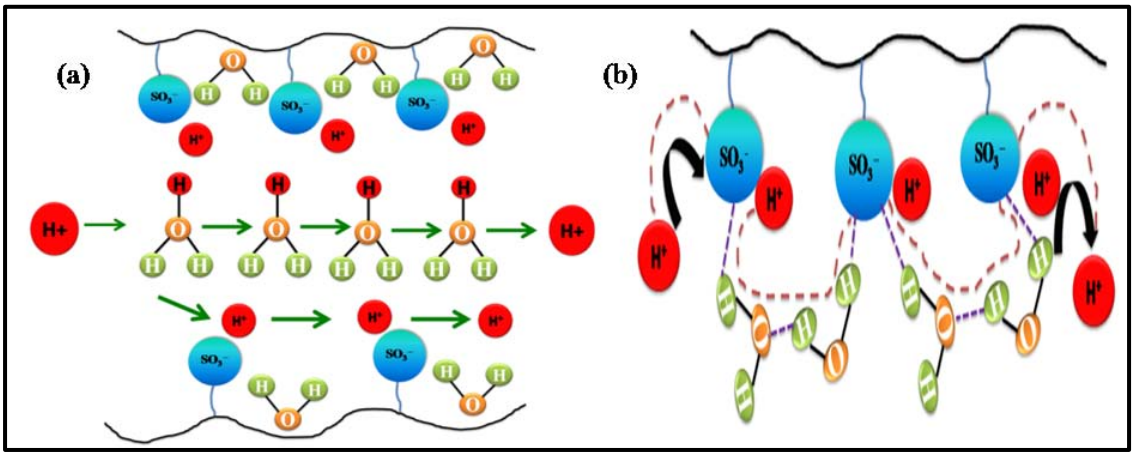

Figure 6.11: *(a) Vehicle and (b) Grotthuss type mechanism for proton Transfer*

6.5. Conclusions

In conclusion, we have synthesized proton exchange Semi-IPN hydrogel membranes using polyacrylamido propane sulfonic acid (PAMPS) and sultone modified PVA polymers. Sultone modified PVA content in the hydrogel membrane was varied from 0-15 mol%. The structural characterization of sultone modified PVA was performed using FT-IR, NMR and

EDAX spectroscopy. The swelling and mechanical strength of the hydrogel membranes were studied. The proton conductivity and ion exchange capacity (IEC) of the hydrogel membranes were determined and the influence of humidity and temperature on the proton conductivity was investigated. The proton conductivities were obtained in the range of (0.6 - 4.30) x 10^{-2} Scm^{-1}. Activation energy (E_a) for proton conductivity was determined and compared with the E_a of commercial membrane, nafion 117. The tensile strength of the hydrogel membranes varied from 5-30 MPa depending on the humidity content in the hydrogel membrane. The % elongation was in the range of 200-400%. The proton conductivity and IEC of the hydrogel membranes increased with increase in water content. The activation energy decreased with increase in $-SO_3H$ content in the membranes and exhibited higher proton conductivity. The mechanism of proton transfer was explained using both "hop" along via Grotthuss method as well as Vehicle transport of hydrated ions. These hydrogel membranes show promise in fuel cell application.

6.6. References

1. Kreuer, K., On the development of proton conducting polymer membranes for hydrogen and methanol fuel cells. *Journal of membrane science* **2001,** *185* (1), 29-39.
2. Yang, Y.; Shi, Z.; Holdcroft, S., Synthesis of Sulfonated Polysulfone-b lock-PVDF Copolymers: Enhancement of Proton Conductivity in Low Ion Exchange Capacity Membranes. *Macromolecules* **2004,** *37* (5), 1678-1681.
3. Glipa, X.; El Haddad, M.; Jones, D. J.; Rozière, J., Synthesis and characterisation of sulfonated polybenzimidazole: a highly conducting proton exchange polymer. *Solid State Ionics* **1997,** *97* (1), 323-331.
4. Kopitzke, R. W.; Linkous, C. A.; Anderson, H. R.; Nelson, G. L., Conductivity and water uptake of aromatic based proton exchange membrane electrolytes. *Journal of the Electrochemical Society* **2000,** *147* (5), 1677-1681.
5. Slade, S. C., S. A.; Ralph, T. R.; Walsh, F. C., Ionic Conductivity of an Extruded Nafion 1100 EW Series of Membranes. *J. Electrochem.Soc.* **2002,** *149*, A1556.
6. St-Pierre, J.; Wilkinson, D. P., Fuel cells: a new, efficient and cleaner power source. *AIChE Journal* **2001,** *47* (7), 1482-1486.
7. Sumner, J.; Creager, S. E.; Ma, J.; DesMarteau, D., Proton conductivity in Nafion® 1 17 and in a novel bis [(perfluoroalkyl) sulfonyl] imide ionomer membrane. *Journal of the Electrochemical Society* **1998,** *145* (1), 107-110.
8. Li, L.; Zhang, J.; Wang, Y., Sulfonated poly (ether ether ketone) membranes for direct methanol fuel cell. *Journal of membrane science* **2003,** *226* (1), 159-167.
9. Fang, J.; Guo, X.; Harada, S.; Watari, T.; Tanaka, K.; Kita, H.; Okamoto, K.-i., Novel sulfonated polyimides as polyelectrolytes for fuel cell application. 1. Synthesis, proton conductivity, and water stability of polyimides from 4, 4'-diaminodiphenyl ether-2, 2'-disulfonic acid. *Macromolecules* **2002,** *35* (24), 9022-9028.
10. Lobato, J.; Canizares, P.; Rodrigo, M. A.; Linares, J. J., PBI-based polymer electrolyte membranes fuel cells: Temperature effects on cell performance and catalyst stability. *Electrochimica acta* **2007,** *52* (12), 3910-3920.

11. Guo, Q.; Pintauro, P. N.; Tang, H.; O'Connor, S., Sulfonated and crosslinked polyphosphazene-based proton-exchange membranes. *Journal of membrane science* **1999,** *154* (2), 175-181.

12. Herranen, J.; Kinnunen, J.; Mattsson, B.; Rinne, H.; Sundholm, F.; Torell, L., Characterisation of poly (ethylene oxide) sulfonic acids. *Solid State Ionics* **1995,** *80* (3), 201-212.

13. Lehtinen, T.; Sundholm, G.; Sundholm, F., Effect of crosslinking on the physicochemical properties of proton conducting PVDF-g-PSSA membranes. *Journal of applied electrochemistry* **1999,** *29* (6), 679-685.

14. Kallio, T.; Slevin, C.; Sundholm, G.; Holmlund, P.; Kontturi, K., Proton transport in radiation-grafted membranes for fuel cells as detected by SECM. *Electrochemistry communications* **2003,** *5* (7), 561-565.

15. Rhim, J.-W.; Park, H. B.; Lee, C.-S.; Jun, J.-H.; Kim, D. S.; Lee, Y. M., Crosslinked poly (vinyl alcohol) membranes containing sulfonic acid group: proton and methanol transport through membranes. *Journal of membrane science* **2004,** *238* (1), 143-151.

16. Manea, C.; Mulder, M., Characterization of polymer blends of polyethersulfone/sulfonated polysulfone and polyethersulfone/sulfonated polyetheretherketone for direct methanol fuel cell applications. *Journal of membrane science* **2002,** *206* (1), 443-453.

17. Travas Sejdic, J.; Easteal, A., Study of free radical copolymerization of acrylamide with 2-acrylamido-2-methyl-1-propane sulphonic acid. *J Appl Polym Sci* **2000,** *75* (5), 619-628.

18. Karlsson, L. E.; Wesslén, B.; Jannasch, P., Water absorption and proton conductivity of sulfonated acrylamide copolymers. *Electrochimica acta* **2002,** *47* (20), 3269-3275.

19. Walker, C. W., Proton-conducting polymer membrane comprised of a copolymer of 2-acrylamido-2-methylpropanesulfonic acid and 2-hydroxyethyl methacrylate. *Journal of Power Sources* **2002,** *110* (1), 144-151.

20. Zukowska, G.; Williams, J.; Stevens, J.; Jeffrey, K.; Lewera, A.; Kulesza, P., The application of acrylic monomers with acidic groups to the synthesis of proton-conducting polymer gels. *Solid State Ionics* **2004,** *167* (1), 123-130.

Summary and Conclusions

Chapter – VII

In the seventh chapter, we have discussed the summary and conclusions of the thesis work.

The objective of this thesis was to design and synthesize the hydrogels for novel applications such as metal nanoparticles incorporated hydrogels for catalytic applications, conducting hydrogels as proton exchange membranes in fuel cell applications and hydrogels as sensor materials for toxic metals. Although extensive work has been done on hydrogels in terms of their synthesis, stimuli-sensitive properties, structure-property relations and their wide variety of applications in bio-medical, controlled drug delivery, health-care, tissue engineering, robotics, actuators etc., still there is enormous scope in looking at other novel applications. Therefore, in this thesis we have undertaken work on synthesizing hydrogels with metal nanoparticles for catalytic and sensor applications and making conducting hydrogel membranes for fuel cell applications.

In the first chapter, a detailed literature survey was done on hydrogels in terms of their introduction, classification, properties and on a few reports on their applications in catalysis, conducting membranes and sensors field. The characterization techniques such as XPS, XRD, TEM, Electrospinning, etc., used for studying the atomic composition, surface morphology and making nanofibers were briefly explained. The scope and objectives of thesis was discussed in second chapter.

In the third chapter, we have synthesized Ag-NPs embedded Semi-IPN hydrogels based on combination of PAm and PAS by free radical polymerization and its application in catalytic reduction of 4-NP to 4-AP. The presence of PAS enhances swelling and diffusion of more Ag^+ ions into the hydrogel through electrostatic interaction between -COO^- groups of PAS and Ag^+ ions. The presence of Ag-NPs in hydrogels was clearly evidenced by TEM, EDAX and UV-Vis analysis. The swelling studies on PAm/PAS hydrogels showed Non-Fickian diffusion of transport. The catalytic reduction of 4-NP to 4-AP was performed using Ag-NPs embedded Semi-IPN hydrogel where the completion of reaction occurred in ≈ 16 minutes. The completion of the reaction was indicated by slow fading of yellow colour of the reaction mixture. The Ag-NPs embedded hydrogel could be easily separated and reused for subsequent repeated cycles without losing the catalytic activity which is most desired in catalytic applications.

In the forth chapter, we have demonstrated the green synthesis of Ag-NPs by SA (polysaccharides) as a reducing as well as capping agent and further incorporated them

into SA/EHM-200 blend beads. EHM-200 with long alkyl phenol helped in stabilizing the nanoparticles. EHM-200 also helped in enhancing the swelling of the hydrogel as a result there could be better diffusion of reactants through the hydrogel. The conformation of formation of Ag-NPs was done by UV-Vis spectroscopy, which gave a surface plasmon resonance in the range of 410-425 nm. The TEM images indicated the size of nanoparticles in the range of 15-30 nm. SEM images indicated that beads are more or less spherical in nature. Finally, we demonstrated the use of this Ag-NPs embedded hydrogel blend for the catalytic reduction reaction of 4-NP to 4-AP. The completion of the reaction was achieved in ≈ 8 minutes and could be recycled for atleast 2 times. The combination of SA and EHM-200 makes the system biodegradable and helps in the green synthesis of Ag-NPs.

In the fifth chapter, we synthesized Ag-NPs incorporated PVA/PAS electrospun nanofibers as a sensor for detecting toxic metals such as Hg. It is known that, Ag-NPs on their own are susceptible to oxidation and degradation and using them in liquid state is highly cumbersome. Therefore, incorporating them into a nanofiber polymer matrix can resolve the above issues to a great extent. Accordingly, we have prepared PVA/PAS electrospun nanofibers and made in-situ synthesis of Ag-NPs in the nanofibers. In order to get good films of nanofibers, the fibers were post-crosslinked with glutaraldehyde. Morphology of the nanofibers was studied by SEM and the average diameter of the fibers was in the range of 195-285 nm. Presence of Ag-NPs in the nanofibers was confirmed by TEM analysis. Finally, we demonstrated the use of Ag-NPs embedded nanofibers for sensing toxic metal, mercury.

In the sixth chapter, we synthesized PAMPS/sultone modified PVA hydrogel as a proton conducting membrane for fuel cell applications. The structural characterization of sultone modified PVA was performed using FT-IR, NMR and EDAX spectroscopy. The swelling and mechanical strength of the hydrogel membranes were studied. The tensile strength of the hydrogel membranes varied from 5-30 MPa depending on the humidity content in the hydrogel membrane. The % elongation was in the range of 200-400%. The proton conductivities were obtained in the range of (0.6 - 4.30) x 10^{-2} Scm^{-1}. These hydrogels can have potential in fuel cell application.

In the overall thesis work, we have demonstrated the synthesis, characterization and new applications of hydrogels in the areas of catalysis, fuel cell and sensing toxic metals.

List of Publications

1. An efficient Ag-Nanoparticle embedded Semi-IPN hydrogel for catalytic Applications; **Manjusha V. Patwadkar**, Chinnakonda S. Gopinath, Manohar V. Badiger; *RSC Advances*, **2015**, 5, 7567-7574.

2. PAMPS/sultone modified PVA hydrogel as proton conducting membrane; **Manjusha V. Patwadkar**, Rajith Illathvalappil, Sreekumar Kurungot, Manohar V. Badiger (Under preparation)

3. Capturing a novel metastable polymorph of the anticancer drug gefitinib; Shridhar Thorat, **Manjusha V. Patwadkar**, Rajesh G. Gonnade, and R. Vaidhyanathanc; *CrystEngComm,* **2014**, 16, 8638–8641.

4. Drug-Drug Molecular Salt Hydrate of an Anticancer Drug Gefitinib and a Loop Diuretic Drug Furosemide: An Alternative for Multidrug Treatment; Shridhar Thorat, Sanjay Kumar Sahu, **Manjusha V. Patwadkar**, Manohar V. Badiger, Rajesh G. Gonnade; *Journal of Pharmaceutical Sciences*, **2015**, 104, 4207–4216.

Conferences

1. Participation in the "Macro-2006 International conference on Polymer Science", National Chemical Laboratory, Pune, Maharashtra, India, 2006

2. Silver Nanoparticle embedded hydrogels based on Poly(acrylamide) and Poly(aspartic acid): Synthesis ,Characterization and Biomedical Applications; **Manjusha V. Patwadkar and M. V. Badiger**; APA International Conference, Delhi, India, 2014

3. An efficient Ag-Nanoparticle embedded Semi-IPN hydrogel for catalytic Applications; **Manjusha V. Patwadkar and M. V. Badiger**; APA International Conference, Rajkot, Gujarat, India, 2015

4. An efficient Ag-Nanoparticle embedded Semi-IPN hydrogel for catalytic Applications; **Manjusha V. Patwadkar and M. V. Badiger**; National Science Day Celebrations, National Chemical Laboratory, Pune, Maharashtra, India, 2015